TISSUE SPECIFIC ROLES OF FATTY ACID OXIDATION

by
Jieun Lee

A dissertation submitted to Johns Hopkins University in conformity with the requirements for the degree of Doctor of Philosophy

Baltimore, Maryland

September, 2016

ABSTRACT

The oxidation of long chain fatty acids facilitates mitochondrial respiration in diverse cell types. In this thesis, the role of fatty acid oxidation primarily in the adipose tissue and liver are discussed. To address this question, we generated mice with an adipose- or liver-specific knockout of carnitine palmitoyltransferase 2 (Cpt2), an obligate step in long chain mitochondrial fatty acid oxidation. In adipocyte-specific KO mice ($Cpt2^{A-/-}$), the brown adipose tissue (BAT) of $Cpt2^{A-/-}$ mice was unable to utilize fatty acids and therefore caused hypothermia after an acute cold challenge. Surprisingly, $Cpt2^{A-/-}$ BAT was also unable to up-regulate thermogenic genes such as *Ucp1* and *Pgc1a* in response to agonist-induced stimulation *in vivo* or *ex vivo*. The adipose specific loss of CPT2 did not result in changes in body weight on low or high fat diets, although paradoxically, low fat diets promoted and high fat diets suppressed adiposity. Additionally, a high fat diet increased oxidative stress and inflammation in gonadal white adipose tissue (WAT) of control mice but this effect was greatly suppressed in $Cpt2^{A-/-}$ mice. However, this suppression did not improve high fat diet induced glucose intolerance. In hepatocyte-specific KO ($Cpt2^{L-/-}$) mice, fasting induced hepatic steatosis and serum dyslipidemia with an absence of circulating ketones while blood glucose remained normal. Systemic energy homeostasis was largely maintained in fasting $Cpt2^{L-/-}$ mice by adaptations in hepatic and systemic oxidative gene expression mediated in part by Pparα target genes including procatabolic hepatokines Fgf21, Gdf15 and Igfbp1. However, feeding a ketogenic diet to $Cpt2^{L-/-}$ mice resulted in severe hepatomegaly, liver damage and death with a complete absence of adipose triglyceride stores. These results

provided the first functional and physiological characterizations of Cpt2 and established its importance in energy homeostasis.

Thesis Advisor: Dr. Michael J. Wolfgang

Thesis Reader: Dr. Daniel M. Raben

ACKNOWLEDGEMENT

I am grateful to my advisor, Dr. Michael J. Wolfgang, for his support and guidance during my PhD training. We have been a very productive team and had a great time working together. I am especially thankful for his enthusiasm and support for helping me publish manuscripts for all of my different projects. My PhD training was hard, but it was exciting because I had a great mentor like him.

I am also thankful to my colleagues who helped me generously during my PhD training. I would especially like to thank my lab partner and good friend, Joseph Choi, for all the latenight experiments and mouse work we did together. I would not have been able to publish as many manuscripts without his effort and help in all of my projects. I am also thankful to the rest of the members of the Wolfgang Lab, Elsie Gonzales-Huartado, Ebru Selen-Alpergin, Caitlyn Bowman, Cory White, and past members Susana Rodriguez and Jessica Ellis, for being friends with me and making lab work fun. Drs. Susanna Scafidi, G. William Wong, Daniel M. Raben, Steven Claypool and Seth Margolis provided training and help for most of the experiments, therefore made great contributions toward the completion of the projects.

Finally, I am deeply thankful to the love and support from my family, my father, Jae Seok Lee, mother, Kyungsin Kim Lee, and sisters Esther J. Lee and Sarah J. Lee. Whatever I achieve in life and wherever I am, they are the source of inspiration and strength for me to move forward and pursue my goals.

TABLE OF CONTENTS

LIST OF FIGURES

LIST OF TABLES

TISSUE SPECIFIC ROLES OF FATTY ACID OXIDATION

CHAPTER 1. Overview

Dysregulated fatty acid metabolism is strongly linked to the development and progression of obesity, diabetes, fatty liver and cardiovascular disease. In particular, obesity results when caloric intake exceeds expenditure, directing metabolic flux into storing energy, primarily as triglyceride in adipose tissue. Conversely, when caloric expenditure exceeds intake, these reserves are mobilized to provide physiological fuel for other tissues. To alter body weight, in particular adiposity, either energy intake or expenditure or both must be altered. Energy intake can be managed either behaviorally or via bariatric surgery to physically constrain intake. One popular notion is that increasing energy expenditure would be sufficient to decrease adiposity and improve glycemic control (1-12). Indeed, in the early 1900s, chemical uncoupling agents such as 2,4 Dinitrophenol were used effectively in humans to reduce adiposity (13). It was eventually rendered impractical and banned in 1938 due to a high incidence of mortality which is unfortunately still seen today as weight loss enthusiasts purchase it over the internet (14).

More recently, there has been great interest in harnessing the capacity of brown and beige adipocytes to rapidly oxidize fatty acids via natural uncoupling as a bioenergetic means of "burning fat" and reducing adiposity (1-12). This idea has gained further momentum since the rediscovery of active brown and beige adipocytes in adult humans (15-18). In fact, the entire field of metabolic biochemistry and physiology seems to have pivoted towards this idea. Mouse models that are resistant to high fat diet induced weight gain are often mechanistically explained based on a change in energy expenditure via increased adipocyte fatty acid oxidation (19-24). However, it has never been directly demonstrated that the suppression or enhancement of fatty acid oxidation in

adipocytes leads to changes in adiposity or insulin sensitivity. In fact, the idea that body weight can be suppressed by increasing oxidative capacity in the absence of uncoupling has recently been challenged (25-27).

Mitochondrial long chain fatty acid oxidation is governed by the regulated translocation of activated fatty acids (acyl-CoAs) from the cytoplasm to the matrix of the mitochondria (**Figure 1-1**). This is mediated by successive carnitine acyltransferases. CPT1 isoenzymes mediate acyl transfer from long chain acyl-CoAs to carnitine. Acylcarnitines can then traverse organic cation transporters in the mitochondrial membranes and enter the mitochondrial matrix. Within the mitochondrial matrix, CPT2 transfers the acyl group from the acylcarnitine back onto CoA. The acyl-CoA is then used by the beta-oxidation machinery in the matrix. CPT1 isoenzymes are highly allosterically regulated by malonyl-CoA, the rate setting metabolite in de novo fatty acid synthesis. This provides the metabolic logic whereby synthesis and oxidation do not occur simultaneously.

The significance of fatty acid oxidation in many biological processes is made evident from multiple mutations in this pathway that cause human disease (28). For example, hypomorphic mutations in CPT2 result in metabolic disease (OMIM #s, 255110 adult onset, 600649 infantile, and 600650 infantile lethal). The most severe form presents as hypothermia, cardiomegaly, hepatomegaly and hypoglycemia in the first days of life presumably from the important roles of fatty acid beta-oxidation in brown adipocytes, heart and liver respectively. Additionally, hypomorphic mutations in CPT1a result in hypoketotic hypoglycemia (OMIM # 255120) and a loss of CPT1a or CPT1b in mice is lethal (29, 30). Clearly, fatty acid oxidation is an essential metabolic process,

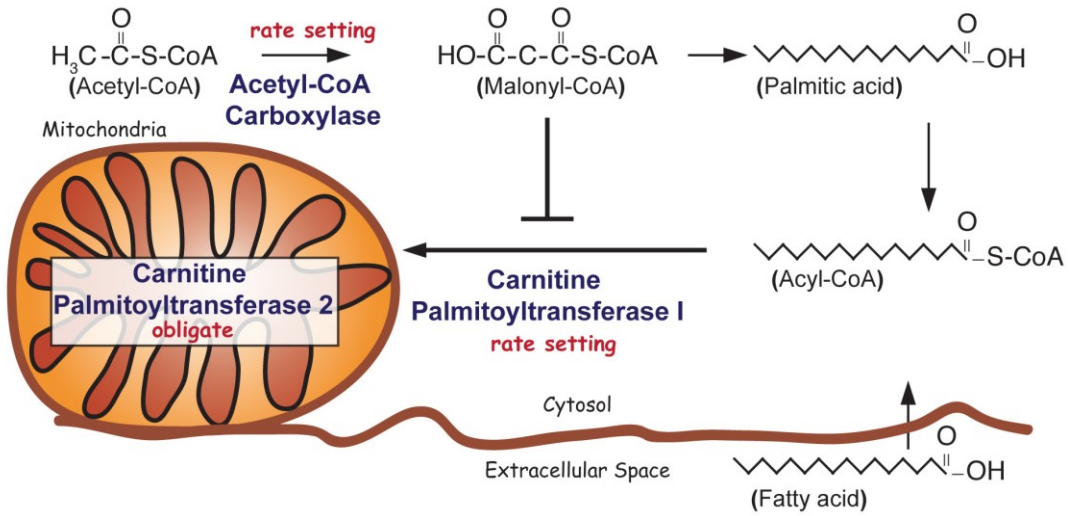

Figure 1-1. Diagram of fatty acid oxidation

however, it is not apparent from these studies what the cell autonomous role for fatty acid oxidation is in vivo. Many laboratories around the world have suggested that the oxidation of fatty acids in adipose tissue is an important component for weight gain, adiposity and glucose tolerance (1-12, 31-34). Therefore, to test this hypothesis and determine the cell autonomous role of fatty acid oxidation in vivo, we have generated a mouse model that targets CPT2 specifically in the adipose tissue and liver to determine the effect of loss of fatty acid oxidation in these tissues.

Fatty acid oxidation: Brown adipocytes.

Brown adipose tissue is essential for heat generation during cold exposure in perinatal and adult mammals (1, 26, 35). Brown adipocytes mediate heat generation by uncoupling mitochondrial respiration from ATP generation via an uncoupling protein, UCP1, which dissipates the chemiosmotic gradient. Therefore, protons are diverted from the ATP Synthase. The chemiosmotic gradient forms when reducing equivalents (NADH, $FADH_2$) donate electrons to the electron transport chain. The loss of UCP1 results in cold intolerant mice (36) however, the role of UCP1 in obesity remains controversial (26). The requirement of fatty acid oxidation during cold thermogenesis is exemplified by cold intolerant phenotypes of whole body knockout mouse models of the acyl-CoA dehydrogenase enzymes (37-40). Therefore, fatty acid oxidation is critical for brown adipocyte function.

Fatty acid oxidation: White adipocytes.

WAT is a remarkably dynamic organ that can dramatically expand and contract in triglyceride content depending on the metabolic state of the individual. It is an insulin responsive tissue that can greatly influence insulin resistance (41-43). In lean humans,

~5% of resting metabolic rate can be attributed to white adipocytes. In obese individuals, where >50% of total body weight can be from adipose, this value can double (44). Oxygen consumption in white adipose tissue goes down with age and is negatively correlated with human obesity (45, 46). Many genetic forms of obesity in rodents are accompanied by suppressed WAT oxidation (19-23). Furthermore, monozygotic twins discordant for obesity showed ~2 fold difference in mitochondrial content in WAT (47). Although the oxidation of fatty acids in the fed state is low, fasting doubles the rate of white adipocyte fatty acid oxidation and is presumably the major fuel in insulin suppressed states (48). This has led to the hypothesis that mitochondrial dysfunction and suppressed fatty acid oxidation in WAT is a contributor to increasing adiposity and impaired glucose tolerance (22, 31, 32, 49-52).

Fatty acid oxidation: Liver.

Lipid metabolism is also a critical component in the development of fatty liver disease (FLD) that could progress on to hepatic steatosis or cirrhosis. Energy combustion in the liver is primarily regulated via the peroxisome proliferator-activated receptor (PPAR)-alpha dependent fatty acid oxidation in mitochondria and peroxisomes. Disrupted lipid metabolism or ineffective PPARα in the liver have been shown to increase triglyceride storage in hepatocytes and initiate a series of events that lead to FLD (53). In fact, many studies have suggested that FLD begins when energy consumption exceeds PPARα-mediated energy expenditure through fatty acid oxidation in the liver. When the hepatocytes become apoptotic, they rupture and release triglycerides and long chain fatty acids that cause liver injury. Therefore the balance between fatty acid synthesis and fatty acid oxidation is crucial to prevent the development of FLD (54-59).

The liver is also crucial when the body goes under prolonged fasting. Starvation initiates a series of metabolic adaptations to enable continuous production and delivery of nutrients to critical organs, tissues and cells (53). The liver responds to starvation by liberating glucose to the circulation initially from glycogen stores followed by de novo glucose production (i.e. gluconeogenesis). Fatty acid oxidation is critical for as it provides the carbon substrate for ketone production (acetyl-CoA) and mitochondrial bioenergetics (ATP, NADH) to facilitate gluconeogenesis. Therefore, humans with disparate inborn errors in mitochondrial fatty acid oxidation exhibit life-threatening hypoketotic-hypoglycemia following a fast (54). The liver is thought to dominate fasting gluconeogenesis with minor contributions from the kidney and gut.

TISSUE SPECIFIC ROLES OF FATTY ACID OXIDATION

CHAPTER 2. Adipose fatty acid oxidation is required for thermogenesis and potentiates oxidative stress-induced inflammation

Introduction

Ingestion of a calorically dense diet, generally high in fat content, coupled with inactivity leads to increased adiposity and eventual obesity. Obesity in turn is highly correlated with the development of type 2 diabetes, the metabolic syndrome, and cardiovascular disease, among others. The molecular mechanisms by which high-fat diets contribute to these pathologies are not well understood, but several themes have emerged. Implicated in the etiology and progression of obesity-related pathologies is oxidative stress, endoplasmic reticulum stress, and inflammation originating locally at adipose depots but acting systemically to promote insulin resistance (48, 62-64). Reversing or preventing local adipose tissue inflammation may have beneficial systemic effects against insulin resistance. Alternatively, strategies to reverse obesity by increasing adipose energy expenditure have been suggested to improve systemic obesity-related complications (1).

Adult mammals have at least two functionally distinct adipose lineages: unilocular white adipocytes, which function mainly to store fat, and multilocular brown adipocytes, which function mainly to burn fat for thermogenesis. Dysfunctional white adipose tissue (WAT) and brown adipose tissue (BAT) have been implicated in the pathogenesis of obesity and diabetes. BAT is densely packed with mitochondria and requires fatty acid oxidation to fuel heat generation (27, 35-38). Although the oxidation of fatty acids in WAT in the fed state is relatively low, fasting doubles the rate of white adipocyte fatty acid oxidation and is presumably a major fuel in insulin suppressed states (46). Changing macronutrient metabolism specifically in adipocytes can lead to changes in adiposity, body weight, and glucose tolerance (22, 39, 65, 66). However, the

autonomous contribution of adipose fatty acid oxidation to obesity and insulin resistance remains unknown.

Mitochondrial long-chain fatty acid β-oxidation requires successive carnitine acyltransferases to translocate acyl-coenzyme As (acyl-CoAs) from the cytoplasm into the mitochondrial matrix (67). The initial and rate-setting enzyme, CPT1, generates acylcarnitines that can traverse the mitochondrial membranes via specific transporters. CPT1 is allosterically inhibited by the rate-determining metabolite in de novo fatty acid synthesis, malonyl-CoA; therefore, the balance of fatty acid synthesis and oxidation is metabolically coordinated posttranslationally. Once inside the mitochondrial matrix, CPT2 generates acyl-CoAs from acylcarnitines to initiate the b-oxidation of long-chain fatty acids to acetyl-CoA. Fatty acids contain an abundant energy potential, making them ideal for storage during energy surplus and mobilization during energy deficits. Fatty acid oxidation efficiently generates energy but can also promote the generation of reactive oxygen species (ROS). ROS can potentiate oxidative stress and inflammation, which can impair insulin sensitivity (68).

Although it is clear that fatty acid oxidation is a critical and fundamental metabolic endpoint in humans (26) and rodents (27, 28), it is not clear how adipocyte fatty acid oxidation affects whole-body metabolism in an autonomous manner. Therefore, we generated a conditional loss-of-function allele for CPT2, an obligate step in mitochondrial long-chain fatty acid β-oxidation that is encoded by a single gene. Here we show that adipose tissue fatty acid oxidation is required not only for acute cold adaptation but also for the induction of thermogenic genes in BAT. The loss of adipose fatty acid oxidation altered adiposity in a diet-dependent manner but did not lead to diet-induced

changes in body weight. Furthermore, we show that in WAT, the loss of fatty acid oxidation reduces high-fat-induced oxidative stress and inflammation but does not alter the progression of obesity or glucose intolerance.

Experimental Procedures

Animals and Diets

$CPT2^{lox/lox}$ mice were generated by targeting loxP sequences to introns flanking exon 4 of the mouse Cpt2 gene by homologous recombination in C57Bl/6 embryonic stem cells by standard methods. To produce mice with a loss of CPT2 specifically in adipocytes, we bred $CPT2^{lox/lox}$ mice to adiponectin-Cre transgenic mice (69). $CPT2^{A-/-}$ and littermate $CPT2^{lox/lox}$ mice were housed in a facility with ventilated racks on a 14 hr light/10 hr dark cycle with access to a standard chow diet (Etruded Global Rodent Diet, Harlan Laboratories). For the diet study, mice were fed a 10% low fat (D12450J, Research Diets) or a 60% high fat diet (D12492, Research Diets) from 6 weeks to 18 weeks of age (12 weeks on diet). At week 10 of the diet, mice were subjected to a glucose tolerance test by intraperitoneal injection of glucose (0.75 g/kg) and measuring tail blood glucose at 0, 15, 30, 60, and 120 min. At week 11 of the diet, insulin tolerance tests were performed via intraperitoneal injection of insulin (0.6 U/kg) and measuring tail blood glucose at 0, 15, 30, 60, and 90 min (Nova Max Plus). Body weights were measured on a weekly basis. For thermogenesis experiments, 12-week-old mice had food withdrawn for 4 hr and placed in a 4°C environment for 3 hr. Body temperature was measured hourly by a rectal probe thermometer (BAT-12, Physitemp). BAT, iWAT, gWAT, liver, and muscle were collected and frozen in liquid nitrogen. Serum was collected from all mice, and free glycerol and TAG (Sigma), b-hydroxybutyrate (StanBio), total cholesterol (Wako), and

NEFA (Wako) were measured colorimetrically. BAT collected from thermogenesis experiments was homogenized in Media I (10mMTris [pH 8.0], 1mMEDTA, and 0.25M sucrose) to measure TAG (Sigma). For in vivo studies, 20-week-old $CPT2^{A-/-}$ and littermate $CPT2^{lox/lox}$ mice were injected with CL-316243 (10 mg/kg, Santa Cruz) or vehicle. To determine the protein expression of phospho-CREB, CREB, phospho-mTOR and mTOR, CL-316243 (10 mg/kg) or vehicle was injected to 20-week old mice and tissues were collected after 30min. For cold acclimation, 12–14 week old $CPT2^{A-/-}$ and littermate $CPT2^{lox/lox}$ mice were housed in an animal incubator at 18°C on a 12 hr light/12 hr dark cycle with access to a standard chow diet for one week. The incubator was lowered to 15°C the following week. Then mice had food withdrawn for 4 hr and placed in a 4°C environment for 4 hr. For thermoneutral adaptation, 12-week-old $CPT2^{A-/-}$ and littermate $CPT2^{lox/lox}$ mice were housed in an animal incubator at 30°C on a 12 hr light/12 hr dark cycle with access to a standard chow diet for 2 weeks. At 14 weeks of age, the mice were injected with either CL-316243 (10 mg/kg) or vehicle for 3 hr. All procedures were performed in accordance with the NIH's Guide for the Care and Use of Laboratory Animals and under the approval of the Johns Hopkins Medical School Animal Care and Use Committee.

Body Composition and Metabolic Analysis

Body fat and lean mass were determined by magnetic resonance imaging (minispec MQ10) in 18-week-old mice. To measure whole-animal energy utilization, 12-week-old male $CPT2^{A-/-}$ and $CPT2^{lox/lox}$ littermates that were fed a standard chow diet were individually housed in Comprehensive Laboratory Animal Monitoring System (Columbus Instruments) cages on a 12 hr light/12 hr dark cycle. O_2 and CO_2 consumption

and production, respectively, food and water intake, and home-cage activity were measured continuously. After a 2-day acclimation period, data were collected for 48 hr for ad libitum and a 24 hr fasting period. At the end of the study, the same mice were injected with CL-316243 (10 mg/kg) and were monitored for 3 hr.

In Vivo Acetate Incorporation Experiment

Six-week-old $CPT2^{A-/-}$ and $CPT2^{lox/lox}$ littermates were fed a 10% low-fat diet for 2 weeks. At 8 weeks of age, mice were injected with 10 mCi of [^{3}H] acetate for 3 hr. BAT, gWAT, and liver were collected, and lipid was extracted using the Folch method. Aliquots of the samples were counted for [^{3}H] labeled lipids. All samples were counted using the Beckman Coulter scintillation counter (LS 6000SC, Beckman Coulter).

Cell Culture

$CPT2^{lox/lox}$ primary MEFs were derived from embryos and cultured in Dulbecco's modified Eagle's medium (DMEM) supplemented with 10% fetal bovine serum (FBS) and 1% penicillin/streptomycin. To generate CPT2lox/lox and CPT2KO MEFs, cells were first transduced with large T antigen-expressing lentiviral particles (LVP016-Neo, GenTarget) for 48 hr and G418 (300 mg/mL) was added to select for positive cells. The selected cells were then transduced with red fluorescent protein (LVP023, GenTarget) or CRE-2A-RFP (LVP013, GenTarget) lentiviral particles and selected with blasticidin (10 mg/mL) to generate $CPT2^{lox/lox}$ and CPT2KO MEFs, respectively. MEFs were plated in T25 flasks at 70% confluency and incubated in DMEM supplemented with 10% FBS and 1% penicillin/streptomycin overnight. The cells were washed with PBS and the reaction mixture for [U-^{14}C] glucose (DMEM [A14430-01], 2 mM glutamine, 2.5 mM glucose, 0.5 mM sodium pyruvate, 0.1 mCi of [U-^{14}C] glucose) or [2-^{14}C] pyruvate (DMEM

[A14430-01], 2mM glutamine, 2.5 mM glucose, 0.5 mM sodium pyruvate, 0.1 mCi of [2-^{14}C] pyruvate) was added to cells. The flasks were sealed with a rubber stopper containing a hanging well filled with filter paper and incubated in a 37°C incubator for 4 hr. Carbon dioxide was trapped by adding 150 ml of 1 M NaOH to the filter paper in the center well and 200 ml of 1 M perchloric acid to the reaction mixture. Then the samples were incubated at 55°C for 1 hr and the filter paper was placed in scintillation fluid and counted. For [1-^{14}C] oleate oxidation, the reaction mixture (DMEM supplemented with 0.1 mCi of [1-^{14}C] oleate, 100 mM L-carnitine hydrochloride [Sigma], and 0.2% BSA) or the reaction mixture containing 100 mM etomoxir was added to cells and incubated in a 37_C incubator for 4 hr. Carbon dioxide was collected and counted as described above. For [1-14C] lignoceric acid oxidation, the reaction mixture (DMEM supplemented with 0.1 mCi of [1-14C] lignocerate and 0.2% BSA) was added to cells and incubated overnight in a 37°C incubator. Carbon dioxide was collected and counted as described above. For substrate flux into lipids, MEFs were plated in 24-well plates and incubated in DMEM supplemented with 10% FBS and 1% penicillin/streptomycin overnight and washed with PBS the next day. The cells were incubated in [2-^{14}C] pyruvate (DMEM [A14430-01], 2 mM glutamine, 2.5 mM glucose, 0.5 mM sodium pyruvate, 0.1 mCi of [2-^{14}C] pyruvate) or [^{3}H] acetate (DMEM supplemented with 0.3 mCi [^{3}H] acetate) reaction mixture and incubated at 37°C for 4 hr. Lipid was extracted using the Folch method, and aliquots of the samples were counted for [^{3}H]-labeled lipids.

Adipose Tissue Oxidation Experiments

BAT, iWAT, and gWAT were collected from 20-week-old CPT2$^{A-/-}$ and littermate CPT2$^{lox/lox}$ male mice and placed in an incubation chamber containing the reaction

mixture (DMEM supplemented with 0.1 mCi of [1-^{14}C] oleate, 100 mM L-carnitine (Sigma), and 0.2% BSA). The chamber contained a center well filled with filter paper and sealed with a rubber stopper. The incubation chambers were in a 37°C shaking water bath for 4 hr. Trapping carbon dioxide was collected as described above. In vivo fatty acid oxidation was carried out as previously described (*70, 71*).

BAT Explant Experiments

BAT was collected from 20-week-old mice. Each BAT nugget was cut in half and placed in media (DMEM, 10% FBS, 200 mM total of palmitate and oleate at a 1:2 molar ratio, BSA at a 1:3 molar ratio with total fatty acids). Forskolin (10 mM, Sigma), isoproterenol (10 mM, Sigma), or CL-316243 (10 mM, Santa Cruz) was added to tubes and incubated in a 37°C water bath for 3 hr. The tissues were frozen in liquid nitrogen for further analysis.

Analysis of Gene Expression and Mitochondrial DNA by Quantitative PCR

Total RNA was isolated using the RNeasy Mini Kit (QIAGEN). A total of 1–2 mg of RNA was reverse transcribed using the High Capacity cDNA Reverse Transcription Kit (Applied Biosciences). The cDNA was diluted to 2 ng/mL and was amplified by specific primers in a 20 ml reaction using SsoAdvanced SYBR Green Supermix (Bio-Rad). WAT cDNA from CPT2$^{A-/-}$ and littermate CPT2$^{lox/lox}$ mice on a high-fat diet was prepared according to the manufacturer's protocol for the mouse oxidative stress PCR array (SA Biosciences). Analysis of gene expression was carried out in a CFX Connect Real-Time System (Bio-Rad). For each gene, mRNA expression was calculated as 2^deltaCT relative to cyclophilin A expression. For mitochondrial DNA analysis, total DNA was prepared using the QIAmp DNA mini Kit (QIAGEN). Mitochondrial DNA was amplified

using primers Co1 and Nd1 and was normalized to genomic DNA by primers amplifying H19 from genomic DNA as previously described (*72*).

Western Blot Analysis

BAT collected after acute CL-316243 or vehicle injection was homogenized in RIPA buffer with protease inhibitors (Complete Mini, Roche) and phosphatase inhibitors (PhosSTOP, Roche). All other tissues from the diet study were homogenized in 13 RIPA buffer with protease inhibitors (Complete Mini, Roche). BAT, gWAT, iWAT, and liver samples from thermogenesis experiments were homogenized in Media I with protease inhibitors. All samples were spun down at 10,000 rpm for 20 min, and supernatant was collected and assayed by the Pierce BCA Protein Assay Kit (Thermo Scientific) to determine the concentration of protein. A total of 30 mg of protein was subjected to SDS-PAGE and transferred to a nitrocellulose membrane (Protran BA 83, Whatman). The blots were probed with the following antibodies: Uqcrc2 (mitoprofile Total OXPHOS, Abcam), Sdhb (mitoprofile Total OXPHOS, Abcam), Acsf3 (Pierce), phospho-CREB (Ser-133, Millipore), CREB (Pierce), phospho-mTOR (Cell Signaling), and mTOR (Cell Signaling) using the appropriate secondary antibodies conjugated to horseradish peroxidase. Fasn (BD Biosciences), Aco2 (Cell Signaling), Mcad (GeneTex), Hsc70 (Santa Cruz), Sod2, and Hadha (GeneTex) used the appropriate Cy5 (Life Technologies) or Cy3 (Life Technologies) fluorescent secondary antibodies.

Oxidative Damage

Thiobarbituric acid reactive substances (TBARS) were determined in gWAT, and serum from 20-week-old male $CPT2^{A-/-}$ and littermate $CPT2^{lox/lox}$ mice fed a high- or low-fat diet. WAT was prepared by homogenizing 100 mg of tissue in 500 ml of 13 RIPA buffer

with protease inhibitors (Complete Mini, Roche). Homogenates were centrifuged at 1,600 3 g for 10 min, and 25 ml of supernatant was used to determine oxidative damage via the TBARS Assay Kit (Cayman Chemical Company).

Acylcarnitine Analysis

iWAT from $CPT2^{A-/-}$ and littermate $CPT2^{lox/lox}$ mice were collected and frozen in liquid nitrogen. Approximately 100 mg of tissue was analyzed for acylcarnitine content at the University of Michigan Metabolomics Core Services.

Statistical Analysis

When only two genotypes were analyzed, statistical significance was determined using a student's t test. Two-way ANOVA was utilized for repeated measures such as body temperature over time, weight gain over time, GTT, and insulin tolerance test. Significance was determined for p values < 0.05.

Results

Generation of Mice with an Adipose Tissue-Specific Deletion of CPT2

Mitochondrial long-chain fatty acid oxidation requires sequential carnitine acyltransferases to translocate acyl-CoAs into the mitochondrial matrix. The regulated and rate setting enzyme, CPT1, is encoded by multiple isoenzymes that can functionally compensate in some tissues (*73*). Therefore, to generate a mouse model to assess the tissue-specific roles and requirements of fatty acid oxidation, we generated a conditional loss-of-function allele for CPT2, an enzyme required in mitochondrial long-chain fatty acid b-oxidation that is encoded by a single gene. C57BL/6 embryonic stem cells were used to target loxP recombination sites

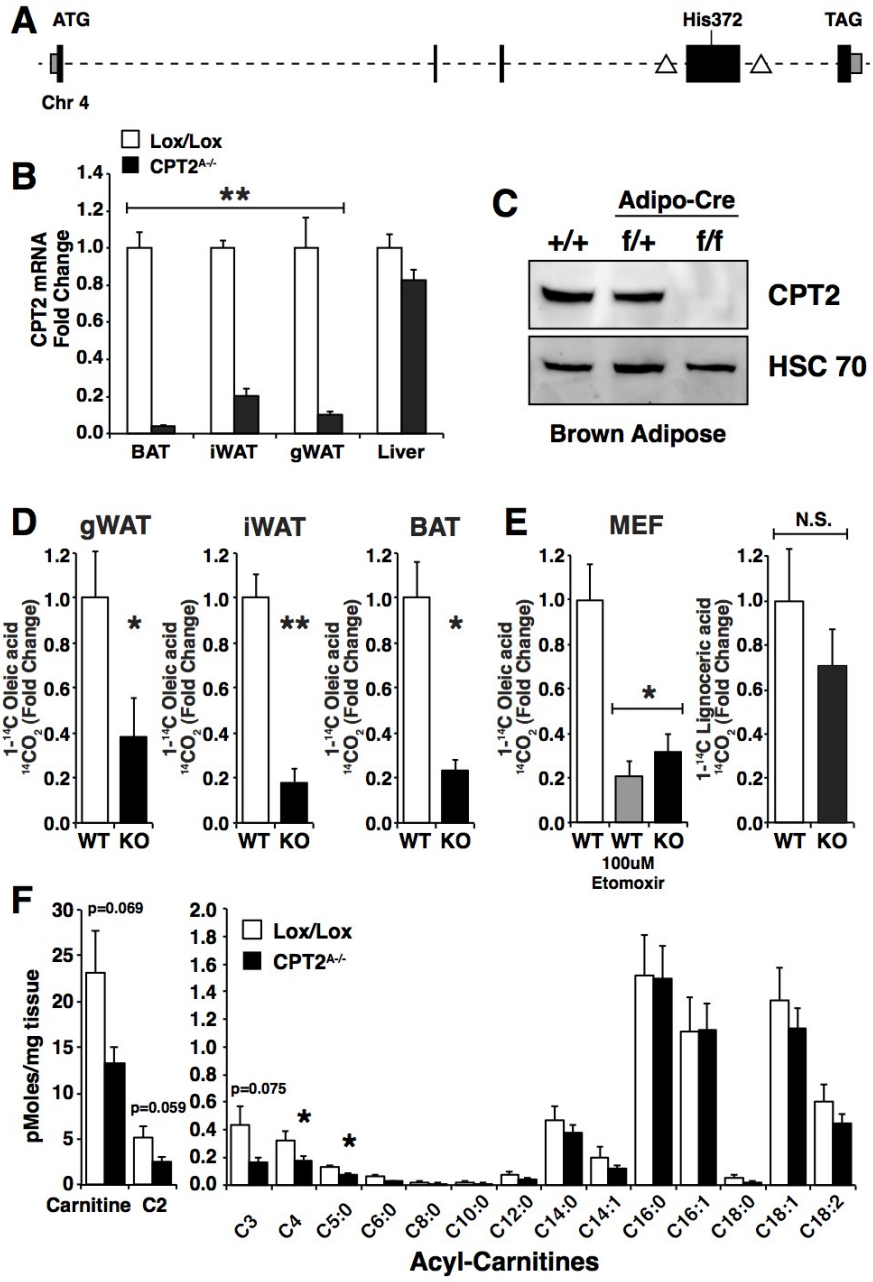

Figure 2-1. Generation of mice with an adipose-specific KO of CPT2.

(A) Gene targeting strategy for the *Cpt2* gene (Triangles represent lox sites).
(B) mRNA for *Cpt2* in adipose depots and liver of control and $Cpt2^{A-/-}$ mice (n=8).
(C) Western blot of CPT2 in BAT of control and $Cpt2^{A-/+}$ and $Cpt2^{A-/-}$ mice.
(D) Oxidation of 1-^{14}C-oleic acid to $^{14}CO_2$ in control and $Cpt2^{A-/-}$ adipose depot explants (n=3).
(E) Oxidation of 1-^{14}C-oleic acid or 1-^{14}C-lignoceric acid to $^{14}CO_2$ in control and *Cpt2* KO MEFs (n=3).
(F) Acylcarnitine profile of iWAT in control and $Cpt2^{A-/-}$ mice (n=8).

Data are expressed as mean ± SEM. *p<0.05; **p<0.01; N.S., not significant. White bars represent control and black bars represent loss of *Cpt2*.

surrounding exon 4 of the Cpt2 gene (**Figure 2-1A**). Exon 4 encompasses approximately one-third of the protein coding sequence including all of the critical catalytic residues (*74*). Loss of exon 4 is predicted to additionally cause a frameshift in the remaining exons. To produce mice with a loss of CPT2 specifically in adipocytes, we bred $CPT2^{lox/lox}$ mice to adipocyte specific adiponectin-Cre transgenic mice (*69*). The resulting adipose-specific CPT2 knockout (KO) mice, $CPT2^{A-/-}$, have a loss of Cpt2 mRNA in all adipose depots examined (**Figure 2-1B**). Furthermore, CPT2 protein is substantially reduced in BAT of $CPT2^{A-/-}$ mice (**Figure 2-1C**). As expected, ex vivo gonadal WAT (gWAT), inguinal WAT (iWAT), and BAT explants derived from $CPT2^{A-/-}$ mice had a greatly suppressed ability to oxidize radiolabeled 1-^{14}C-oleic acid (**Figure 2-1D**). Long chain mitochondrial fatty acid β-oxidation cannot proceed in the absence of CPT2. The remaining oxidation of oleic acid in tissues was presumably due to either peroxisomal fatty acid oxidation or oxidation in nonparenchymal cells within the adipose depots. To test this directly, we derived and immortalized mouse embryonic fibroblasts (MEFs) from $CPT2^{lox/lox}$ embryos and infected them with a control or Cre recombinase expressing virus. The oxidation of 1-^{14}C-oleic acid in $CPT2^{lox/lox}$ MEFs was severely blunted by incubating cells with a large dose (100 mM) of the mitochondrial fatty acid oxidation inhibitor etomoxir. The genetic loss of CPT2 in MEFs suppressed oleic acid oxidation to the same degree as etomoxir (**Figure 1E**). However, the oxidation of the very long chain lignoceric acid (C24:0), which is oxidized mainly in peroxisomes, was not significantly changed (**Figure 2-1E**). Therefore, the deletion of CPT2 represents an effective strategy for inhibiting long chain mitochondrial fatty acid β-oxidation. To determine how the loss of CPT2 alters white adipose fatty acid oxidative metabolites, we measured the steady-

state concentration of carnitine and acyl-carnitine species in iWAT of control and CPT2$^{A-/-}$ mice. Although CPT2 deficiency results in the inability to utilize long chain acyl-carnitines and people with CPT2 mutations are diagnosed by the elevation of these metabolites in serum, CPT2$^{A-/-}$ mice did not have increased long chain acyl-carnitine species in iWAT. Instead, CPT2$^{A-/-}$ iWAT had a strong trend toward suppressed free carnitine and acetyl-carnitine and statistically significant reductions in several short chain acyl-carnitines (**Figure 2-1F**). We conclude that long chain acylcarnitines do not build up in WAT but are readily transported out of the adipocyte resulting in a tissue specific carnitine deficiency due to the inability to properly recycle carnitine in CPT2$^{A-/-}$ WAT. In summary, we have generated mice with an adipose-specific defect in mitochondrial long-chain fatty acid oxidation that is mediated by the loss of an obligate noncompensatory step in fatty acid oxidation.

Adipose Fatty Acid Oxidation Is Required for Cold-Induced Thermogenesis

BAT is essential for heat generation during an acute cold exposure in perinatal and adult mammals (*1, 25, 33*). The requirement of fatty acid oxidation during cold thermogenesis is made evident by cold-intolerant phenotypes of whole-body KO mouse models of the acyl-CoA dehydrogenase enzymes (*11, 37, 38*). To determine the autonomous requirement of adipose fatty acid oxidation during adaptive thermogenesis, we placed 12-week-old control and CPT2$^{A-/-}$ female mice at 4_C and measured their body temperature over 3 hr. Although all of the mice visibly shivered, cold intolerance was evident in CPT2$^{A-/-}$ mice, reaching critical hypothermia (30°C) within 3 hr (**Figure 2-2A**). The body weights of 12-week-old female CPT2$^{A-/-}$ mice were not different (**Figure**

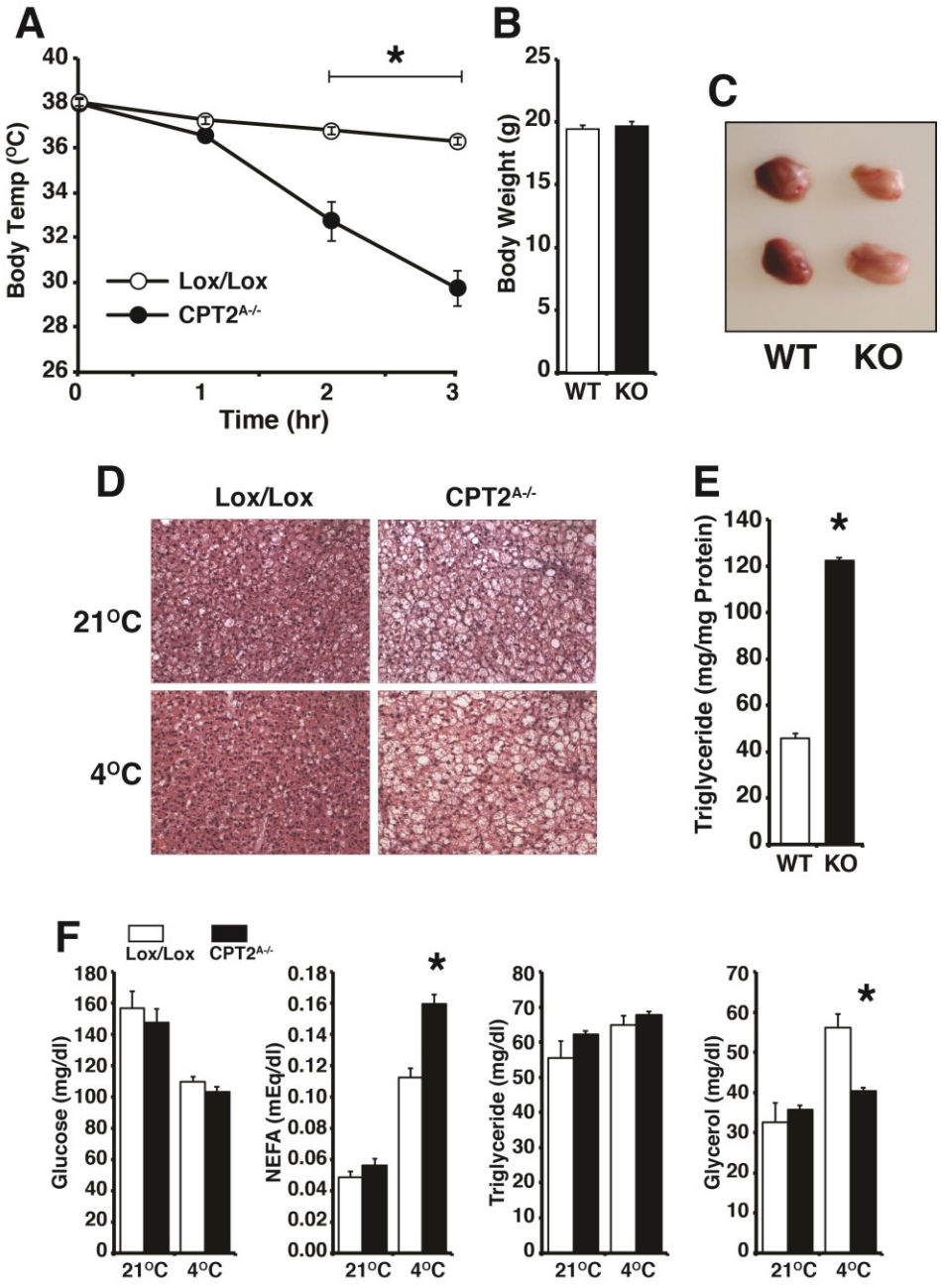

Figure 2-2. Adipose fatty acid oxidation is required for acute cold-induced thermogenesis.

(A) Body temperature of control and Cpt2$^{A-/-}$ mice subjected to a 3hr cold challenge (n=10-13).

(B) Body weights of 12-week-old female control and Cpt2$^{A-/-}$ mice (n=22-26).

(C) Gross morphology of control and Cpt2$^{A-/-}$ mouse BAT after a 2hr cold exposure.

(D) Hematoxylin and eosin (H&E)-stained sections of BAT from control and Cpt2$^{A-/-}$ mice at 21°C and 3hr at 4°C (Scale bar is 100μM).

(E) Triglyceride content of BAT of control and Cpt2$^{A-/-}$ mice after a 3hr cold exposure (n=5).

(F) Serum metabolites of control and Cpt2$^{A-/-}$ mice at 21°C and 3hr at 4°C (n=8).

Data are expressed as mean ± SEM. *p<0.05; **p<0.01; N.S., not significant. White bars represent control and black bars represent loss of *Cpt2*.

2-2B). Upon dissection, CPT2$^{A-/-}$ interscapular BAT was visibly lipid laden, displaying a milky appearance in contrast to the dark brown color of control BAT (**Figure 2-2C**). Histologic evaluation demonstrated increased lipid droplet accumulation that did not dissipate upon cold stimulation (**Figure 2-2D**). Consistent with these morphologic changes, cold-exposed CPT2$^{A-/-}$ BAT maintained ~3-fold increase in triglyceride content compared to BAT from control mice (**Figure 2-2E**). Evaluation of serum metabolites showed normal responses of serum glucose, ketone bodies, and triglycerides to cold stimulation in CPT2$^{A-/-}$ mice. However, compared to controls, CPT2$^{A-/-}$ mice had increased serum free fatty acids and decreased glycerol during cold stimulation, likely due to their inability to utilize the mobilized fatty acids in CPT2 null BAT (**Figure 2-2F**). These data show that adipose fatty acid oxidation is required for acute cold-induced thermogenesis.

BAT Fatty Acid Oxidation Is Required for Agonist-Induced Thermogenic Gene Expression

To understand the transcriptional control of BAT metabolism in CPT2$^{A-/-}$ mice, we determined the expression of fatty acid catabolic and anabolic genes. After a 3 hr cold stimulation, the fatty acid oxidative genes *Acox1, Cpt1b*, and *Lcad* were suppressed in CPT2$^{A-/-}$ BAT (**Figure 2-3A**). Malonyl-CoA decarboxylase (Mlycd), which decarboxylates malonyl-CoA and therefore disinhibits CPT1, was greatly suppressed in both basal and cold stimulated CPT2$^{A-/-}$ BAT. Additionally, fatty acid biosynthetic genes *Pcx, Acaca*, and *Elovl6* were suppressed after a 3 hr cold stimulation in CPT2$^{A-/-}$ BAT compared to controls (**Figure 2-4A**). These data suggest that the loss of fatty acid oxidation in BAT feeds back to inhibit genes in fatty acid oxidation. To better understand

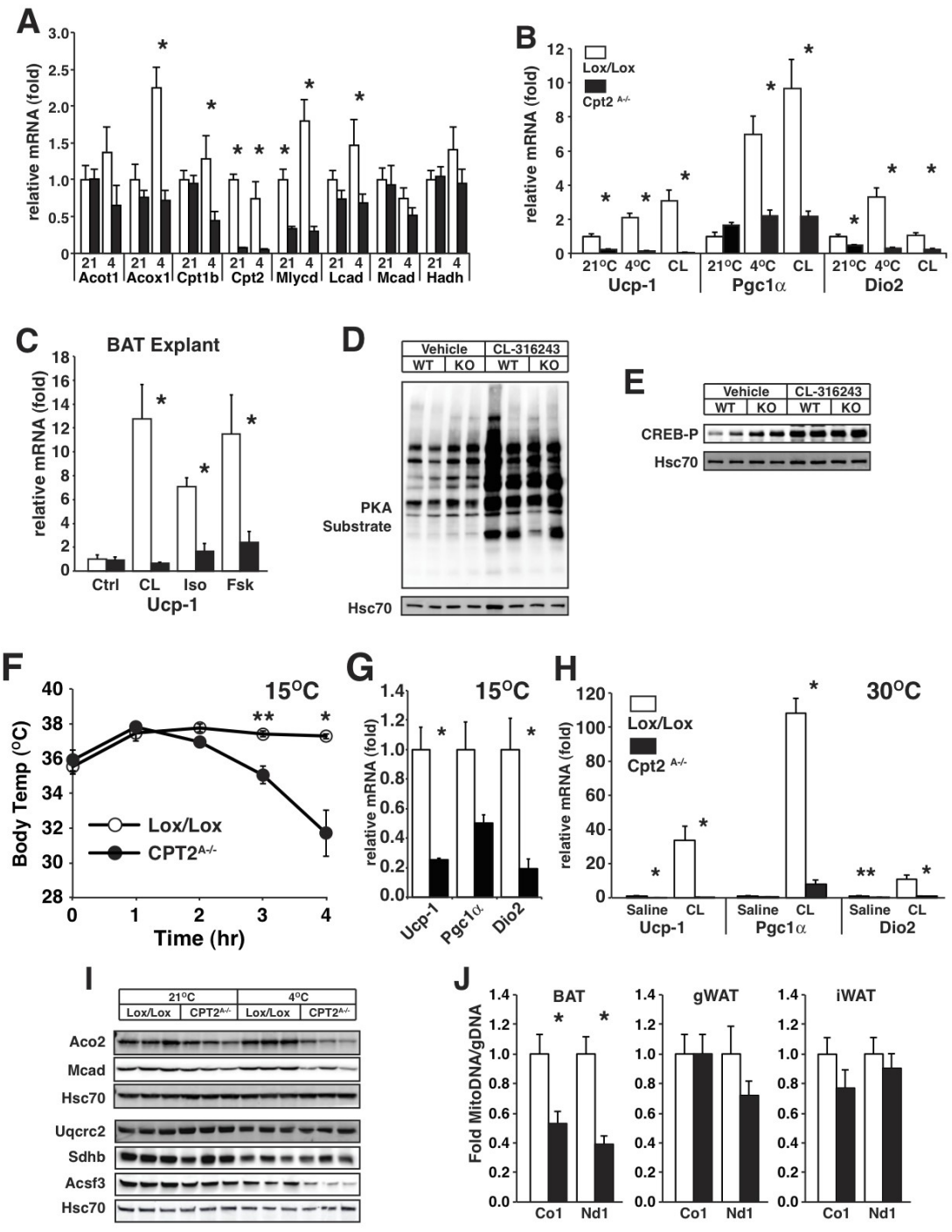
A
relative mRNA (fold)
21 4
Acot1
Acox1
Cpt1b
Cpt2
Mlycd
Lcad
Mcad
Hadh
B
Lox/Lox
Cpt2 A-/-
relative mRNA (fold)
21°C 4°C CL
Ucp-1
Pgc1α
Dio2
C
BAT Explant
relative mRNA (fold)
Ctrl CL Iso Fsk
Ucp-1
D
Vehicle
CL-316243
WT KO WT KO
PKA Substrate
Hsc70
E
Vehicle
CL-316243
WT KO WT KO
CREB-P
Hsc70
F
15°C
Body Temp (°C)
Lox/Lox
CPT2A-/-
Time (hr)
G
15°C
relative mRNA (fold)
Ucp-1
Pgc1α
Dio2
H
30°C
Lox/Lox
Cpt2 A-/-
relative mRNA (fold)
Saline CL
Ucp-1
Pgc1α
Dio2
I
21°C
4°C
Lox/Lox
CPT2A-/-
Aco2
Mcad
Hsc70
Uqcrc2
Sdhb
Acsf3
Hsc70
J
BAT
gWAT
iWAT
Fold MitoDNA/gDNA
Co1 Nd1

Figure 2-3. Adipose fatty acid oxidation is required for agonist-induced thermogenic gene expression and mitochondrial homeostasis.

(A) mRNA expression of fatty acid oxidative genes in BAT of control and $Cpt2^{A-/-}$ mice at 21°C or after 3hr at 4°C.

(B) mRNA expression of *Ucp1, Pgc1α* and *Dio2* in BAT of control and $Cpt2^{A-/-}$ mice at 21°C (n=8), after 3hr at 4°C (n=8) or 3hr after injection with 10mg/kg CL-316243 (n=5).

(C) mRNA expression of *Ucp1* in BAT explants treated with 10μM CL-316243, isoproterenol or forskolin (n=5).

(D) Western blot for PKA phosphorylated substrates in BAT of control and $Cpt2^{A-/-}$ mice treated with 10mg/kg CL-316243 for 30min *in vivo*.

(E) Western blot for phosphorylated-CREB (Ser-133) in BAT of control and $Cpt2^{A-/-}$ mice treated with 10mg/kg CL-316243 for 30min *in vivo*.

(F) Body temperature of control and $Cpt2^{A-/-}$ mice acclimatized to 15°C and subjected to a 4hr cold challenge (n=5).

(G) mRNA expression of *Ucp1, Pgc1α* and *Dio2* in BAT of 15°C acclimatized control and $Cpt2^{A-/-}$ mice after a 4hr cold challenge (n=5).

(H) mRNA expression of *Ucp1, Pgc1α* and *Dio2* in BAT of control and $Cpt2^{A-/-}$ mice acclimatized to 30°C and injected with vehicle or 10mg/kg CL-316243 for 3hr (n=4-5).

(I) Western blot of mitochondrial proteins in BAT of control and $Cpt2^{A-/-}$ mice at 21°C or after 3hr at 4°C.

(J) Mitochondrial DNA content of BAT and gWAT from control and $Cpt2^{A-/-}$ mice (n=10-12).

Data are expressed as mean ± SEM. *$p<0.01$; **$p<0.05$. White bars represent control and black bars represent loss of *Cpt2*.

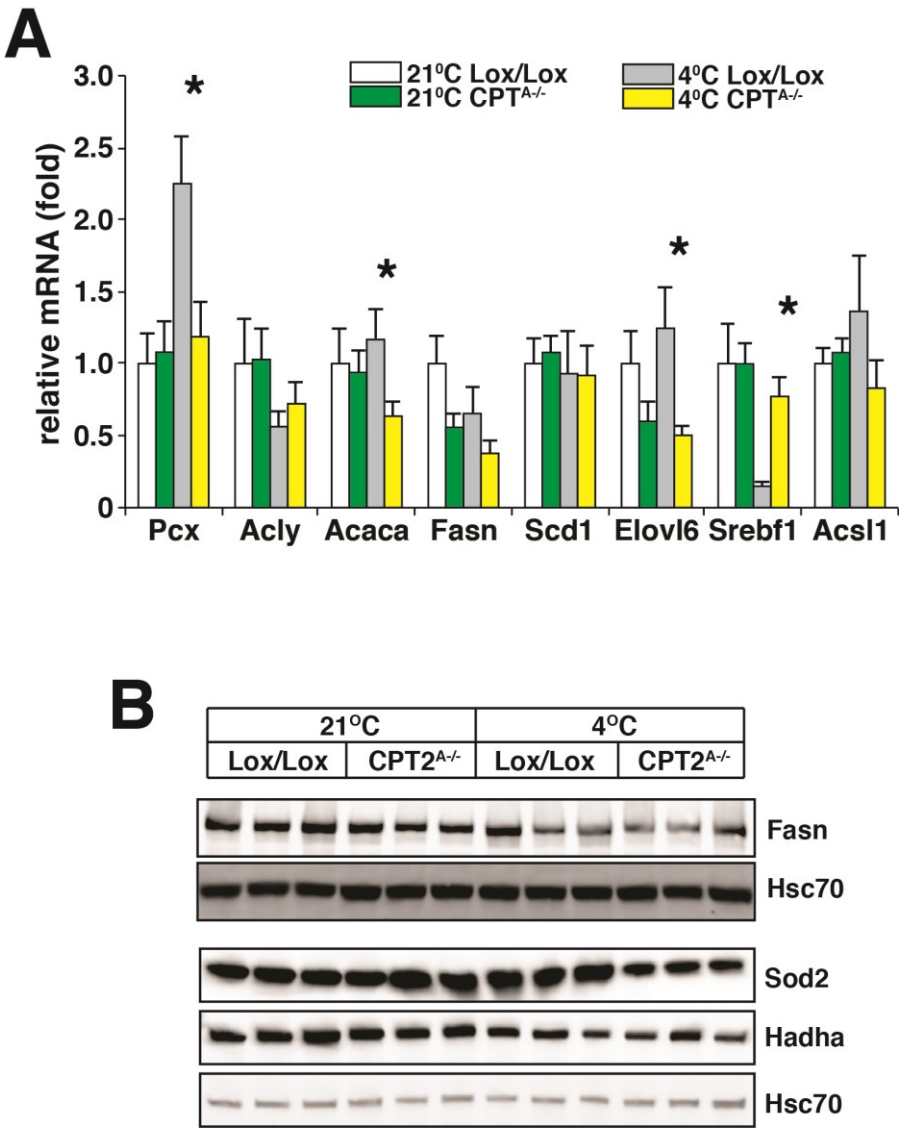

Figure 2-4. Expression of fatty acid metabolic genes in BAT of control and Cpt2$^{A-/-}$ mice.

(A) mRNA expression of fatty acid biosynthetic genes from BAT of control and Cpt2$^{A-/-}$ mice housed at 21°C or after 3hr at 4°C (n=8). Data are expressed as mean ± SEM. *p,0.05.

(B) Western blot of mitochondrial proteins in BAT of control and Cpt2$^{A-/-}$ mice at 21°C or after 3hr at 4°C.

the role of fatty acid oxidation on thermogenic programing in BAT, we measured the transcriptional response of BAT to cold stimulation. The canonical cold-induced genes *Ucp1, Pgc1a*, and *Dio2* were induced robustly in BAT of control mice after 3 hr at 4°C but were unresponsive in $CPT2^{A-/-}$ BAT (**Figure 2-3B**). In fact, *Ucp1* and *Dio2* were suppressed constitutively even at room temperature. *Ucp1* and *Pgc1a* are thermogenic genes regulated by adrenergic signaling upon cold exposure. Therefore, we determined if $CPT2^{A-/-}$ BAT was responsive to adrenergic stimulation by injecting $CPT2^{A-/-}$ and control mice with the selective β3-adrenergic agonist CL-316243 (10 mg/kg) and collected BAT 3 hr later. Unlike the control, $CPT2^{A-/-}$ BAT elicited no increase in the mRNA abundance of *Ucp1* or *Pgc1a* (**Figure 2-3B**). This suggests a strong defect in $CPT2^{A-/-}$ BAT thermogenic gene expression.

To determine where in the adrenergic signaling pathway $CPT2^{A-/-}$ BAT was impaired, we collected control and $CPT2^{A-/-}$ BAT explants and stimulated them ex vivo with 10mM CL-316243, the β-adrenergic agonist isoproterenol, or the adenylyl cyclase activator forskolin, in the presence of 200mM fatty acids (2:1 oleate: palmitate). All of these activators robustly induced Ucp1 in control explants; however, $CPT2^{A-/-}$ BAT was unable to induce Ucp1 (**Figure 2-3C**). These data suggest that the defect in cold-induced thermogenic gene expression is mediated downstream of the adrenergic receptor.

To determine if $CPT2^{A-/-}$ BAT was activating signaling downstream of adrenergic stimulation, we probed for protein kinase A (PKA) targets of adrenergic signaling after a 30 min stimulation with 10 mg/kg CL-316243 in vivo. Utilizing a PKA phosphorylated substrate specific antibody, both control and $CPT2^{A-/-}$ BAT showed robust CL-316243 mediated phosphorylation (**Figure 2-3D**). Additionally, cAMP response element-binding

protein (CREB) phosphorylation, the canonical transcription factor downstream of adrenergic stimulation, elicited a robust phosphorylation in both control and CPT2$^{A-/-}$ BAT (**Figure 2-3E**). These data show that CPT2$^{A-/-}$ BAT can activate adrenergic signaling and phosphorylation of downstream targets such as CREB. This suggests the defect in agonist-induced thermogenic gene expression is likely at the level of transcriptional regulation. Taken together, these experiments show that CPT2$^{A-/-}$ BAT is resistant to agonist-induced thermogenic gene expression and further suggest that fatty acid oxidation in BAT is coupled to agonist-induced transcription.

CPT2$^{A-/-}$ Mice Are Defective in Environmental Temperature Adaptation

Mammals can dramatically alter their physiology to adapt to the ambient temperature. Cold acclimation of UCP1KO mice is sufficient to rescue their acute cold intolerance (*75, 76*). To test the role of adipose fatty acid oxidation on this adaptation, we cold acclimatized CPT2$^{A-/-}$ mice to 15°C and then subjected them to an acute 4°C cold challenge. At 15°C, CPT2$^{A-/-}$ and control mice had lower body temperatures (~35.5°C) that upon cold challenge initially rose rapidly. However, CPT2$^{A-/-}$ mice could not maintain body temperature and after 4 hr reached critical hypothermia (**Figure 2-3F**). Again, *Ucp1* and *Dio2* mRNA abundance was suppressed in CPT2$^{A-/-}$ BAT (**Figure 2-3G**). This suggests that adipose fatty acid oxidation has additional roles other than merely activating UCP1 in BAT. Next, we asked if the inhibition of agonist-induced thermogenic gene expression at 21°C and 15°C was due to tonic activation of thermogenic signaling and therefore constitutively inhibited via negative feedback. To eliminate tonic basal thermogenic signaling, we acclimatized CPT2$^{A-/-}$ and control mice to a thermoneutral environment (30°C). We then injected the mice with 10 mg/kg CL-316243 or vehicle and

collected BAT 3 hr later. Thermoneutral acclimatization did not improve agonist-induced thermogenic gene expression in CPT2$^{A-/-}$ mice. In fact, the difference between control and CPT2$^{A-/-}$ mice was further exacerbated, suggesting that the transcriptional defect is not due to tonic inhibition but is a primary defect (**Figure 2-3H**). These data show that adipose fatty acid oxidation is critical for thermal adaptation.

Loss of Adipose Fatty Acid Oxidation Disrupts Mitochondrial Homeostasis in BAT

The lack of agonist-induced Pgc1a expression, a gene key to mitochondrial biogenesis, prompted us to examine mitochondrial proteins and mitochondrial density in CPT2$^{A-/-}$ BAT. Several mitochondrial proteins were suppressed in CPT2$^{A-/-}$ BAT under basal (21°C) conditions, including ACO2 and MCAD (**Figures 2-3I and 2-4**). These changes were exacerbated after 3 hr of cold stimulation. To determine mitochondrial number, we quantified BAT mitochondrial DNA and found that gWAT and iWAT maintained normal mitochondrial DNA content whereas CPT2$^{A-/-}$ BAT had about a 2-fold suppression in mitochondrial DNA (**Figure 2-3J**). These data show that mitochondrial long-chain fatty acid oxidation in BAT is important not only for cellular bioenergetics but also for nuclear-encoded mitochondrial gene expression, mitochondrial protein abundance, and density.

Bioenergetic Contribution of Adipose Fatty Acid Oxidation

In the absence of cold stimulation, it was not clear what the contribution of adipose fatty acid oxidation is to whole-body energy expenditure under standard physiological conditions or perturbations. To determine the physiological contributions of adipose fatty acid oxidation, we housed control and CPT2$^{A-/-}$ mice individually in

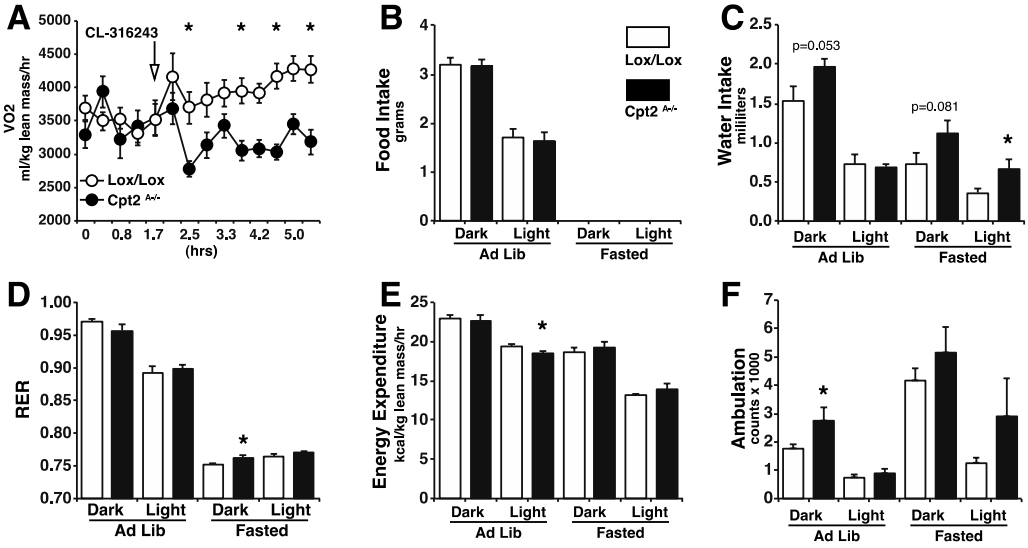

Figure 2-5. Contribution of adipose fatty acid oxidation to energy expenditure.

(A) VO2 consumption of control and Cpt2$^{A-/-}$ mice treated with 10mg/kg CL-316243.

(B) Food intake of control and Cpt2$^{A-/-}$ mice.

(C) Water intake of control and Cpt2$^{A-/-}$ mice under ad libitum and fasting under dark and light cycles.

(D) Respiratory exchange ratio of control and Cpt2$^{A-/-}$ mice under ad libitum and fasting under dark and light cycles.

(E) Energy expenditure of control and Cpt2$^{A-/-}$ mice under ad libitum and fasting under dark and light cycles.

(F) Ambulation rates of control and Cpt2$^{A-/-}$ mice under ad libitum and fasting under dark and light cycles (n=10-14).

Data are expressed as mean ± SEM. *p<0.05. White bars represent control and black bars represent loss of *Cpt2.*

metabolic cages and measured metabolic parameters continuously during ad libitum feeding and fasting conditions. Consistent with a requirement for fatty acid oxidation during cold exposure, an injection of CL-316243 rapidly increased oxygen consumption in control mice but was completely ineffective in altering oxygen consumption in $CPT2^{A-/-}$ mice (**Figure 2-5A**). Unlike other models where changes in fatty oxidation drive changes in feeding behavior (*77*), $CPT2^{A-/-}$ mice had no changes in food intake compared to control mice (**Figure 2-5B**). Interestingly, $CPT2^{A-/-}$ mice consumed more water than controls during the course of the experiment, particularly during fasting (**Figure 2-5C**). This suggests that adipose tissue fatty acid oxidation may play a role in the generation and balance of water, similar to the role of lipid oxidation during hibernation (*78*). There were minor reductions in energy expenditure and increased respiratory exchange ratio in $CPT2^{A-/-}$ mice relative to controls (**Figures 2-5D and 2-5E**). Additionally, there was a modest increase in ambulatory activity in $CPT2^{A-/-}$ mice that may reflect a compensatory requirement of energy expenditure from skeletal muscle (**Figure 2-5F**). These data show that adipose fatty acid oxidation contributes to overall energy expenditure in the absence of cold stimulation, albeit minimally.

Loss of Adipose Fatty Acid Oxidation Results in Diet-Dependent Changes in Adiposity, but Not Body Weight

It has been suggested that mitochondrial dysfunction and suppressed BAT or WAT fatty acid oxidation contributes to changes in body weight and glucose tolerance (*48, 64*). $CPT2^{A-/-}$ BAT is both bioenergetically and transcriptionally unable to support thermogenesis. Additionally, we have shown that the oxidation of fatty acids in adipose tissue is not a major determinant of whole-animal bioenergetics during ad libitum or

fasting conditions. To determine the consequences of a chronic long-term inability to oxidize fatty acids in adipocytes on body weight, we placed control and CPT2$^{A-/-}$ mice on matched low- and high-fat diets for 12 weeks and measured their body weights weekly. CPT2$^{A-/-}$ mice elicited no change in body weight, compared to control littermates, fed either a high-fat or low-fat diet (**Figure 2-6A**). Evaluation of fat and lean content revealed a 64% increase in fat mass in low fat-fed CPT2$^{A-/-}$ mice (**Figures 2-6B and 2-6C**). Measurement of fat pad weights of low-fat-fed CPT2$^{A-/-}$ mice showed 67% increases in both gonadal and inguinal fat pads (**Figure 2-6D**).

High-fat-fed CPT2$^{A-/-}$ mice displayed a suppression of fat mass that was mainly the result of changes in inguinal adiposity (**Figures 2-6C and 2-6D**). These seemingly paradoxical results are actually consistent with other models with dysfunctional adipose fatty acid oxidation or uncoupling (*36, 79*) and likely reflect compensatory increases in energy expenditure in tissues other than adipose. The expression of fatty acid biosynthetic genes was largely unchanged between control and CPT2$^{A-/-}$ gWAT; however, there were increases in fatty acid oxidative genes *Cpt1a* and *Mlycd* in low-fat-fed CPT2$^{A-/-}$ gWAT (**Figure 2-7A**). This suggests distinct regulatory mechanisms in CPT2$^{A-/-}$ BAT and gWAT, since *Cpt1b* and *Mlycd* were decreased in CPT2$^{A-/-}$ BAT. Consistent with increased compensatory energy expenditure, high-fat-fed CPT2$^{A-/-}$ mice displayed about a 2-fold increase in circulating ketones compared to control high-fat-fed mice (**Figure 2-6E**).

Analysis of gene expression in iWAT and liver of control and CPT2$^{A-/-}$ mice shows that under high-fat conditions, many of the changes between the genotypes were concentrated in the iWAT (**Figure 2-7B**). Conversely, liver from control and CPT2$^{A-/-}$

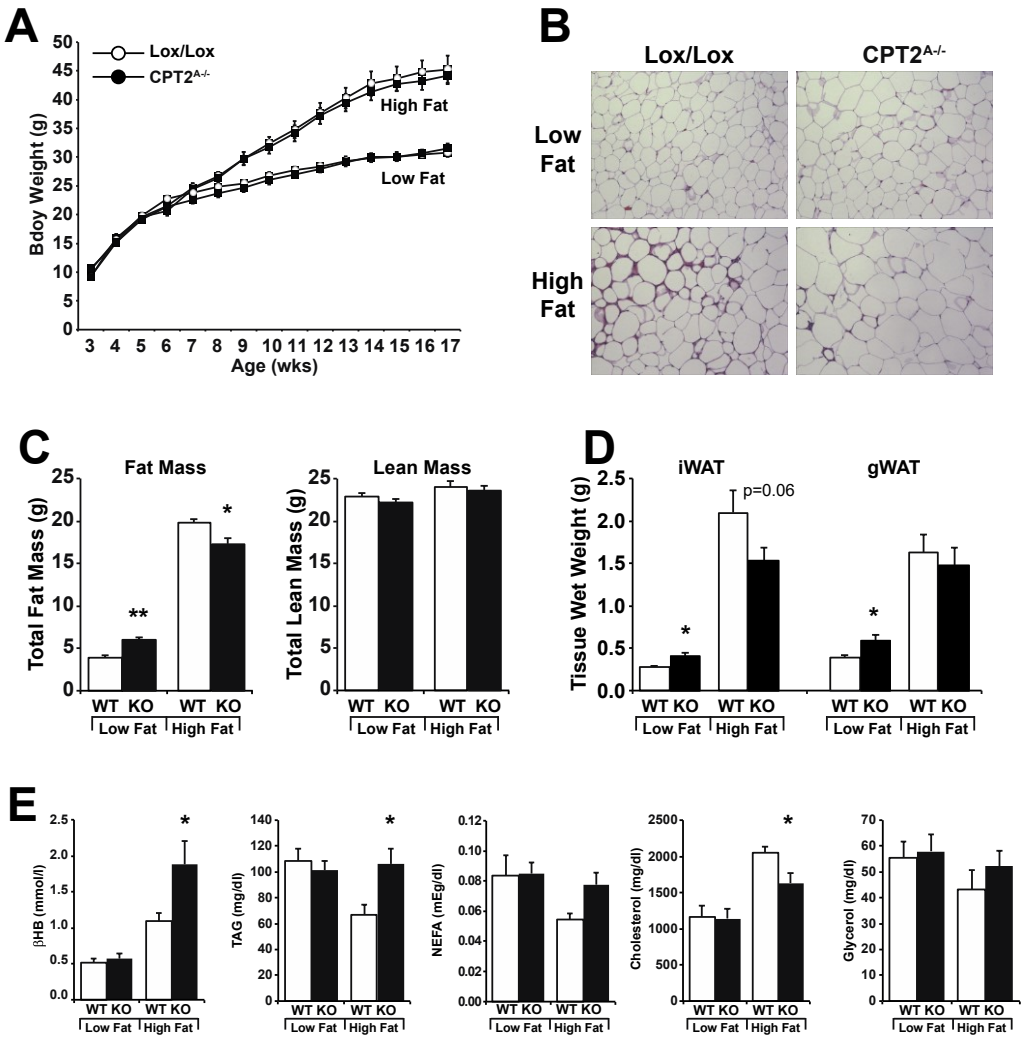

Figure 2-6. The loss of adipose fatty acid oxidation affects diet-dependent adiposity but not body weight.

(A) Body weights of control and Cpt2$^{A-/-}$ mice fed a low- or high-fat diet (n=13-18).

(B) H&E stained sections of gWAT from control and Cpt2$^{A-/-}$ mice fed a low- or high-fat diet (Scale bar is at 250μM).

(C) Body compositions measured by EchoMRI for control and Cpt2$^{A-/-}$ mice fed a low- or high-fat diet (n=13-18).

(D) Wet weights of iWAT and gWAT unilateral depots for control and Cpt2$^{A-/-}$ mice fed a low- or high-fat diet (n=13-18).

(E) Serum metabolites in control and Cpt2$^{A-/-}$ mice fed a low- or high-fat diet (n=8).

Data are expressed as mean ± SEM. **p<0.01; *p<0.05. White bars represent control and black bars represent loss of *Cpt2*.

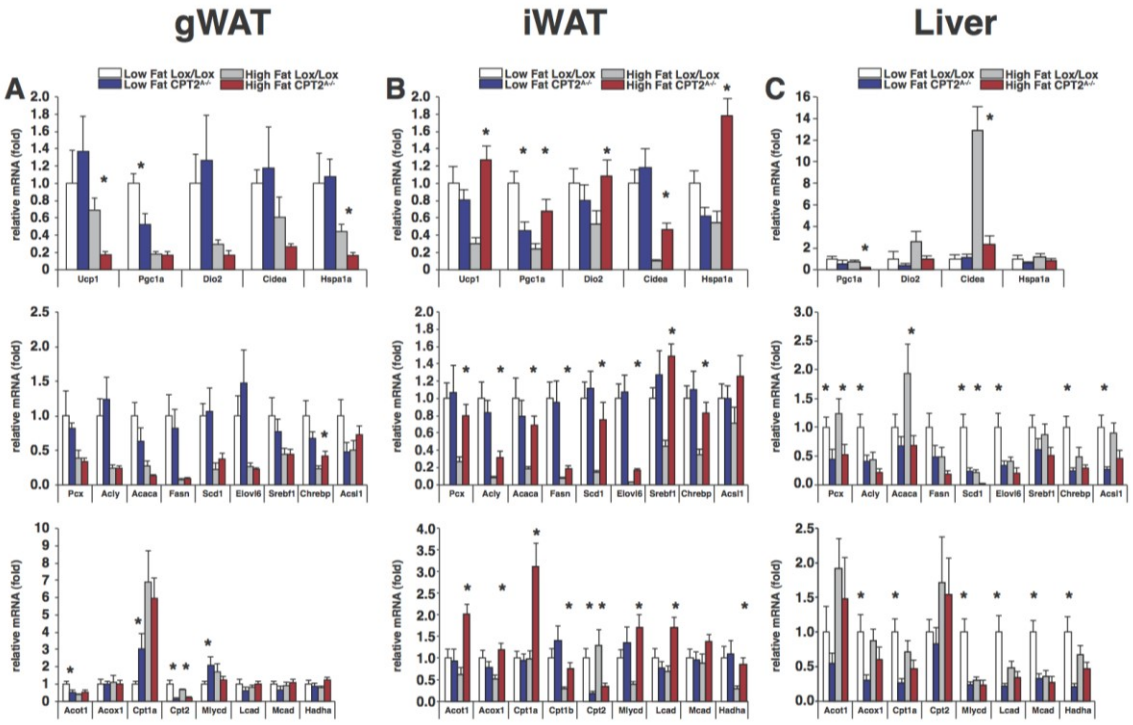

Figure 2-7. Expression of thermogenic and fatty acid metabolic genes in gWAT, iWAT and liver of control and Cpt2$^{A-/-}$ mice fed a low- or high-fat diet.

(A) mRNA expression of metabolic genes from gWAT of control and Cpt2$^{A-/-}$ mice fed a low- or high-fat diet.

(B) mRNA expression of metabolic genes from iWAT of control and Cpt2$^{A-/-}$ mice fed a low- or high-fat diet.

(C) mRNA expression of metabolic genes from liver of control and Cpt2$^{A-/-}$ mice fed a low- or high-fat diet.

Data are expressed as mean ± SEM. *$p<0.05$.

mice showed most differences after low-fat feeding (**Figure 2-7C**). This shows that individual tissues and even different adipose depots respond disparately. These data demonstrate that the loss of adipose fatty acid oxidation does not contribute to changes in total body weight regardless of dietary lipid content, but that $CPT2^{A-/-}$ mice displayed differences in adiposity that were diet dependent.

Loss of Adipose Fatty Acid Oxidation Is Compensated in Part by Altered Carbohydrate Metabolism

The diet-dependent changes in adiposity in $CPT2^{A-/-}$ mice are consistent with other cold-intolerant models (*36, 79*). Nonetheless, we were interested in determining the flux of macronutrients in tissues lacking CPT2. First, we directly tested the ability of $CPT2^{A-/-}$ mice to fully oxidize radiolabeled 1-^{14}C oleic acid in vivo. Consistent with the indirect calorimetry data, we did not observe differences in whole-body fatty acid oxidation between control and $CPT2^{A-/-}$ mice (**Figure 2-8**).

Next, we determined the rate of de novo fatty acid synthesis by injecting 3H-acetate to control and $CPT2^{A-/-}$ mice for 3 hr and extracting lipids from liver, gWAT, and BAT. Although the livers of control and $CPT2^{A-/-}$ mice had equal incorporation of ^{3}H-acetate into lipids, both gWAT and BAT had an ~2-fold increase in incorporation **(Figure 2-9A**). This suggested that there was an increase in carbohydrate utilization in cells where CPT2 was deleted. Therefore, we assayed ^{3}H-acetate incorporation into lipids in control and CPT2KO MEFs. Consistent with the in vivo data, CPT2KO MEFs had a 2-fold increase in de novo lipogenesis from both ^{3}H-acetate and 2-^{14}C-pyruvate (**Figure 2-9B**). Additionally, we examined the oxidation of radiolabeled 2-^{14}Cpyruvate and U-^{14}C-glucose to 14CO2. While pyruvate oxidation was increased ~20%, glucose oxidation was

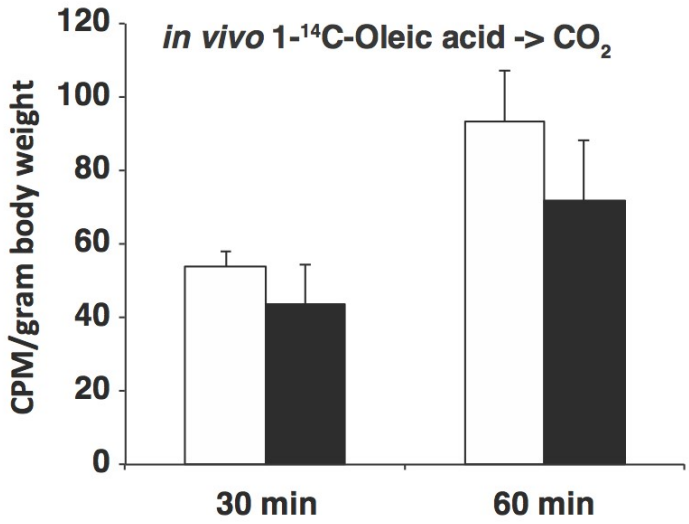

Figure 2-8. ***In vivo*** **oxidation of 1-^{14}C-oleic acid.**

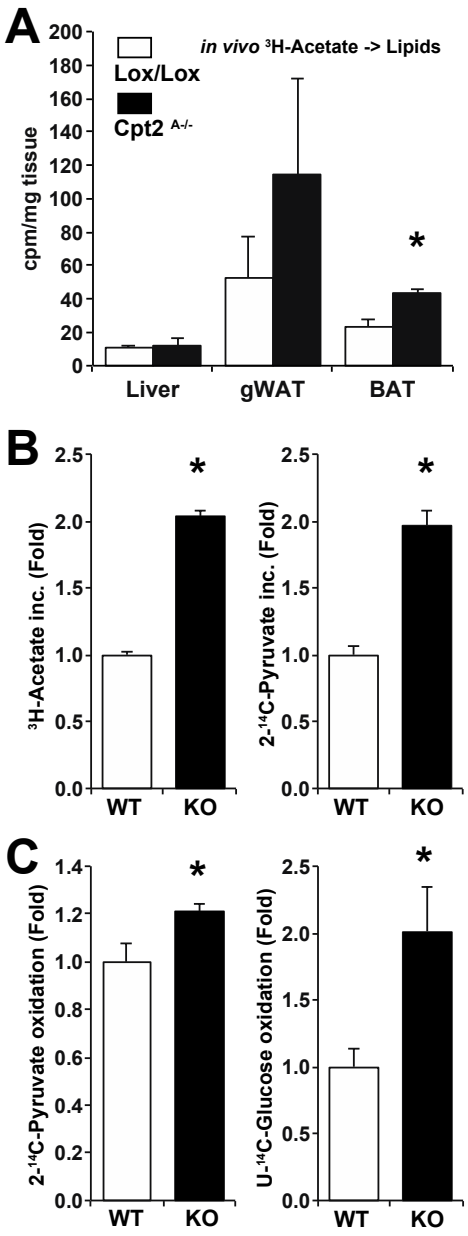

Figure 2-9. The loss of fatty acid oxidation alters carbohydrate metabolic flux.

(A) *De novo* lipogenesis of control and Cpt2$^{A-/-}$ liver, gWAT and BAT from a 1hr injection of ^{3}H-acetate normalized to tissue wet weight (n=4-5).

(B) *De novo* lipogenesis of control and Cpt2$^{A-/-}$ MEFs from ^{3}H-acetate or 2-^{14}C-pyruvate normalized to protein concentration (n=6).

(C) Substrate oxidation of control and Cpt2$^{A-/-}$ MEFs from 2-^{14}C-pyruvate or U-^{14}C-glucose normalized to protein concentration (n=5).

Data are expressed as mean ± SEM. *$p<0.05$. White bars represent control and black bars represent loss of *Cpt2*.

increased 2-fold over control cells (**Figure 2-9C**). These data show that the loss of fatty acid oxidation is compensated in part by increased carbohydrate flux.

Adipose Fatty Acid Oxidation Potentiates High-Fat Diet-Induced Oxidative Stress and Inflammation

The oxidation of fatty acids generates a substantial oxidative burden. It has been previously demonstrated that high-fat feeding increases oxidative stress and damaging oxidative end products particularly within gWAT (*80*). Given the role of fatty acid oxidation in the generation of ROS, we profiled genes known to be involved in oxidative stress in high-fat fed control and $CPT2^{A-/-}$ gWAT by quantitative PCR (qPCR) array. Multiple genes involved in detoxifying ROS were increased and several more involved in generating ROS were suppressed (**Figure 2-10**). To confirm and extend this data, we analyzed the genes and pathways identified in the qPCR screen in gWAT RNA isolated from both low- and high-fat-fed control and $CPT2^{A-/-}$ mice. *Sod1* and *Sod2* trended toward an increase under high-fat conditions, and *Sod2* was significantly increased ~2-fold in low-fat-fed $CPT2^{A-/-}$ gWAT. Genes that increase oxidative stress were suppressed in $CPT2^{A-/-}$ gWAT specifically in high-fat-fed conditions (**Figure 2-11A**). Therefore, $CPT2^{A-/-}$ gWAT gene expression was consistent with greater ROS detoxification and lower ROS generation. This led us to look at the mRNA abundance of adipokines, cytokines, and inflammatory markers in gWAT of control and $CPT2^{A-/-}$ mice. *Cox2* mRNA abundance, which produces inflammatory mediators, was robustly suppressed in high-fat-fed $CPT2^{A-/-}$ gWAT compared to controls (**Figure 2-11A**). Adiponectin mRNA abundance, which is regulated by redox and suppressed in diabetes, rebounded in high-fat-fed $CPT2^{A-/-}$ gWAT back to low-fat-fed levels (**Figure 2-11B**). Although Leptin

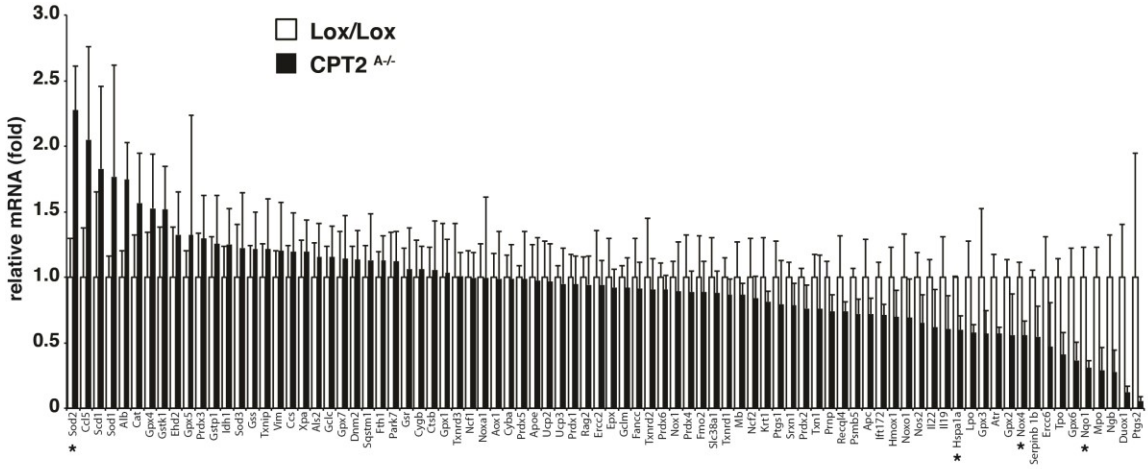

Figure 2-10. Expression of oxidative stress genes in gWAT of control and Cpt2$^{A-/-}$ mice fed a high-fat diet, related to Figure 2-7.

mRNA abundance in gWAT was unchanged between genotypes, Fgf-21 and Adipsin were significantly suppressed in low-fat-fed CPT2$^{A-/-}$ mice (**Figure 2-11B**).

Since Adipsin, also known as complement factor D, is involved in the inflammatory response, we next looked at inflammatory markers in CPT2$^{A-/-}$ gWAT. Although, the macrophage marker F4/80 was unchanged between CPT2$^{A-/-}$ and control mice, there was a suppression in *Cd11b* (*Mac-1*), a marker for activated macrophages, in high-fat-fed CPT2$^{A-/-}$ gWAT (**Figure 2-11C**). Consistent with these changes, there was a marked suppression in inflammatory gene expression as evidenced by lower mRNA abundance of *Mip-1a* and *Il-1b*, as well as a trend for the suppression in *Mip1b* in high-fat-fed CPT2$^{A-/-}$ gWAT (**Figure 2-11C**).

Additionally, the mRNA abundance of the anti-inflammatory cytokine Il-10 was significantly suppressed in high-fat-fed CPT2$^{A-/-}$ gWAT. There were no changes in the mRNA abundance of several important inflammatory and insulin-resistance-promoting cytokines/chemokines *Tnf-a*, *Il-6*, or *Mcp1* in control and CPT2$^{A-/-}$ gWAT (**Figure 2-11C**). Finally, we measured oxidized lipids in gWAT and serum of low- and high-fat-fed control and CPT2$^{A-/-}$ mice. The high-fat diet-induced increase in lipid peroxidation observed in control gWAT and serum was repressed in CPT2$^{A-/-}$ mice (**Figure 2-11D**). These data show that high-fat feeding requires mitochondrial oxidation to potentiate high-fat diet-induced oxidative stress and inflammation.

Improvements in CPT2$^{A-/-}$ Adipose Tissue Oxidative Stress Did Not Lead to Improved Systemic Glucose Tolerance

Adipose oxidative stress and inflammation induced by high-fat feeding has been suggested to initiate a cascade that leads to systemic insulin resistance (62, 63). Because

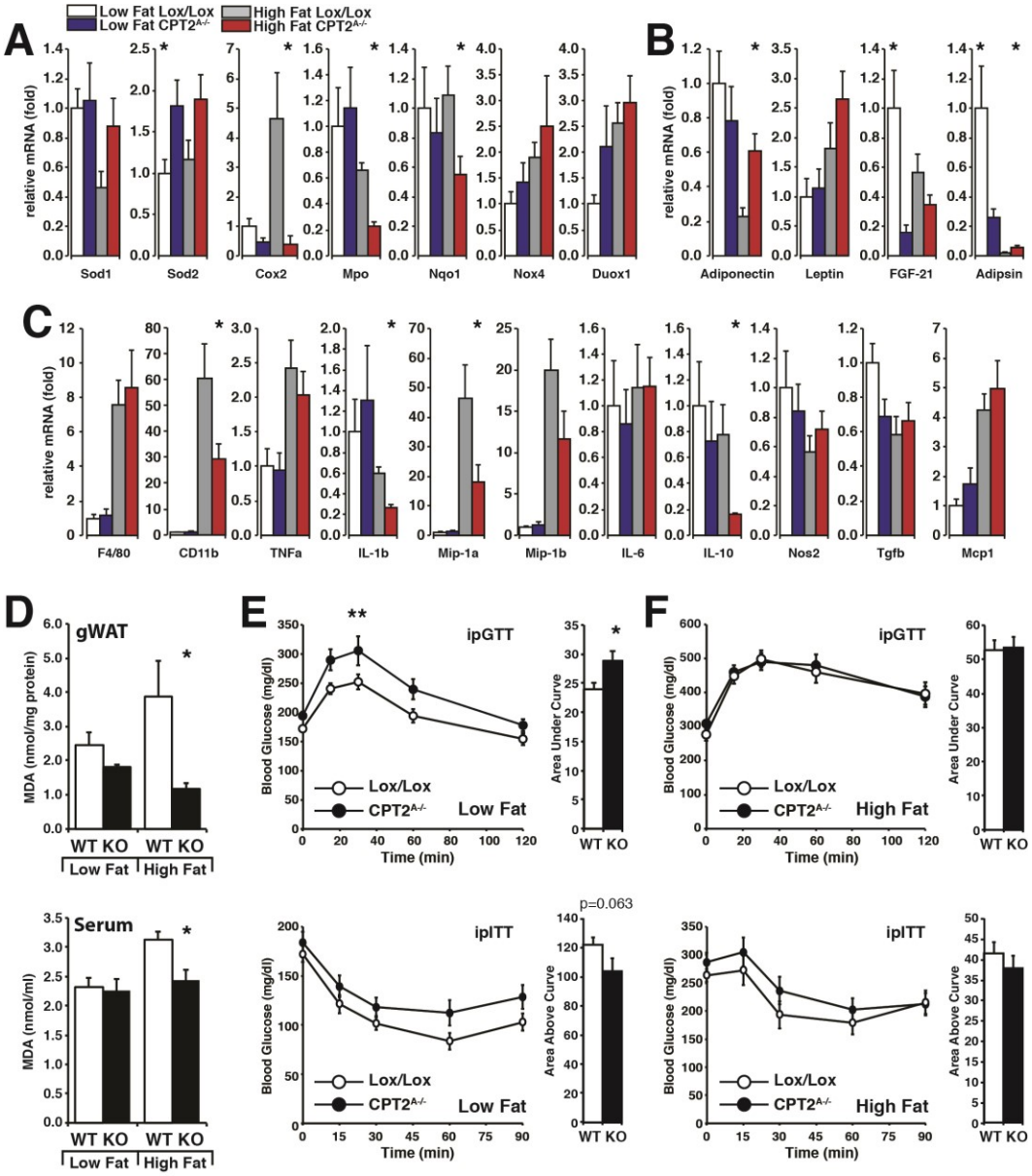

Figure 2-11. Adipose fatty acid oxidation potentiates high-fat induced oxidative stress and inflammation.

(A) Quantitative RT-PCR (qRT-PCR) of oxidative stress genes from gWAT of control and Cpt2$^{A-/-}$ mice fed a low- or high-fat diet (n=8).

(B) qRT-PCR of adipokines from gWAT of control and Cpt2$^{A-/-}$ mice fed a low- or high-fat diet (n=8).

(C) qRT-PCR of inflammatory genes from gWAT of control and Cpt2$^{A-/-}$ mice fed a low- or high-fat diet (n=8).

(D) TBARS assay from gWAT and serum of control and Cpt2$^{A-/-}$ mice fed a low- or high-fat diet (n=5).

(E) Intraperitoneal glucose tolerance test (ipGTT) and intraperitoneal insulin tolerance test (ipITT) including area under the curve and area above the curve, respectively, for control and Cpt2$^{A-/-}$ mice fed a low fat diet (n=9).

(F) Intraperitoneal glucose tolerance test (ipGTT) and intraperitoneal insulin tolerance test (ipITT) including area under the curve and area above the curve, respectively, for control and Cpt2$^{A-/-}$ mice fed a high fat diet (n=13-18).

Data are expressed as mean ± SEM. **p,0.005; *p<0.05.

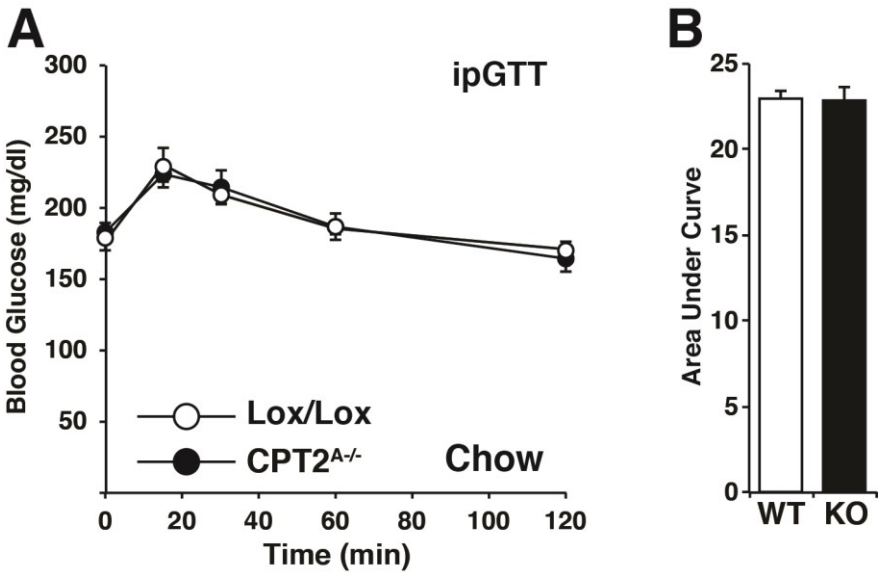

Figure 2-12. Glucose tolerance of chow fed control and Cpt2$^{A-/-}$ mice, related to Figure 2-7.

(A) ipGTT for control and Cpt2$^{A-/-}$ mice fed a chow diet.

(B) Area under the curve for GTT of control and Cpt2$^{A-/-}$ mice fed a chow diet (n=10-14). Data are expressed as mean ± SEM.

we have greatly suppressed oxidative stress and improved inflammatory markers in $CPT2^{A-/-}$ mice fed a high-fat diet, we determined glucose tolerance for control and $CPT2^{A-/-}$ mice fed both low- and high-fat diets by glucose and insulin tolerance tests. Consistent with an increase in adiposity, low-fat-fed $CPT2^{A-/-}$ mice exhibited greater glucose intolerance exhibited by impaired glucose disposal during the glucose tolerance test (GTT) and a strong trend toward impaired glucose clearance in response to insulin in the ITT (**Figure 2-11E**). These defects in glucose tolerance are not seen in chow-fed mice, suggesting that the high content of simple sugars (i.e., sucrose) promote lipid deposition and glucose intolerance in adipose in the absence of fatty acid oxidation (**Figure 2-12**). In contrast, high-fat-fed control and $CPT2^{A-/-}$ mice had similar glucose dynamics (**Figure 2-11F**). Therefore, the improvements in adiposity, oxidative stress, and inflammation in high-fat-fed $CPT2^{A-/-}$ mice were not sufficient to reverse systemic insulin resistance and glucose intolerance and are not consistent with a requirement for adipose-derived ROS in mediating systemic glucose intolerance.

Discussion

Obesity is the result of energy imbalance. As caloric intake exceeds expenditure, metabolic flux is directed into energy reserves, primarily as triglyceride in adipose tissue. Conversely, when caloric expenditure exceeds intake, these reserves are mobilized to provide physiological fuel. Alterations in adipocyte-specific metabolism can lead to systemic changes in adiposity, body weight, and glucose tolerance (*39, 50, 65, 66*). The suppression of adipocyte fatty acid oxidation is often invoked as a mechanism to explain mouse models that are obese in the absence of increased food intake. Although this is not an implausible idea, it has lacked an experimental underpinning. Contrary to this notion,

we have shown that the lack of adipocyte long-chain fatty acid oxidation does not lead to changes in body weight under standard laboratory conditions even when challenged by calorically dense diets.

BAT can dramatically increase metabolic rate and dissipate large amounts of stored lipids in a relatively short time once activated. Transgenic mice with increased BAT mass correlate nicely with resistance to weight gain (24). The transplantation of large amounts of BAT into mice improves their glucose tolerance but does little to improve their body weight (3). This may point to a robust endocrine rather than bioenergetic contribution of BAT. In fact, in the absence of cold-induced activation, the role of brown adipocyte bioenergetics in obesity remains controversial (25). Similar to $CPT2^{A-/-}$ mice, UCP1KO mice are resistant to, rather than prone to, diet-induced obesity at 20°C (79). Aging or a thermoneutral environment can alter this phenotype to produce obese-prone UCP1KO mice (81, 82). Additionally, the loss of ACSL1 in adipocytes, which renders mice unable to efficiently activate fatty acids for oxidation, leads to an increase in adiposity with low fat feeding similar to $CPT2^{A-/-}$ mice (36). Activation of catabolic processes in tissue other than adipose, needed to maintain body temperature, likely accounts for their lack of body-weight change and altered adiposity (83). These experiments illuminate a compensatory role of basal metabolic rate to compensate for the loss of BAT mediated thermogenesis; however, little is known about how the basal metabolic rate is regulated, where it emanates from, or mechanistically how it contributes to body temperature or body weight.

The phosphorylation of CREB by adrenergic stimulation induces the robust expression of thermogenic genes in BAT, including *Ucp1* and *Pgc1a*. Conversely, several

nuclear hormone receptors and corepressors such as LXRa and RIP140 negatively regulate thermogenic genes (84, 85). LXRa selectively represses *Ucp1* induction by binding adjacent to CREB on the *Ucp1* promoter. The crosstalk between fatty acid metabolism and thermogenic programing is likely mediated by fatty acid metabolites acting as ligands for nuclear hormone receptors to suppress agonist induced transcriptional control. The fact that ACSL1$^{A-/-}$ mice are cold intolerant but still retain thermogenic gene induction suggests the defect in CPT2$^{A-/-}$ BAT gene expression lies between the activation of fatty acids and their oxidation (36). Similar to CPT2$^{A-/-}$ mice, systemic carnitine deficiency also results in a suppression of *Ucp1* expression in BAT (86). These data suggest that an accumulation of fatty acid metabolites, such as long chain acyl-CoAs, for example, may be critical nuclear hormone ligands acting as negative metabolic feedback sensors to link metabolic capacity to nuclear encoded mitochondrial gene expression.

Although CPT2$^{A-/-}$ mice were unable to generate heat or oxidize fatty acids in BAT and WAT, they did not have changes in body weight when fed standard chow, low-fat, or high-fat diets. Under low-fat feeding, the mice gained more adiposity, but this was likely due to the high sucrose content in the diet, as chow feeding did not elicit increased adiposity. Low-fat-fed mice have enhanced de novo fatty acid synthesis in WAT, likely in part due to decreased concentrations of cellular L-carnitine and acetylcarnitine. Lower L-carnitine and acetylcarnitine levels can shift mitochondria to increased de novo lipogenesis by the inability to dissipate mitochondrial acetyl-CoA and thereby its allosteric effects on the pyruvate dehydrogenase complex and pyruvate carboxylase (87). High-fat feeding elicited a suppression in adiposity in CPT2$^{A-/-}$ mice and a concomitant

~2-fold increase in circulating ketones. Severe forms of cold intolerance such as ACSL1$^{A-/-}$, CPT2$^{A-/-}$ mice, and UCP1KO mice are either neutral or mildly resistant to high fat diet-induced obesity at room temperature (36, 79). However, mouse models with mild cold intolerance are obese prone at room temperature (88, 89). One possible explanation for this paradox is that mild BAT dysfunction may evade the reflexive compensation required to maintain body temperature, resulting in increased weight gain. Long-term housing of mice at thermoneutrality may relieve this compensation and generate obese-prone CPT2$^{A-/-}$ mice similar to UCP1KO mice (81). It is not clear, however, what the role of uncoupling and heat generation is at thermoneutrality. Is there still a need for BAT thermogenesis, or is uncoupling required for something else entirely, such as the generation of metabolic water (78, 90)?

It is clear that fatty acid oxidation is important in BAT; however, how does fatty acid oxidation in WAT contribute? The high oxidative stress and inflammation seen after long-term high-fat feeding has been attributed to fatty acid metabolism, which we confirm here (80). Here, we have evidence that the rate setting step in fatty acid oxidation is transcriptionally upregulated 6-fold in high-fat-fed gWAT (**Figure 2-7A**). We also observed increases in oxidative stress and inflammation under a high-fat diet, and these changes are greatly reduced in the absence of adipose fatty acid oxidation. Systemic glucose intolerance attributed to local adipose dysfunction was not, however, ameliorated by the loss of CPT2. We observed a suppression in gWAT inflammation in CPT2$^{A-/-}$ mice, as evidenced by a suppression in *Cd11b, Cox2, Mip1a*, and *Il1b*. The major and likely most relevant inflammatory mediators for insulin resistance such as *Tnf-a* and *Mcp1*, for example, were unchanged (63). Therefore, these important mediators of

obesity-induced insulin resistance were not dependent on adipose mitochondrial long-chain fatty acid β-oxidation.

In summary, adipose tissue fatty acid oxidation is critical for acute adaptation to the cold by providing both the energy required to fuel heat generation and the transcriptional regulation of BAT thermogenesis. Additionally, white adipose fatty acid oxidation potentiates high-fat diet-induced oxidative stress and inflammation; however, the improvements seen in $CPT2^{A-/-}$ mice were not sufficient to reverse systemic insulin resistance. Taken together, adipose fatty acid oxidation is an important metabolic process for environmental and nutritional homeostasis.

TISSUE SPECIFIC ROLES OF FATTY ACID OXIDATION

CHAPTER 3. Loss of adipose fatty acid oxidation does not potentiate obesity at thermoneutrality

Introduction

Obesity is driven by energy imbalance. Overconsumption of a calorie-dense diet increases energy storage mainly as triglyceride in white adipose tissue (WAT). Concomitantly, the inability to use this energy potentiates adiposity and body weight gain. Although great strides are being made in understanding the regulation of food intake, less is known about the regulation and contribution of energy expenditure to obesity. Determining the tissue-specific contribution of macronutrient metabolism to energy expenditure is critical for understanding the balance of energy intake and expenditure.

WAT plays an important role in energy storage but contains few mitochondria and contributes minimally to organismal bioenergetics in an autonomous manner. Alternatively, brown adipose tissue (BAT) is densely packed with mitochondria and can rapidly and robustly affect whole animal energy expenditure when deployed during a cold challenge (24). The physiological role of BAT is to produce heat to maintain body temperature during a cold challenge. This is accomplished via uncoupling cellular respiration from ATP generation via the mitochondrial transporter uncoupling protein-1 (Ucp1). Fatty acid oxidation is critical for this process (35, 38, 91) and provides the biophysical activator of uncoupling in BAT (92). Mice with an adipose-specific loss of fatty acid oxidation are severely cold intolerant, demonstrating an autonomous requirement for adipose fatty acid oxidation in cold-induced thermogenesis (36, 93).

Because of the large potential to alter energy expenditure, it is tempting to suggest that defects in brown or beige adipocytes can lead to an obesogenic phenotype. Therefore, it was somewhat surprising that uncoupling protein-1 knockout (Ucp1KO)

mice were resistant to rather than prone to diet-induced obesity (34, 79). One caveat is that standard laboratory animal housing is below the thermal preference for mice, generating a mild cold stress. Mice have a large surface-to-volume ratio and need to expend large amounts of energy defending their body temperature against the environment. Removing this cold stress by rearing mice at thermoneutrality (30°C) acutely reversed this phenotype and generated obesity-prone Ucp1KO mice, revealing a strong environmental impact on body weight and energy expenditure (81).

Recently, we generated mice with a loss of adipose fatty acid oxidation by knocking out carnitine palmitoyltransferase 2 (Cpt2), an obligate step in mitochondrial long-chain fatty acid β-oxidation (93). Similar to Ucp1KO mice, $Cpt2^{A-/-}$ mice were severely cold intolerant, but mildly resistant to high fat diet-induced adiposity. To understand the effect of ambient temperature on BAT deficient in fatty acid oxidation, we acclimatized $Cpt2^{A-/-}$mice to thermoneutrality (30°C) and demonstrate a severe loss of agonist-induced thermogenic gene induction and loss of interscapular BAT after long-term housing of $Cpt2^{A-/-}$ mice at thermoneutrality. Surprisingly, given the severity of cold intolerance and suppression of molecular and cellular thermogenic programming in $Cpt2^{A-/-}$ BAT, thermoneutral housing did not affect diet-induced obesity in $Cpt2^{A-/-}$ mice. These data show that bioenergetically and transcriptionally incompetent BAT does not potentiate obesity, even at thermoneutrality.

Experimental Procedures

Animals

$Cpt2^{lox/lox}$ and $Cpt2^{A-/-}$ mice and diets were previously described (93). Control mice are defined as sex-matched $Cpt2^{lox/lox}$ littermates. For the diet study, $Cpt2^{lox/lox}$ and $Cpt2^{A-/-}$

mice were fed a 60% high-fat diet (D12492, Research Diets) starting at 6 weeks of age and continuing for 12 weeks. For temperature acclimation studies, $Cpt2^{lox/lox}$ and $Cpt2^{A-/-}$ mice were housed at the indicated temperatures for 2 weeks in an animal incubator (Key Scientific) on a 12 hr light/12 hr dark cycle. Serum was collected from all mice to measure free glycerol and triacylglycerol (Sigma), β-hydroxybutyrate (Stan-Bio), total cholesterol (Wako), and non-esterified fatty acid (Wako). Blood acylcarnitines were quantified from dried blood spots (DBSs) with modifications (94, 95). Punched one-eighth-inch DBS samples were submerged in 100 ml of methanol solution containing internal acylcarnitine standards (NSKB, Cambridge Isotopes). Samples were incubated at 4°C for 20 min and dried under the nitrogen; then 60 ml 3N HCl in n-butanol was added. The samples were incubated for 15 min at 65°C and then dried under LN_2, and butylated acylcarnitines were reconstituted in 100 ml of mobile phase acetonitrile/water/formic acid (H_2O:CH_3CN:HCOOH, 80:19.9:0.1 v/v%). Samples were vortexed, transferred to a centrifuge filter, spun, and transferred to injection vial. Acylcarnitines were analyzed on an API 3200 (AB Sciex) operated in positive ion mode employing a precursor ion scan for m/z 85, which is generated as a characteristic product ion of butyl ester of acylcarnitine species. Quantitation of acylcarnitines was achieved by Chemoview (AB Sciex) application. Body composition was measured using quantitative nuclear magnetic resonance technology (Echo-MRI-100) to determine fat and lean mass. Energy expenditure and RER were measured using Oxymax indirect calorimetry cages (Columbus Instruments). All procedures were performed in accordance with the NIH's Guide for the Care and Use of Laboratory Animals and under the approval of the Johns Hopkins Medical School Animal Care and Use Committee.

Analysis of gene expression and mitochondrial DNA.

Trizol followed by the RNeasy Mini Kit (QIAGEN) was used to obtain total RNA. Microarray analysis was done using affymetrix mouse exon arrays (GSE72210). For qRT-PCR, 1-2 μg of RNA was reverse transcribed using the High Capacity cDNA Reverse Transcription Kit (Applied Biosciences). cDNA was diluted to 2 ng/μL and was amplified by specific primers in a 20μL reaction using SsoAdvanced SYBR Green Supermix (Bio-Rad). Analysis of gene expression was carried out in a CFX Connect Real-Time System (Bio-Rad). For each gene, mRNA expression was calculated as 2ΛdeltaCT relative to cyclophilin A expression. For mitochondrial DNA analysis, total DNA was prepared using the QIAmp DNA mini Kit (QIAGEN).

Western Blots

For western blots, protein was obtained by homogenizing tissues in 1x RIPA buffer (50 mM Tris-Cl pH 7.4, 150 mM NaCl, 1 mM EDTA, 1% Triton X-100, 0.25% deoxycholate). The concentration of the protein was obtained using the BCA Protein Assay Reagent (Pierce, Rockford, IL). 30 μg of protein was used in an SDS-PAGE and transferred to either a nitrocellulose (Protran BA 83, Whatman) or a polyvinylidene difluoride (PVDF) membrane and blocked with 3% BSA-TBST (tris buffer saline with tween 20). The blots were probed with the following antibodies: CPT2 (Thermoscientific), ACADM (GeneTex), UCP1 (Abcam), Pgc1α (Abcam), ATP5A (Abcam), and Hsc70 (Santa Cruz Biotechnology). Cy3 fluorescent antibody was used for Hsc70 and the corresponding secondary antibodies conjugated to horseradish peroxidase were used for other primary antibodies.

Statistical Analyses

Multiple comparisons were calculated using a two-way ANOVA. Acylcarnitines were analyzed using repeated-measures ANOVA with a Bonferroni post hoc correction. Pairwise comparisons were calculated using a two-tailed Student's T-test. Significance was determined as: *$p<0.05$; **$p<0.01$; ***$p<0.001$.

Results

The loss of adipose fatty acid oxidation results in broad transcriptional dysregulation at thermoneutrality.

Previously, we showed that the loss of an obligate step in mitochondrial long chain fatty acid β-oxidation specifically in adipocytes ($Cpt2^{A-/-}$) resulted in severe cold intolerance (93). Cold intolerance was expected given the critical role of fatty acid oxidation for providing the mitochondrial bioenergetics as well as biophysical activator of uncoupling in BAT (2, 37, 38). Unexpectedly, $Cpt2^{A-/-}$ BAT failed to up-regulate thermogenic programming in response to cold, β3-adrenergic agonists or forskolin (93). To better understand the role of fatty acid oxidation on the transcriptional control of BAT, we acclimatized $Cpt2^{A-/-}$ and littermate control mice to thermoneutrality (30°C) for two weeks. Thermoneutrality relieves facultative thermogenesis and reduces the requirement for basal tonic adrenergic signaling in BAT. We then injected the mice with the selective β3-adrenergic agonist CL-316243 (10mg/kg) or saline and collected interscapular BAT 3hrs later and preformed genome wide gene expression profiling on BAT mRNA via DNA microarrays (**Figure 3-1A,B**). Microarray analysis revealed broad transcriptional dysregulation upon the loss of fatty acid oxidation particularly in response to the β3-adrenergic agonist.

To validate the microarray results in a larger cohort of mice, we analyzed a subset

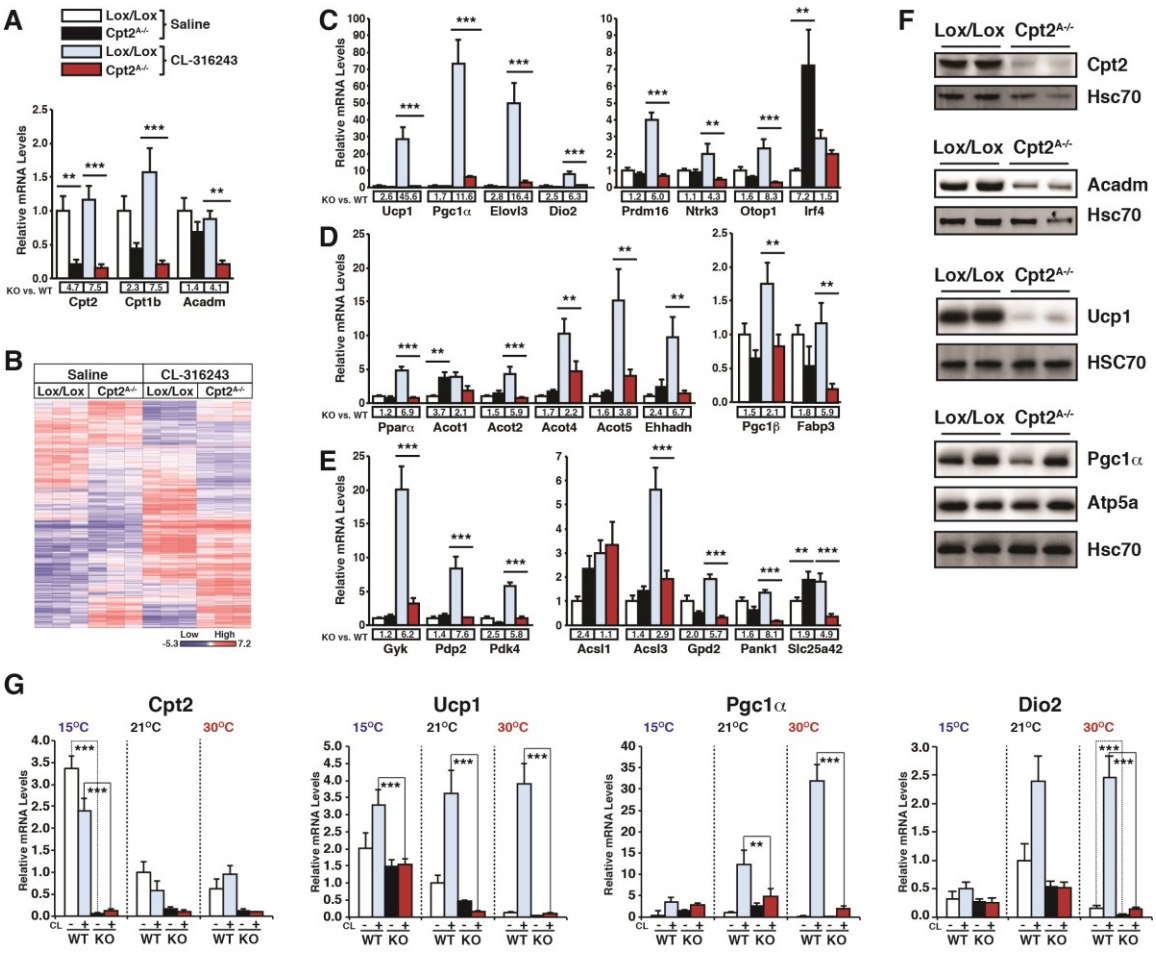

Figure 3-1. Transcriptional response of Cpt2$^{A-/-}$ BAT to adrenergic stimulation at thermoneutrality.

(A) Gene expression profiling via microarray of *Cpt2, Cpt1b* and *Acadm* at thermoneutrality 3hrs after injection with vehicle or CL-316243 injected control and Cpt2 $^{A-/-}$ BAT (n=5).

(B) Heat map of genes exhibiting statistically significant ($p<0.05$) changes from microarray analyses are shown for vehicle or CL-316243 injected control and Cpt2$^{A-/-}$ BAT (n=3).

(C) mRNA expression in BAT of thermogenic and brown fat enriched genes (n=5).

(D) mRNA expression in BAT of *Pparα* and Pparα target genes (n=5).

(E) mRNA expression in BAT of metabolic genes (n=5).

(F) Western blots of BAT from control and Cpt2$^{A-/-}$ mice at thermoneutrality.

(G) mRNA expression of *Cpt2, Ucp1, Pgc1α* and *Dio2* in BAT of control and Cpt2A-/- mice after 2wks at 15°C, 22°C and 30°C injected with vehicle of CL-316243 (n=5).

Data are expressed as mean ±SEM. *$p<0.05$; **$p<0.01$; ***$p<0.001$.

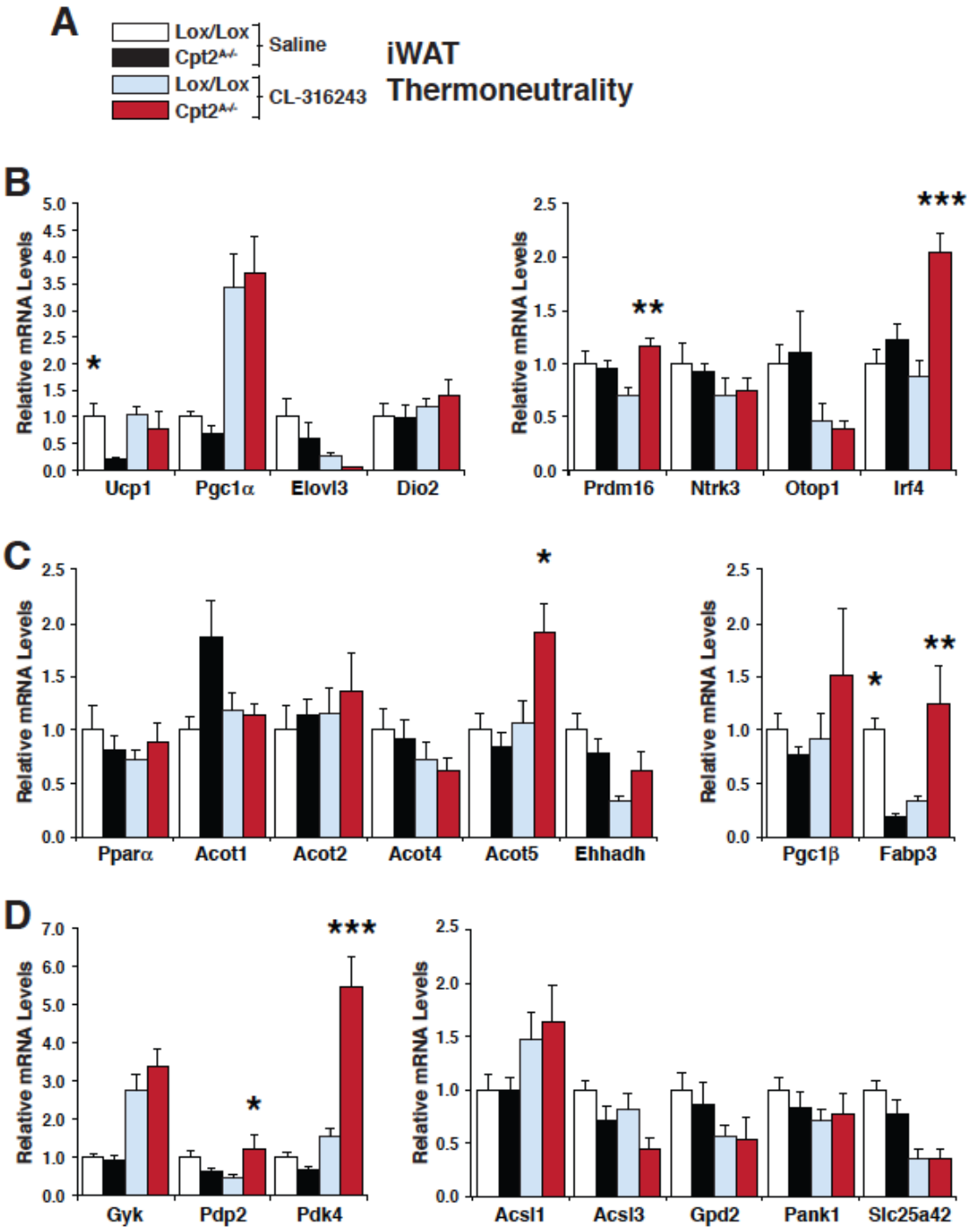

Figure 3-2. Transcriptional response of control and Cpt2$^{A-/-}$ iWAT to adrenergic stimulation at thermoneutrality, related to Figure 3-1.

(A) Figure Legend.
(B) mRNA expression in iWAT of thermogenic and brown fat enriched genes (n=5).
(C) mRNA expression in iWAT of Pparα and Pparα target genes (n=5).
(D) mRNA expression in iWAT of metabolic genes (n=5).

Data are expressed as mean ± SEM. *p<0.05; **p<0.01; ***p<0.001.

of genes identified in the microarray analysis by qRT-PCR. In agreement with our previous studies (93), thermogenic genes *Ucp1, Pgc1a, Elovl3*, and *Dio2* failed to be induced upon β3-adrenergic stimulation *in vivo* (**Figure 3-1C**). Alternatively, inguinal white adipose tissue (iWAT) of $Cpt2^{A-/-}$ mice exhibited significant suppression of *Ucp1* but was still responsive to β3-adrenergic stimulation (**Figure 3-2**). Other models of BAT dysfunction have shown a switch in identity from BAT to WAT (96, 97); however, $Cpt2^{A-/-}$ BAT largely maintained its transcriptional identity but again lost β3-adrenergic induction (**Figure 3-1C**). Loss of triglyceride hydrolysis results in defects in β-oxidation and a loss of Pparα signaling (65, 98-100). $Cpt2^{A-/-}$ BAT did not exhibit a defect in *Pparα*, and the canonical Pparα target *Acot1* was increased at baseline; however, these genes were again not induced by the β3-adrenergic agonist (**Figure 3-1D**). Consistent with the metabolic defects induced upon the loss of β-oxidation, $Cpt2^{A-/-}$ BAT exhibited defects in β3-adrenergic induction of genes in several metabolic pathways, such as *Gyk* (glycerolipid synthesis), *Pdp2*, and *Pdk4* (pyruvate-tricarboxylic acid cycle flux) (**Figure 3-1E**). Alternatively, iWAT remained sensitive to β3-adrenergic stimulation, and *Pdp2* and *Pdk4* showed increased expression following CL-316243 injection (**Figure 3-2**). The transcriptional deficits in BAT were mirrored by alterations in the protein abundance for *Ucp1, Pgc1α*, and *Acadm* (**Figure 3-1F**). These data show that the loss of fatty acid b-oxidation via genetic perturbation of *Cpt2* results in a defective transcriptional response to β3-adrenergic stimulation specifically in BAT.

The difference between agonist induced thermogenic gene induction between control and $Cpt2^{A-/-}$ BAT at 30°C was much larger than we observed at lower ambient temperatures (93). To understand if this was due to a change in basal expression or

inducibility, we acclimatized control and Cpt2$^{A-/-}$ mice for two weeks to 15°C, 21°C, or 30°C and then injected them with saline or CL-316243 (10mg/kg) and collected interscapular BAT 3hrs later. We then analyzed the expression of *Ucp1, Pgc1α*, and *Dio2* (**Figure 3-1G**). Basal *Ucp1* expression in WT BAT increased with decreasing temperature but was induced to the same degree. *Ucp1* expression in Cpt2$^{A-/-}$ BAT also increased with decreasing temperature but was not induced at any temperature. Basal *Pgc1α* expression was minimally altered by temperature acclimatization or genotype. However, it was induced by adrenergic stimulation in WT BAT to a greater degree upon increasing temperature, while Cpt2$^{A-/-}$ BAT remained non-induced under all conditions (**Figure 3-1G**). These data show that the primary transcriptional defect in Cpt2$^{A-/-}$ BAT is a failure in agonist-induced rather than basal thermogenic gene expression.

Role of adipose fatty acid oxidation on thermogenic plasticity.

Adipose fatty acid oxidation is required for acute cold-induced thermogenesis (36, 93). Preacclimatization to different ambient temperatures has dramatic effects on the response to cold challenge. To understand the role of adipose fatty acid oxidation on the physiology of thermogenic plasticity, Cpt2$^{A-/-}$ mice were acclimatized at thermoneutrality (30°C) for two weeks and then placed in individual metabolic cages also housed at 30°C. After several days to further acclimatize the mice to the metabolic cages, control and Cpt2$^{A-/-}$ mice were injected with CL-316243 (10mg/kg) and their energy expenditure was monitored. As expected, Cpt2$^{A-/-}$ mice failed to increase their energy expenditure in response to β3-adrenergic stimulation and also did not drop their RER, showing that they exhibited less fatty acid oxidation in response to the adrenergic challenge (**Figure 3-3A,B**). We then measured the energy expenditure of control and Cpt2$^{A-/-}$ mice at 30°C,

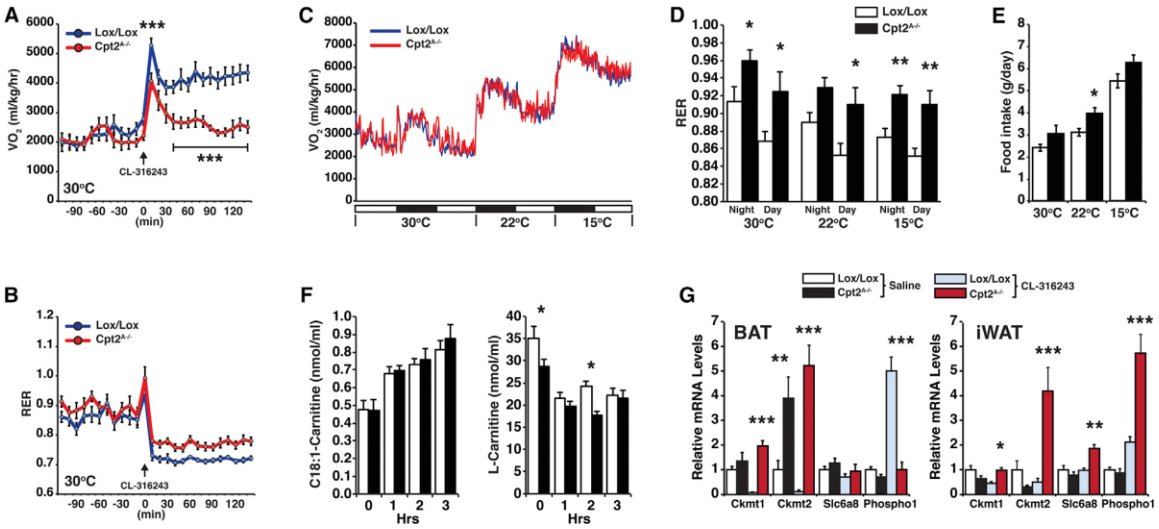

Figure 3-3. Contribution of adipose fatty acid oxidation to energy expenditure at different temperatures

(A) O_2 consumption of control and Cpt2$^{A-/-}$ mice injected with vehicle or CL-316243 (10 mg/kg) at thermoneutrality (n=7).

(B) RER of control and Cpt2$^{A-/-}$ mice injected with either vehicle or CL-316243 (10 mg/kg) at thermoneutrality (n=7).

(C) O_2 consumption of control and Cpt2$^{A-/-}$ mice at 30°C, 22°C, and 15°C (n=7).

(D) RER of control and Cpt2$^{A-/-}$ mice at 30°C, 22°C, and 15°C under dark and light cycles (n=7).

(E) Food intake of control and Cpt2$^{A-/-}$ mice at 30°C, 22°C, and 15°C (n=7).

(F) Hourly blood C18:1-carntine and L-carnitine concentrations of thermoneutral acclimatized control and Cpt2$^{A-/-}$ mice injected with CL-316243 (10 mg/kg) over 3 hr (n=5).

(G) mRNA expression in BAT and iWAT of genes in creatine metabolism (n=5).

Data are expressed as mean ± SEM. *p < 0.05; **p < 0.01; ***p < 0.001.

and directly before the dark cycle, the temperature was reduced (~1°C/4min) to 22°C (standard housing temperature) for 24hrs and then to 15°C for an additional 24hrs. Surprisingly, the energy expenditure during this paradigm of temperature shifting was unchanged between control and $Cpt2^{A-/-}$ mice (**Figure 3-3C**). However, consistent with the lack of adipose fatty acid oxidation in $Cpt2^{A-/-}$ mice, there was a strong shift towards carbohydrate oxidation as revealed by the RER (**Figure 3-3D**). Additionally, all mice showed an increase in food intake, and there was a modest increase in food consumption of $Cpt2^{A-/-}$ mice during this experimental paradigm (**Figure 3-3E**). These data show that although the $Cpt2^{A-/-}$ mice could not increase energy expenditure via fatty acid oxidation in adipose tissue, a systemic compensation enables homeostatic regulation of energy expenditure at different temperatures.

Next, we wanted to better understand how mice that could not oxidize fatty acids in adipose tissue could maintain systemic energy homeostasis. First, we measured blood acylcarnitines of thermoneutral acclimatized control and $Cpt2^{A-/-}$ mice injected with CL-316243 (10 mg/kg) over 3 hr. $Cpt2^{A-/-}$ mice were slightly carnitine deficient but exhibited a rise in blood long-chain acylcarnitines and a suppression of short-chain acylcarnitines similar to controls (**Figure 3-3F; Table 3-1**). These data support a systemic redistribution of fatty acids (93, 101). To understand possible compensatory adaptations in $Cpt2^{A-/-}$ adipose tissue, we mined our microarray data for genes in creatine metabolism (102). Consistent with Ucp1KO mice, $Cpt2^{A-/-}$ BAT exhibited an increase in *Ckmt2*; however, $Cpt2^{A-/-}$ BAT exhibited a loss of β3-adrenergic- induced *Phospho1* expression, consistent with other thermogenic genes (**Figure 3-3G**). In addition, $Cpt2^{A-/-}$ iWAT exhibited increased β3-adrenergic induction of *Ckmt1, Ckmt2, Slc6a8*, and *Phospho1* (**Figure 3-**

3G). These data support the notion that when BAT thermogenesis is lost, temperature acclimatization results in systemic compensation to maintain energy homeostasis during gradual changes in temperature.

Thermoneutrality induces a mitochondrial DNA stress that is potentiated by the loss of fatty acid oxidation.

To determine the role of adipose fatty acid oxidation during long term housing at thermoneutrality, we placed control and $Cpt2^{A-/-}$ male mice on a high fat diet for 12 weeks housed in a temperature- and light-controlled animal cabinet at 30°C. Upon necropsy, control mice had normal interscapular BAT. However, we could not identify morphologically distinct BAT in $Cpt2^{A-/-}$ mice (**Figure 3-4A**). Upon histological examination of interscapular adipose tissue, almost all of the classical BAT morphology was absent (**Figure 3-4B**). The loss of adipose tissue triglyceride lipase results in a suppression of Pparα, and therefore a switch of identity from BAT to a more WAT-like identity (65; 100). We do not observe defects in Pparα or Pparα target genes at baseline (**Figure 3-1D**). Additionally $Cpt2^{A-/-}$ BAT does not exhibit alterations in BAT specific identity (**Figure 3-1C**). However, increasing ambient temperature potentiated the loss of mitochondrial DNA in $Cpt2^{A-/-}$ BAT (**Figure 3-4C**). These data suggest that adipose fatty acid oxidation is required to maintain BAT at thermoneutrality.

The loss of mitochondrial DNA via genetic deletion of the mitochondrial transcriptional regulator *Tfam* was shown to induce Interferon Stimulated Genes (ISG) and initiate an innate antiviral response (103). Microarray analysis of thermoneutral acclimatized $Cpt2^{A-/-}$ BAT identified a similar gene expression profile. A broad range of ISGs such as *Oasl2, Ifih1, Sp110* and p200 family proteins *Ifi203* and *Ifi204* were

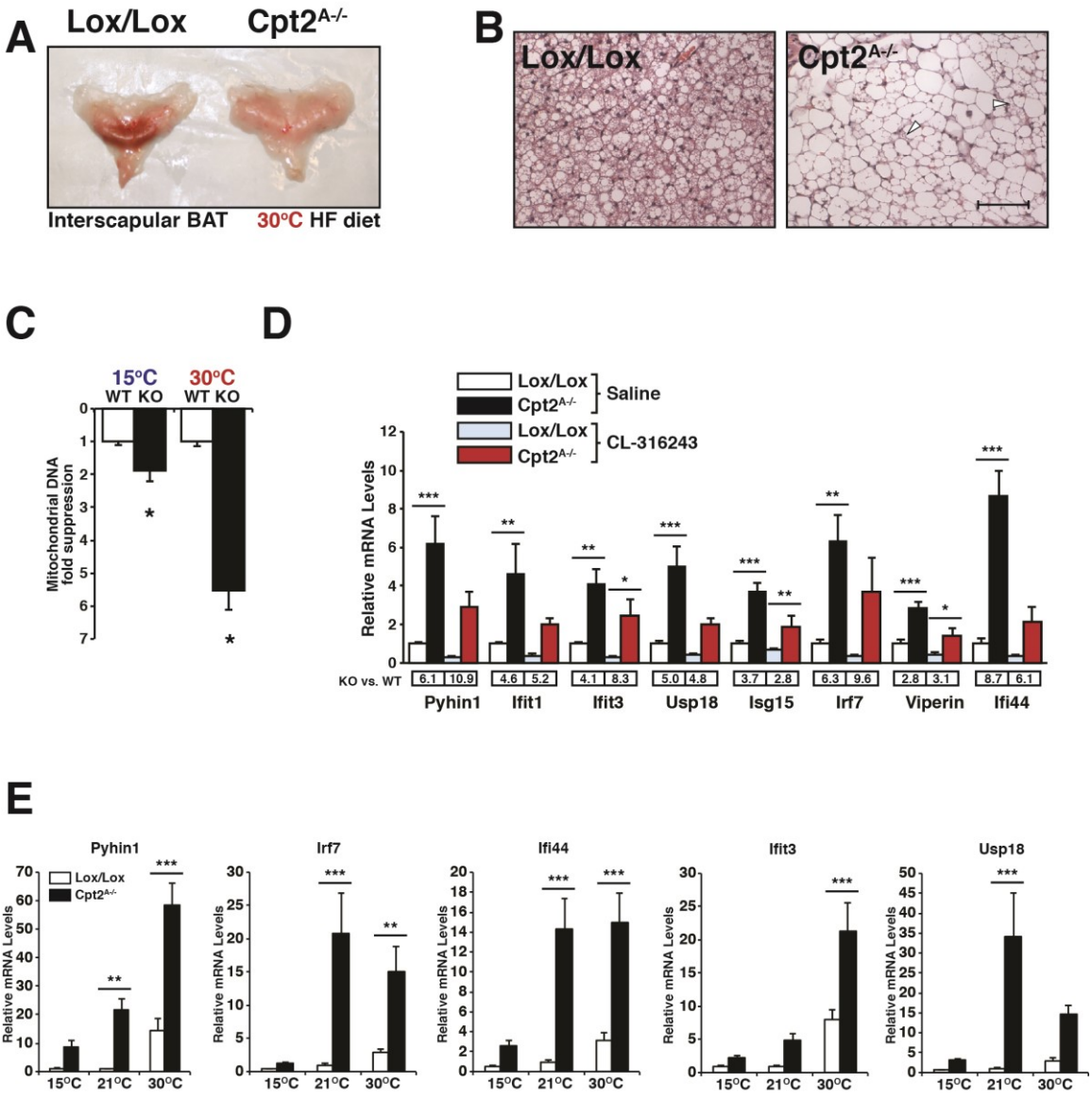

Figure 3-4. Loss of Fatty Acid Oxidation Potentiates Mitochondrial DNA Stress

(A) Gross interscapular BAT morphology of control and Cpt2$^{A-/-}$ mice after 12 weeks of high-fat (HF) diet at thermoneutrality.

(B) H&E-stained BAT from control and Cpt2$^{A-/-}$ mice after 12 weeks of HF diet at thermoneutrality. Arrows indicate BAT morphology. Scale bar, 100 mM.

(C) mtDNA fold suppression of control and Cpt2$^{A-/-}$ BAT at 15°C and 30°C (n=5).

(D) mRNA expression in BAT of ISGs in BAT of control and Cpt2$^{A-/-}$ mice injected with vehicle or CL-316243 at thermoneutrality (n=5).

(E) mRNA expression in BAT of ISGs in control and Cpt2$^{A-/-}$ mice after 2 weeks at 15°C, 21°C, and 30°C (n=5).

Data are expressed as mean ± SEM. *p < 0.05; **p < 0.01; ***p < 0.001.

induced in Cpt2$^{A-/-}$ BAT. We went on to verify a subset of these genes (*Pyhin1, Ifit1, Ifit3, Usp18, Isg15, Irf7, Viperin* and *Ifi44*) by qRT-PCR (**Figure 3-4D**). Interestingly, these genes were induced regardless of adrenergic stimulation. In fact, adrenergic stimulation suppressed these genes in both control and Cpt2$^{A-/-}$ BAT (**Figure 3-4D**). To determine the role of ambient temperature on the regulation of these ISGs, we profiled a subset of genes (*Pyhin1, Irf7, Ifi44, Ifit3, Usp18* and *Viperin*) in control and Cpt2$^{A-/-}$ BAT from mice acclimatized to 15°C, 21°C, and 30°C. All of the ISGs increased in BAT as ambient temperature increased, and the loss of fatty acid oxidation greatly potentiated this response (**Figure 3-4E**). These data show that temperature imparts a mitochondrial DNA stress in BAT and this is greatly potentiated by a loss in mitochondrial fatty acid β-oxidation.

The absence of adipose fatty acid oxidation does not affect obesity at thermoneutrality.

Thermoneutrality has been shown to dramatically and acutely increase weight gain of Ucp1KO mice, particularly when they are fed a high fat diet (81). We predicted that thermoneutrality would impart an obesogenic phenotype on Cpt2$^{A-/-}$ mice since Ucp1KO and Cpt2$^{A-/-}$ mice have a similar degree of cold intolerance. Cpt2$^{A-/-}$ BAT is bioenergetically and transcriptionally incompetent for thermogenesis, and long-term housing at 30°C facilitates an almost complete loss of BAT. Therefore, we measured the body weight weekly of control and Cpt2$^{A-/-}$ mice for 12 weeks fed a high fat diet and housed at 30°C. Surprisingly, thermoneutral housing did not affect weight gain in Cpt2$^{A-/-}$ mice (**Figure 3-5A**). Adiposity was also not affected and even trended lower (**Figure 3-5B,C**), similar to high fat feeding at room temperature (93). Additionally, there was no change in glucose tolerance (**Figure 3-5D**), little change in serum chemistry

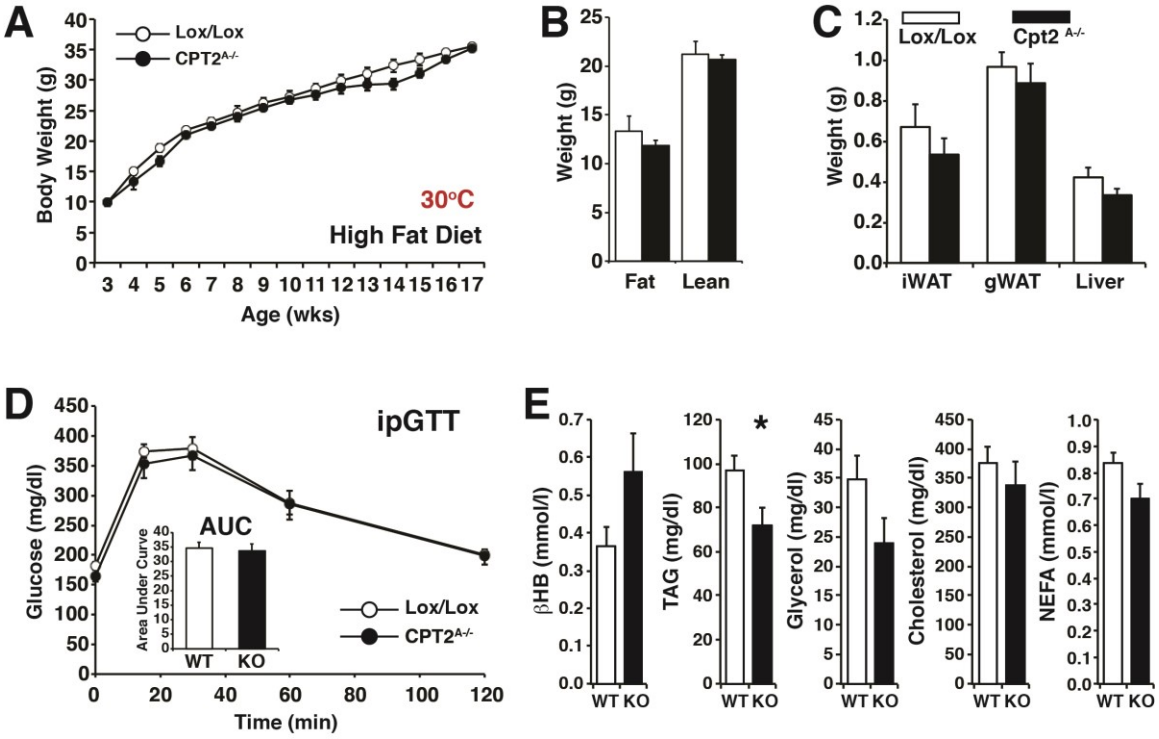

Figure 3-5. The Loss of Adipose Fatty Acid Oxidation Does Not Potentiate Diet-Induced Obesity at Thermoneutrality

(A) Body weights of control and Cpt2$^{A-/-}$ male mice fed a high-fat diet from 6 weeks of age at thermoneutrality (n=11–13). Arrow indicates the beginning of the high-fat diet.

(B) Fat and lean mass of control and Cpt2$^{A-/-}$ mice at 18 weeks of age after 12 weeks on a high-fat diet at thermoneutrality (n=11–13).

(C) Wet weights of iWAT, gWAT (unilateral depots), and liver (left lobe) of control and Cpt2$^{A-/-}$ mice (n=11–13).

(D) Intraperitoneal glucose tolerance test (ipGTT), including the area under the curve (AUC), for control and Cpt2$^{A-/-}$ mice at 10 weeks on a high-fat diet at thermoneutrality (n=11–13).

(E) Serum metabolite levels of control and Cpt2$^{A-/-}$ mice fed a high-fat diet at thermoneutrality (n=9).

Data are expressed as mean ± SEM. *p < 0.05; **p < 0.01; ***p < 0.001.

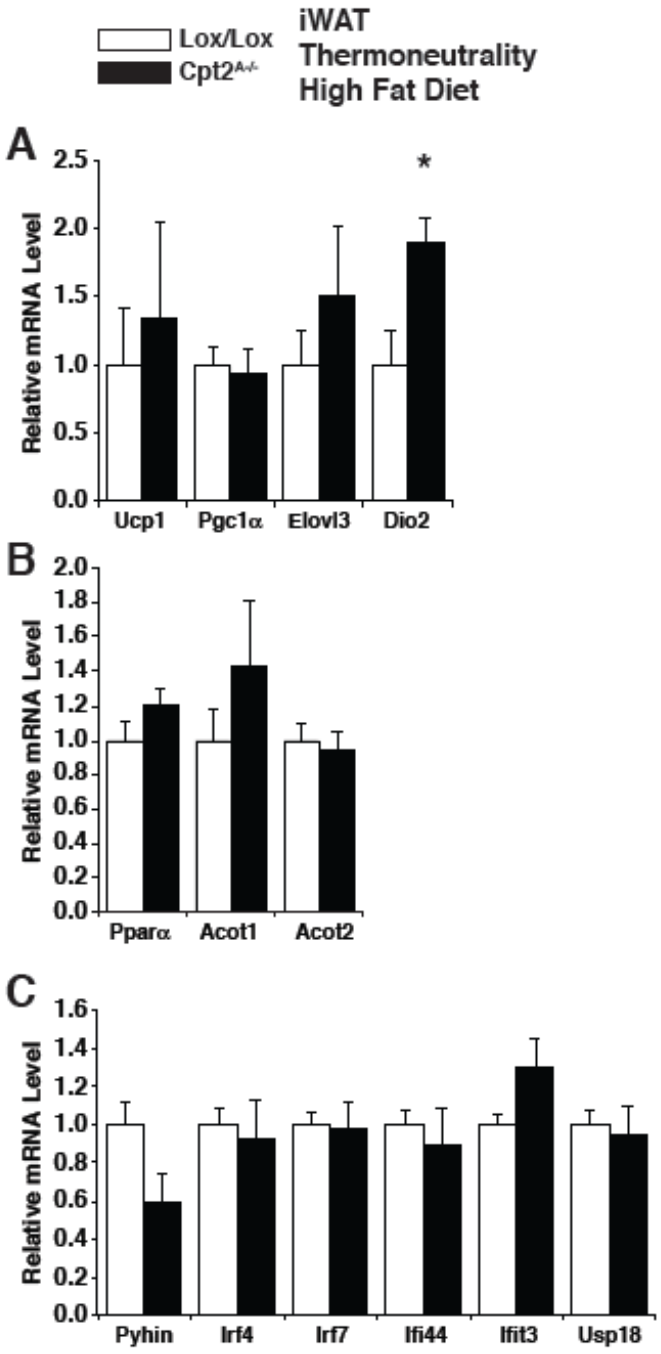

Figure 3-6. Transcriptional response of control and Cpt2$^{A-/-}$ iWAT to a high fat diet at thermoneutrality, related to Figure 3-5.

(A) mRNA expression in iWAT of thermogenic genes (n=5).
(B) mRNA expression in iWAT of Pparα and Pparα target genes (n=5).
(C) mRNA expression in iWAT of interferon responsive genes (n=5).

Data are expressed as mean ± SEM. *$p<0.05$.

(**Figure 3-5E**), and no significant beiging of iWAT (**Figure 3-6**) upon deletion of mitochondrial fatty acid β-oxidation in adipose tissue. These data suggest that defects in adipose tissue bioenergetics alone cannot account for the etiology of obesity or diabetes.

Discussion

BAT gene expression and thermogenic potential are highly correlated with the regulation of body weight and susceptibility to high fat diet induced obesity across many mouse models (24). The loss of Ucp1 (34, 79) or adipose fatty acid oxidation (36, 93) generates severe cold intolerance but does not result in susceptibility to diet induced obesity under standard laboratory housing conditions. Therefore, it seems unlikely that mice with an obesogenic phenotype at room temperature can be explained via a defect in BAT bioenergetics alone. Thermoneutrality revealed an obesogenic phenotype of Ucp1KO mice (81), however, we were not able to recapitulate this effect in $Cpt2^{A-/-}$ mice although they had molecular, cellular and biochemical defects that prevented canonical BAT function. Our results suggest that, although BAT dysfunction is tightly correlated with obesity, BAT function itself is likely correlating with the main driver of whole body energy expenditure that has yet to be defined mechanistically. In support of this notion, Fgf21 has a strong effect on BAT but can increase energy expenditure and induce weight loss equally well in wild-type or Ucp1KO mice even at thermoneutrality (6, 104-106). Additionally, the transplantation of large quantities of BAT in mice produced only mild benefits to body weight gain that were dependent on Il-6, suggesting an endocrine rather than bioenergetic role of BAT (3).

Triglyceride lipolysis and fatty acid oxidation are largely interdependent. Consequently, the loss of the rate-setting step in triglyceride hydrolysis, Adipocyte

Triglyceride Lipase (Atgl), results in cold intolerance (65). Interestingly, the knockout of *Atgl* with ap2/Fabp4-Cre generates mice that are obese with increased adiposity (65). However, the knockout of *Atgl* with the more specific adiponectin-Cre generates mice that are not more prone to obesity even after high fat feeding (100). This suggests that the increase in body weight and adiposity induced by a loss in adipocyte triglyceride hydrolysis requires simultaneous deletion in cells other than adipocytes (such as macrophages). Additionally, the loss of Atgl results in the loss of Pparα directed transcription and the loss of BAT identity presumably from the loss of an endogenous Pparα ligand produced upon hydrolysis (65, 98-100). Cpt2 deficient BAT maintains a BAT-like transcriptional program, and is not deficient in Pparα-mediated transcription. In fact, there is more Pparα target gene expression in $Cpt2^{A-/-}$ BAT likely due in part to the increase in basal adrenergic activity and PKA signaling (93). The main defect in $Cpt2^{A-/-}$ BAT is due to the loss in adrenergic-induced gene expression with limited changes to basal gene expression. Although lipolysis and β-oxidation are intimately linked within a continuous pathway, these data show that fatty acid catabolism affects transcription at multiple independent steps suggesting a complex integration of metabolites and transcriptional programming.

One of the most surprising results from the current study was the increase in ISGs in $Cpt2^{A-/-}$ BAT. The loss of *Cpt2* and the loss of *Tfam* have a high degree of concordance between the ISGs induced (103). However, the suppression in mitochondrial DNA was specific to BAT in $Cpt2^{A-/-}$ mice as mtDNA was unchanged in gWAT, iWAT or MEFs deleted in *Cpt2* (93). This suggests that cells that undergo high fatty acid oxidation may be more susceptible to mtDNA stress, while *Tfam* loss affects mtDNA stress more

globally. It will be interesting to see if other tissue specific KOs of *Cpt2* enhance innate immune priming, particularly macrophages. The mtDNA stress and ISG expression was increased in wild-type mice with increasing temperature, and this was greatly potentiated by the loss of fatty acid oxidation. Thermoneutrality exhibits a broad array of beneficial physiologic adaptations not overtly associated with energy homeostasis, including significant improvements in tumor therapy (107, 108). It is tempting to speculate that thermoneutrality initiates a priming of the innate immune system via mitochondrial metabolism that improves tumor clearance and antiviral activity.

Small mammals with large surface to volume ratios can expend a large amount of energy defending their body temperatures against the environment and have a large capacity for thermogenesis. Altering the ambient temperature results in an amazing array of molecular, cellular and physiological adaptations to maintain body temperature and energy homeostasis. Adipocyte fatty acid oxidation plays a major role in both mediating and regulating these processes. Mice with an adipose specific loss of fatty acid oxidation are unable to maintain their body temperature during an acute cold challenge (93). However, in response to moderate environmental challenges, they are able to maintain energy homeostasis via alternative mechanisms. The control of energy expenditure represents a critical evolutionarily conserved survival mechanism that is likely regulated by multiple overlapping and compensatory systems, which may present a continuing challenge for treatments aimed at reversing human obesity.

Table 3-1. Blood acylcarnitine profile of thermoneutral acclimatized $Cpt2^{lox/lox}$ and $Cpt2^{A-/-}$ mice before and 1, 2, and 3 hours following CL-316243 (10mg/kg).

Acylcamitines	Lox/Lox				Cpt2A-/-			
(nmol/ml)	0	1	2	3	0	1	2	3
Total	24.654 ± 2.462	27.036 ± 0.484	29.56 ± 1.641	27.512 ± 1.377	23.434 ± 2.647	25.364 ± 0.377	27.4 ± 2.325	28.828 ± 1.153
C0	35.074 ± 2.775	21.498 ± 1.35****	24.198 ± 1.216***	22.11 ± 1.741****	28.636 ± 1.592 #	19.814 ± 1.101**	17.604 ± 1.078 #,****	21.526 ± 1.767*
C2	19.124 ± 1.97	20.51 ± 0.507	22.762 ± 1.462	20.798 ± 1.246	18.042 ± 2.386	19.328 ± 0.177	20.888 ± 2.092	21.884 ± 0.924
C3	0.958 ± 0.124	0.624 ± 0.085*	0.586 ± 0.091**	0.494 ± 0.041***	0.744 ± 0.085	0.408 ± 0.05*	0.438 ± 0.044*	0.44 ± 0.048*
C3-DC	0.174 ± 0.015	0.154 ± 0.013	0.206 ± 0.031	0.144 ± 0.012	0.132 ± 0.023	0.144 ± 0.032	0.152 ± 0.012	0.124 ± 0.022
C4	0.726 ± 0.051	0.53 ± 0.055	0.482 ± 0.07	0.476 ± 0.031*	0.58 ± 0.084	0.568 ± 0.04	0.49 ± 0.069	0.542 ± 0.069
C4-OH	0.154 ± 0.016	0.248 ± 0.033*	0.258 ± 0.012*	0.328 ± 0.031****	0.146 ± 0.026	0.248 ± 0.032*	0.266 ± 0.016**	0.302 ± 0.047***
C4-DC	0.13 ± 0.011	0.126 ± 0.011	0.13 ± 0.022	0.124 ± 0.017	0.156 ± 0.013	0.134 ± 0.01	0.116 ± 0.012	0.128 ± 0.015
C5:1	0.014 ± 0.004	0.024 ± 0.005	0.026 ± 0.006	0.022 ± 0.004	0.018 ± 0.006	0.01 ± 0.003	0.018 ± 0.004	0.014 ± 0.002
C5	0.144 ± 0.019	0.078 ± 0.009***	0.098 ± 0.004*	0.064 ± 0.015****	0.116 ± 0.015	0.094 ± 0.007	0.074 ± 0.012*	0.068 ± 0.012*
C5-OH	0.086 ± 0.011	0.08 ± 0.013	0.072 ± 0.009	0.082 ± 0.02	0.09 ± 0.008	0.07 ± 0.005	0.08 ± 0.021	0.076 ± 0.01
C5-DC/C10-OH	0.02 ± 0.003	0.026 ± 0.004	0.034 ± 0.007	0.03 ± 0.009	0.03 ± 0	0.032 ± 0.007	0.034 ± 0.005	0.028 ± 0.005
C6	0.152 ± 0.012	0.108 ± 0.014	0.118 ± 0.01	0.122 ± 0.02	0.11 ± 0.01	0.136 ± 0.009	0.138 ± 0.009	0.138 ± 0.018
C8:1	0.054 ± 0.007	0.054 ± 0.007	0.068 ± 0.006	0.06 ± 0.008	0.052 ± 0.004	0.048 ± 0.009	0.054 ± 0.005	0.054 ± 0.008
C8	0.058 ± 0.011	0.062 ± 0.006	0.078 ± 0.006	0.07 ± 0.014	0.046 ± 0.01	0.056 ± 0.005	0.06 ± 0.008	0.076 ± 0.005
C10:1	0.062 ± 0.004	0.084 ± 0.01	0.104 ± 0.014*	0.09 ± 0.008	0.072 ± 0.01	0.082 ± 0.008	0.088 ± 0.007	0.118 ± 0.01*
C10	0.03 ± 0.005	0.05 ± 0.004	0.07 ± 0.012***	0.046 ± 0.005	0.05 ± 0.006	0.05 ± 0.003	0.046 ± 0.008	0.066 ± 0.007
C12:1	0.034 ± 0.006	0.072 ± 0.011*	0.058 ± 0.011	0.06 ± 0.004	0.042 ± 0.01	0.058 ± 0.007	0.064 ± 0.002	0.06 ± 0.013
C12	0.062 ± 0.008	0.112 ± 0.007**	0.116 ± 0.014**	0.108 ± 0.01*	0.06 ± 0.008	0.072 ± 0.012	0.086 ± 0.01	0.106 ± 0.012*
C12:1-OH	0.056 ± 0.009	0.056 ± 0.013	0.042 ± 0.006	0.046 ± 0.005	0.07 ± 0.007	0.044 ± 0.008	0.044 ± 0.008	0.058 ± 0.007
C12-OH	0.02 ± 0.004	0.028 ± 0.004	0.028 ± 0.006	0.03 ± 0.004	0.016 ± 0.002	0.018 ± 0.002	0.034 ± 0.005	0.03 ± 0.003
C14:2	0.028 ± 0.008	0.046 ± 0.007	0.072 ± 0.014**	0.054 ± 0.002	0.03 ± 0.003	0.058 ± 0.007	0.052 ± 0.006	0.056 ± 0.015
C14:1	0.072 ± 0.009	0.18 ± 0.028**	0.21 ± 0.019****	0.138 ± 0.017	0.11 ± 0.016	0.126 ± 0.012	0.172 ± 0.027	0.192 ± 0.022*
C14	0.15 ± 0.025	0.364 ± 0.041***	0.428 ± 0.044****	0.392 ± 0.058***	0.192 ± 0.03	0.316 ± 0.012	0.41 ± 0.043***	0.316 ± 0.039
C14:1-OH	0.034 ± 0.009	0.042 ± 0.007	0.056 ± 0.009	0.062 ± 0.014	0.03 ± 0.004	0.044 ± 0.004	0.054 ± 0.007	0.056 ± 0.018
C14-OH	0.034 ± 0.005	0.046 ± 0.008	0.056 ± 0.019	0.052 ± 0.004	0.042 ± 0.007	0.038 ± 0.006	0.04 ± 0.007	0.038 ± 0.006
C16:1	0.142 ± 0.024	0.308 ± 0.031***	0.284 ± 0.007**	0.258 ± 0.027**	0.146 ± 0.017	0.286 ± 0.033**	0.346 ± 0.065****	0.286 ± 0.046**
C16	0.974 ± 0.132	1.442 ± 0.137**	1.442 ± 0.091**	1.548 ± 0.067***	1.13 ± 0.109	1.354 ± 0.046	1.44 ± 0.098	1.67 ± 0.137***
C16:1-OH	0.056 ± 0.014	0.06 ± 0.01	0.078 ± 0.004	0.066 ± 0.01	0.048 ± 0.005	0.066 ± 0.009	0.066 ± 0.008	0.078 ± 0.01
C16-OH	0.042 ± 0.011	0.074 ± 0.013	0.082 ± 0.014	0.082 ± 0.012	0.046 ± 0.007	0.062 ± 0.006	0.074 ± 0.01	0.096 ± 0.016*
C18:2	0.22 ± 0.031	0.34 ± 0.033	0.342 ± 0.041	0.35 ± 0.02	0.268 ± 0.043	0.338 ± 0.022	0.4 ± 0.045	0.408 ± 0.048*
C18:1	0.478 ± 0.052	0.678 ± 0.043*	0.728 ± 0.036**	0.814 ± 0.052****	0.47 ± 0.064	0.694 ± 0.032**	0.756 ± 0.062***	0.874 ± 0.081****
C18	0.266 ± 0.041	0.296 ± 0.033	0.318 ± 0.045	0.368 ± 0.015	0.268 ± 0.019	0.26 ± 0.018	0.296 ± 0.035	0.314 ± 0.014
C18:2-OH	0.026 ± 0.004	0.038 ± 0.01	0.036 ± 0.002	0.038 ± 0.012	0.022 ± 0.004	0.036 ± 0.007	0.03 ± 0.003	0.032 ± 0.006
C18:1-OH	0.046 ± 0.014	0.064 ± 0.013	0.052 ± 0.007	0.062 ± 0.012	0.036 ± 0.002	0.062 ± 0.008	0.076 ± 0.014*	0.066 ± 0.006
C18-OH	0.028 ± 0.004	0.032 ± 0.007	0.04 ± 0.005	0.034 ± 0.005	0.024 ± 0.007	0.024 ± 0.002	0.018 ± 0.004 #	0.034 ± 0.006

Symbol	Significance
*	Effect of time; *p<0.05; **p<0.01; ***p<0.005; ****p<0.001
#	Lox/Lox vs. Cpt2A-/-; #p<0.05;

TISSUE SPECIFIC ROLES OF FATTY ACID OXIDATION

CHAPTER 4. Hepatic fatty acid oxidation restrains systemic catabolism during starvation

Introduction

Starvation initiates a series of metabolic adaptations to enable continuous production and delivery of nutrients to critical organs, tissues and cells (*53*). This response is coordinated in large part by the liver that responds by liberating glucose to the circulation initially from glycogen stores followed by *de novo* glucose production (i.e. gluconeogenesis). Additionally, ketones are produced and provide an alternative energy source to glucose for highly oxidative tissues such as the brain (*55*). Fatty acid oxidation is critical for these processes as it provides the carbon substrate for ketogenesis (acetyl-CoA) and mitochondrial bioenergetics (ATP, NADH) to facilitate gluconeogenesis. Therefore, humans with disparate inborn errors in mitochondrial fatty acid oxidation exhibit life-threatening hypoketotic-hypoglycemia following a fast (*54*). Systemically, the liver produces most of the circulating ketones due to its high capacity for β-oxidation and lack of the CoA transferase (Oxct1) in hepatocytes that is required to utilize ketones (*56*). Also, the liver is thought to dominate fasting gluconeogenesis with minor contributions from the kidney and gut. Interestingly, mice with a hepatocyte-specific loss of glucose-6-phosphatase, the obligate terminal enzyme in cellular glucose liberation, do not exhibit reduced blood glucose following fasting or starvation, although ketone production is accelerated (*57*). Therefore, extra-hepatic gluconeogenic tissues can fully compensate for a loss of hepatic production.

Mitochondrial long chain fatty acid β-oxidation is governed by the regulated translocation of activated fatty acids (acyl-CoAs) from the cytoplasm to the mitochondrial matrix mediated by successive carnitine acyltransferases (*58*). Carnitine Palmitoyltransferase 1 (Cpt1) isoenzymes mediate acyl transfer from long chain acyl-

CoAs to carnitine on the outer mitochondrial membrane, generating acylcarnitines that can traverse through the Carnitine-acylcarnitine translocase within the inner mitochondrial membrane. Within the mitochondrial matrix, Cpt2 transfers the acyl group from the acylcarnitine back onto CoA, enabling β-oxidation. Human inborn errors in Cpt2 result in increasing severity of metabolic disease (OMIM #s, 255110 adult onset, 600649 infantile, and 600650 infantile lethal) (*28, 59*). The complete loss of *Cpt1a* or *Cpt1b* is embryonic lethal in mice, and the loss of *Acadl* or *Acadm* results in increased neonatal death (*29, 30, 60*). The loss of other mitochondrial components of β-oxidation result in multisystemic defects as well as cell-specific compensatory mechanisms (*39, 61-63*).

To understand the contribution of hepatic fatty acid oxidation during fasting and starvation, we generated mice with a liver-specific knockout of Carnitine Palmitoyltransferase 2 ($Cpt2^{L-/-}$), an obligate enzyme in mitochondrial long chain fatty acid β-oxidation encoded by a single gene. To our great surprise, $Cpt2^{L-/-}$ mice not only survived the perinatal period but also did not exhibit alterations in blood glucose following a 24hr fast although ketones were absent. Fasting resulted in serum dyslipidemia, hepatic steatosis and alterations in hepatic and systemic oxidative gene expression. Although $Cpt2^{L-/-}$ mice were able to adapt to survive a 24hr fast, feeding them a ketogenic diet resulted in hepatomegaly and death after only 6 days with a complete absence of adipose triglyceride stores. These data show that hepatic fatty acid oxidation is not required for survival during acute food deprivation, but is essential for constraining adipocyte lipolysis and regulating systemic catabolism when glucose is limiting.

Experimental Procedures

Animals

To generate a liver-specific loss-of-function of *Cpt2*, we bred $Cpt2^{lox/lox}$ mice (*64*) to albumin-Cre transgenic mice (*65*). Mice were housed in ventilated racks with a 14 hr light/10 hr dark cycle and fed a standard chow diet (Harlan Laboratories). All mice were euthanized at the same time of day (3p.m.). Fed mice were food deprived from 1 p.m.-3 p.m. to ensure consistent feeding patterns. For fasting studies, mice were deprived of food for 24 hours from 3p.m.-3 p.m. For the ketogenic diet studies, mice were placed on a ketogenic diet at 9 weeks of age (*66*). Serum was collected for all mice to measure free glycerol and TAG (Sigma), β-hydroxybutyrate (StanBio), total cholesterol, NEFA (Wako), and ALT (Sigma). Fgf21, Gdf15, Igfbp1, Corticosterone, Adiponectin (R&D systems) and insulin (Millipore) and Adiponectin were measured by ELISA. Body fat and lean mass of 9-week old mice was measured via magnetic resonance imaging analysis (QNMR EchoMRI100; Echo Medical Systems, LLC). Indirect calorimetry and metabolic cage studies were normalized to total lean mass as described (*67*). All procedures were performed in accordance with the NIH's *Guide for the Care and Use of Laboratory Animals* and under the approval of the Johns Hopkins Medical School Animal Care and Use Committee.

Metabolic measurements

Blood levels of acylcarnitines were quantified from dried blood spots (DBS) with modifications (*68, 69*). Punched 1/8″ DBS samples were submerged in 100 µl of methanol solution containing internal standards for acyl carnitines (NSK B, Cambridge Isotopes). Samples were incubated at 4°C for 20min, dried under nitrogen and then 60 µl

3N HCl in n-butanol was added. The samples were incubated for 15 min at 65 °C then dried under LN_2, and butylated acyl carnitines were reconstituted in 100µl of mobile phase acetonitrile/water/formic acid (H_2O:CH_3CN:HCOOH; 80:19.9:0.1 v/v%). Samples were vortexed, transferred to a centrifuge filter, spun and transferred to an injection vial. Tissue acyl carnitines were isolated from freeze-clamped tissue and homogenized in a methanol solution containing internal standards as above, sonicated for 10min at room temperature and centrifuged for 4min at 13,000rpm at 4°C. Following centrifugation, the liquid phase was collected and evaporated to dryness under LN_2 and processed as above. Acyl carnitines were analyzed on an API 3200 (AB SCIEX, Foster City, CA) operated in positive ion mode employing precursor ion scan for m/z 85, which is generated as a characteristic product ion of butyl ester of acyl carnitine species. Quantitation of acyl carnitines was achieved by Chemoview (AB SCIEX) application. All blood samples are reported as nmol/ml; tissue samples as pmol/mg. Liver fatty acid oxidation, TAG measurement and liver peroxidation was done as previously described (*66, 67*).

Real Time qPCR

RNA was isolated from all tissues using the RNeasy Mini Kit (QIAGEN). Using the High Capacity cDNA Reverse Transcription Kit (Applied Biosystems), we reverse transcribed 1-2 ug of total RNA. The cDNA was diluted to 2ng/uL and amplified by primers in a 20 uL reaction using SsoAdvanced SYBR Green Supermix (Bio-Rad). The analysis was done using a CFX Connect Real-Time System (Bio-Rad). We calculated mRNA using a 2^deltaCT relative to the average of the housekeeping genes *cyclophilin A*, *rpl22* and *18s* expression. All primers and gene information were previously reported (*64*).

Western Blot

Liver and kidney homogenates were prepared using 1× RIPA buffer with protease inhibitors. The protein concentration was measured using the Pierce BCA Protein Assay kit (Thermo Scientific). We used 30 ug of protein on an SDS-PAGE and then transferred it to either a nitrocellulose (Protran BA 83, Whatman) or a polyvinylidene difluoride (PVDF) membrane. We then blocked with 3% BSA-TBST (tris buffer saline with tween 20). The membranes were then probed with antibodies Cpt2 (Pierce), Pgc1α (Abcam), Acsl1 (Cell Signaling), Acot1 (Cell Signaling), Acot2 (Cell Signaling), Cpt1α (Abcam), Acadm (GeneTex), Acsf3 (Pierce), Total Acc (Cell Signaling), Acly (Cell Signaling), Hadha (Genetex), Aco2 (Cell Signaling), Fasn (BD Biosciences), and Hsc70 (Santa Cruz Biotechnology). Hsc70 used the appropriate Cy3 fluorescent secondary antibodies, and the other primary antibodies used the corresponding secondary antibodies conjugated to horseradish peroxidase.

Statistical Analysis

Data were analyzed with the assistance of Prism. Significance was determined using an unpaired two-tailed Student's t-test for single variable experiments and two-way ANOVA with Bonferroni post hoc correction for multiple variable experiments.

RESULTS

Generation of mice with a liver-specific deficiency in fatty acid β-oxidation.

Previously, we generated a mouse model with a conditional loss-of-function allele for *Cpt2*, an obligate step in mitochondrial long chain fatty acid β-oxidation (*64, 70*). To produce mice with a loss of Cpt2 specifically in hepatocytes, we bred $Cpt2^{lox/lox}$ mice to

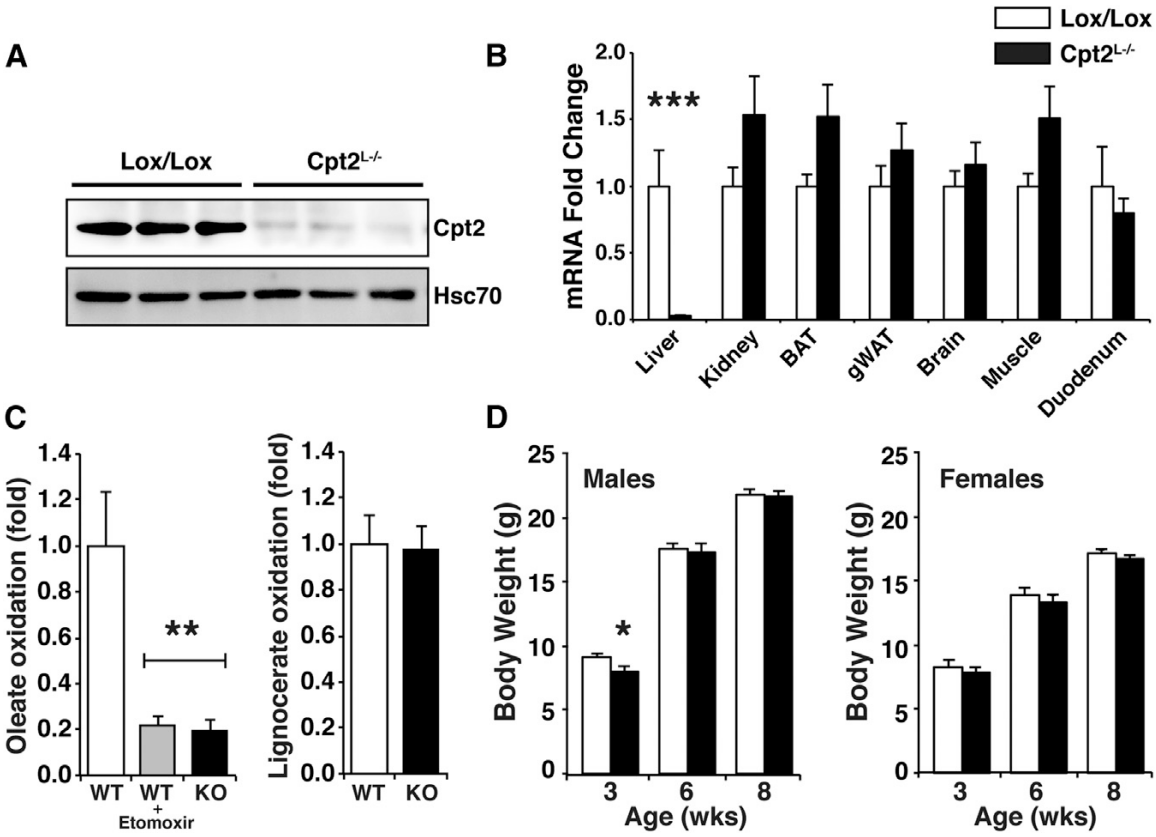

Figure 4-1. Characterization of mice with a liver specific KO of CPT2.

(A) Western blot for CPT2 in liver of $Cpt2^{lox/lox}$ and $Cpt2^{L-/-}$ mice.

(B) mRNA for *Cpt2* across different tissues (n=6).

(C) Oxidation of 1-^{14}C-oleic acid and 1-^{14}C-Lignoceric acid to $^{14}CO_2$ in liver slices of $Cpt2^{lox/lox}$ and $Cpt2^{L-/-}$ mice (n=5).

(D) Body weights of $Cpt2^{lox/lox}$ and $Cpt2^{L-/-}$ male and female mice fed a normal chow diet (males, n=14-23; females, n=8-12).

Data are expressed as mean ± SEM. *p<0.05; **p<0.01; ***p<0.001.

liver-specific albumin-Cre transgenic mice (*65*). The resulting liver-specific Cpt2 knockout (KO) mice ($Cpt2^{L-/-}$) showed a loss of CPT2 protein in the liver (**Figure 4-1A**) and decreased mRNA levels of *Cpt2* specifically in the liver (**Figure 4-1B**). As expected, oleate oxidation was significantly suppressed in the liver of $Cpt2^{L-/-}$ mice to a similar degree as incubation with 100μM of the CPT inhibitor, etomoxir (*71*). There was no change in the oxidation of the very long chain fatty acid, lignoceric acid, which is preferentially oxidized in peroxisomes (**Figure 4-1C**). Although males had a small suppression of body weight after weaning, females did not show suppressed body weight and all mice exhibited normal body weight by 6 weeks of age (**Figure 4-1D**). These data show that the loss of hepatic mitochondrial long chain fatty acid β-oxidation is not required for survival to adulthood. This is surprising given the requirement for fatty acid β-oxidation during the perinatal period (*39, 72, 73*).

Fasting results in hypoketotic dyslipidemia in $Cpt2^{L-/-}$ mice.

To determine the requirements for hepatic fatty acid oxidation upon food deprivation, we fasted $Cpt2^{lox/lox}$ and $Cpt2^{L-/-}$ mice for 24 hours at 9 weeks of age. As expected, there was a significant decrease in serum β-hydroxybutyrate (βHB) in $Cpt2^{L-/-}$ mice even in the fed state. Control $Cpt2^{lox/lox}$ mice dramatically increased serum βHB upon a 24hr fast as expected while $Cpt2^{L-/-}$ mice did not exhibit appreciable serum βHB consistent with the a loss of hepatic fatty acid oxidation (**Figure 4-2A**). Additionally, fasting induced serum dyslipidemia with increased NEFA and cholesterol in $Cpt2^{L-/-}$ mice (**Figure 4-2A**). $Cpt2^{L-/-}$ mice did not become hypoglycemic following the 24hr fast nor was insulin different between genotypes (**Figure 4-2A**). Because the liver plays an integral role in fatty acid metabolism in the body, we determined whole body

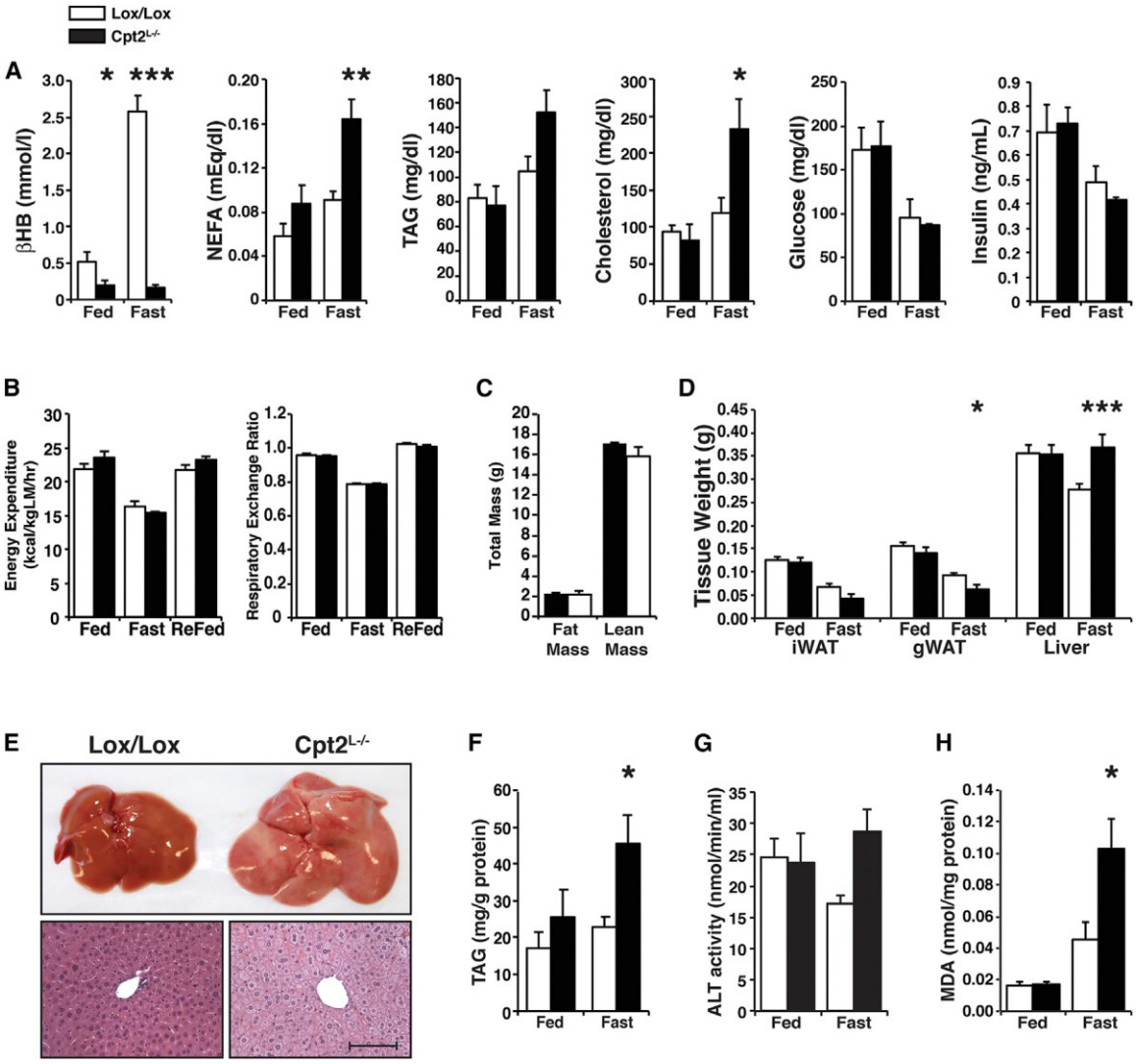

Figure 4-2. Liver and systemic deficits in fed and 24hr fasted Cpt2$^{L-/-}$ mice.

(A) Serum metabolites in Cpt2$^{lox/lox}$ and Cpt2$^{L-/-}$ mice (n=6).
(B) Energy expenditure and respiratory exchange ratio of Cpt2$^{lox/lox}$ and Cpt2$^{L-/-}$ mice under fed, fast and refed conditions (males, n=5-7).
(C) Total fat and lean mass of Cpt2$^{lox/lox}$ and Cpt2$^{L-/-}$ male mice (n=5-7).
(D) Total fat and lean mass of Cpt2$^{lox/lox}$ and Cpt2$^{L-/-}$ male mice (n=5-7).
(E) Wet weights of fed or 24 hour fasted iWAT, gWAT, and liver for Cpt2$^{lox/lox}$ and Cpt2$^{L-/-}$ mice (n=6-10).
(F) Gross and histological morphology of livers from 24 hr fasted Cpt2$^{lox/lox}$ and Cpt2$^{L-/-}$ mice.
(G) Triglyceride levels from liver homogenates of fed and 24 hr fasted Cpt2$^{lox/lox}$ and Cpt2$^{L-/-}$ mice (n=5).
(H) Liver damage measured by serum ALT activity of fed and 24hr fasted Cpt2$^{lox/lox}$ and Cpt2$^{L-/-}$ mice (n=5).
(I) Liver damage measured by serum ALT activity of fed and 24h fasted Cpt2$^{lox/lox}$ and Cpt2$^{L-/-}$ mice (n=5).
(J) TBARS assay measuring lipid peroxidation from liver of fed and 24 hr fasted Cpt2$^{lox/lox}$ and Cpt2$^{L-/-}$ mice (n=5).

Data are expressed as mean ± SEM. *p<0.05; **p<0.01; ***p<0.001.

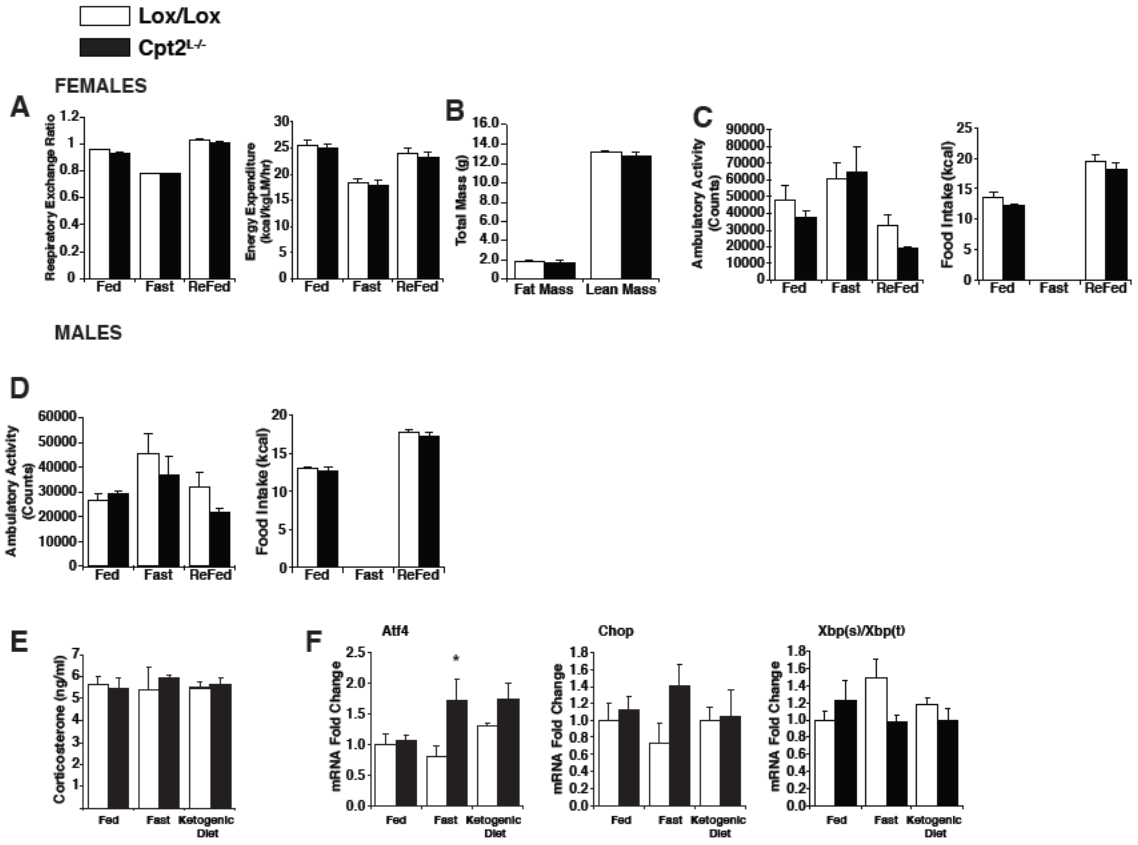

Figure 4-3. Corticosterone, ER stress, body composition and whole body bioenergetics of Cpt2$^{lox/lox}$ and Cpt2$^{L-/-}$ mice.

(A) Respiratory exchange ratio and energy expenditure in fed fast and refed Cpt2$^{lox/lox}$ and Cpt2$^{L-/-}$ female mice (n=6).

(B) Total fat and lean mass of Cpt2$^{lox/lox}$ and Cpt2$^{L-/-}$ female mice (n=6).

(C) Ambulatory activity and food intake during fed, fast and refed Cpt2$^{lox/lox}$ and Cpt2$^{L-/-}$ female mice (n=6).

(D) Ambulatory activity and food intake during fed, fast and refed Cpt2$^{lox/lox}$ and Cpt2$^{L-/-}$ male mice (n=5-7).

(E) Serum concentration of Corticosterone in fed, 24h fasted and ketogenic diet-fed Cpt2$^{lox/lox}$ and Cpt2$^{L-/-}$ male mice (n=5).

(F) Gene expression of *Atf4*, *Chop*, *Xbp(s)* and *Xbp(t)* in the liver of fed, 24h fasted and ketogenic diet-fed Cpt2$^{lox/lox}$ and Cpt2$^{L-/-}$ male mice (n=6).

Data are expressed as mean ± SEM. *p<0.05; **p<0.01; ***p<0.001.

bioenergetics in $Cpt2^{L-/-}$ mice. Interestingly, there was no change in energy expenditure between $Cpt2^{lox/lox}$ and $Cpt2^{L-/-}$ mice in fed, fasted, or refed states (**Figure 4-2B**). Although $Cpt2^{L-/-}$ mice exhibit clear metabolic deficiencies, in the context of whole animal energy homeostasis, $Cpt2^{lox/lox}$ and $Cpt2^{L-/-}$ mice were able to maintain equivalent energy expenditure and respiratory exchange ratio even during fasting (**Figure 4-2B**). Food intake, body composition, and ambulatory activity were not different between male and female $Cpt2^{lox/lox}$ and $Cpt2^{L-/-}$ mice (**Figures 4-2C and 4-3A-3D**). Examination of tissue weights in $Cpt2^{lox/lox}$ and $Cpt2^{L-/-}$ mice showed that fasting resulted in a greater suppression in gonadal white adipose tissue (gWAT) in $Cpt2^{L-/-}$ mice while there was a concomitant increase in liver weight (**Figure 4-2D**). Consistent with the wet weight data, $Cpt2^{L-/-}$ livers were enlarged and lipid laden following a 24-hour fast (**Figure 4-2E**). Liver triglyceride levels were unchanged in the fed state but were significantly increased in $Cpt2^{L-/-}$ mice compared to control $Cpt2^{lox/lox}$ mice upon fasting (**Figure 4-2F**). There were no signs of liver damage by serum ALT activity (**Figure 4-2G**), altered corticosterone levels (**Figure 4-3E**), or significant markers of ER stress (**Figure 4-3F**) following a 24hr fast. There were no signs of liver damage by serum ALT activity (**Figure 4-2G**), altered corticosterone levels (**Figure 4-3E**), or significant markers of ER stress (**Figure 4-3F**) following a 24 hour fast. However, However, $Cpt2^{L-/-}$ livers did show did show significant lipid peroxidation following fasting (**Figure 4-2H**). These data show that mice with a loss of hepatic fatty acid β-oxidation can adapt to maintain systemic energy homeostasis during a fast but not without adverse consequences to the liver and adipose tissue stores.

Fasting increases oxidative and suppresses lipogenic programing in livers of Cpt2$^{L-/-}$ mice.

Given the robust physiological and cellular adaptations in Cpt2$^{L-/-}$ mice, we determined hepatic gene expression of select fatty acid metabolic genes in fed and fasted Cpt2$^{lox/lox}$ and Cpt2$^{L-/-}$ mice. First we determined the expression of fatty acid oxidation genes. In the fed state, there were increases in *acsl1, acot1* and *acot2* mRNA in the livers of Cpt2$^{L-/-}$ mice (**Figure 4-4A**). Acot1 and Acot2 were also increased at the protein level in the livers of fed Cpt2$^{L-/-}$ mice (**Figure 4-4B**). Following a 24-hour fast, the increases in *acot1* and *acot2* in the livers of fed Cpt2$^{L-/-}$ mice were greatly exacerbated as well as increases in the fatty acid oxidative genes, *Acox1*, *AcadL* and *Hadha* (**Figure 4-4A**). These changes were largely mirrored at the protein level by western blotting (**Figure 4-4B**). Many of the fatty acid biosynthetic genes were suppressed following a 24hr fast in livers of Cpt2$^{L-/-}$ mice compared to Cpt2$^{lox/lox}$ mice (**Figures 4-4B and 4-5A**). Gluconeogenic gene expression was not altered in Cpt2$^{L-/-}$ mice with the exception of Pck2 whose contribution to gluconeogenesis is not well defined (**Figure 4-6A**). Gluconeogenic gene expression was not altered in Cpt2$^{L-/-}$ mice with the exception of pck2 whose contribution to gluconeogenesis is not well defined (**Figure 4-6A**). These data show a robust up-regulation of fatty acid catabolic genes and suppression of fatty acid anabolic genes in the livers of Cpt2$^{L-/-}$ mice that were exacerbated by fasting. This suggests that the fatty acid oxidation deficient livers were attempting to compensate for the lack of fatty acid oxidation in the face of a large lipid burden.

Fasting induces Pparα target genes and procatabolic hepatokines Fgf21, Gdf15, and Igfbp1 in Cpt2$^{L-/-}$ mice.

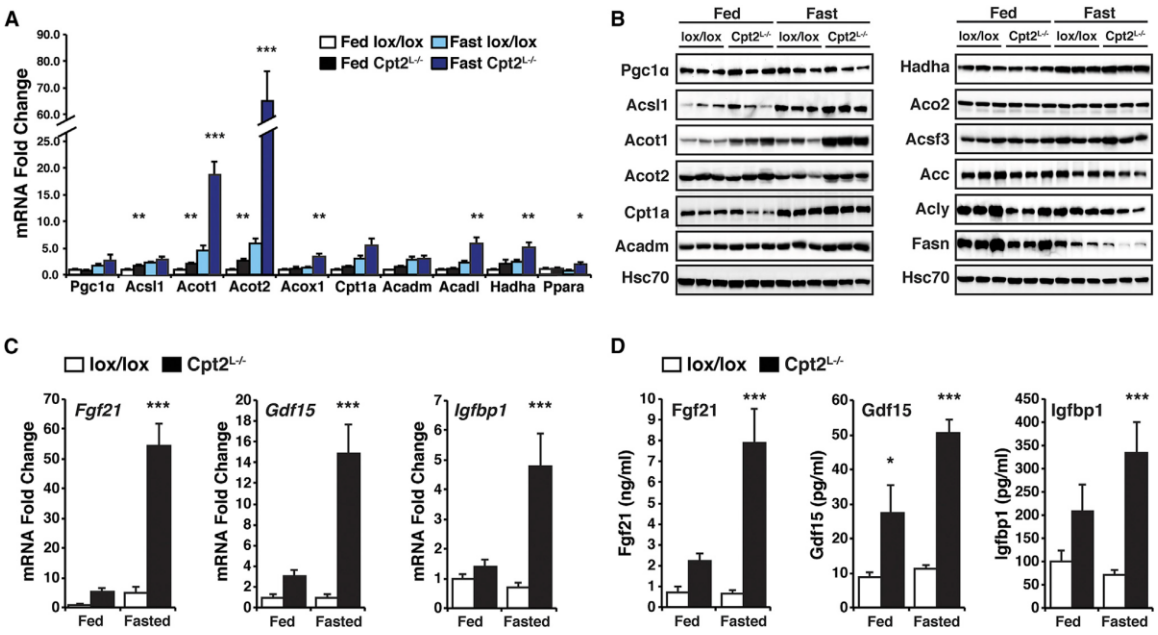

Figure 4-4. Loss of hepatic fatty acid oxidation induces expression of fatty acid oxidative genes.

(A) Gene expression of fatty acid oxidation genes in liver of fed and 24 hr fasted $Cpt2^{lox/lox}$ and $Cpt2^{L-/-}$ mice (n=6).

(B) Western blots of proteins in fatty acid metabolism. Composite of 8 blots. All blots were normalized to Hsc70 (**Figure 4-S2**).

(C) Liver mRNA (n=6) and serum concentrations (n=8) of Fgf21, Gdf15 and Igfbp1 in fed and 24 hr fasted $Cpt2^{lox/lox}$ and $Cpt2^{L-/-}$ mice.

(D) Serum concentration (n=8) of Fgf21, Gdf15 and Igfbp1 in fed and 24-hr fasted $Cpt2^{lox/lox}$ and $Cpt2^{L-/-}$ mice.

Data are expressed as mean ± SEM. *p<0.05; **p<0.01; ***p<0.001.

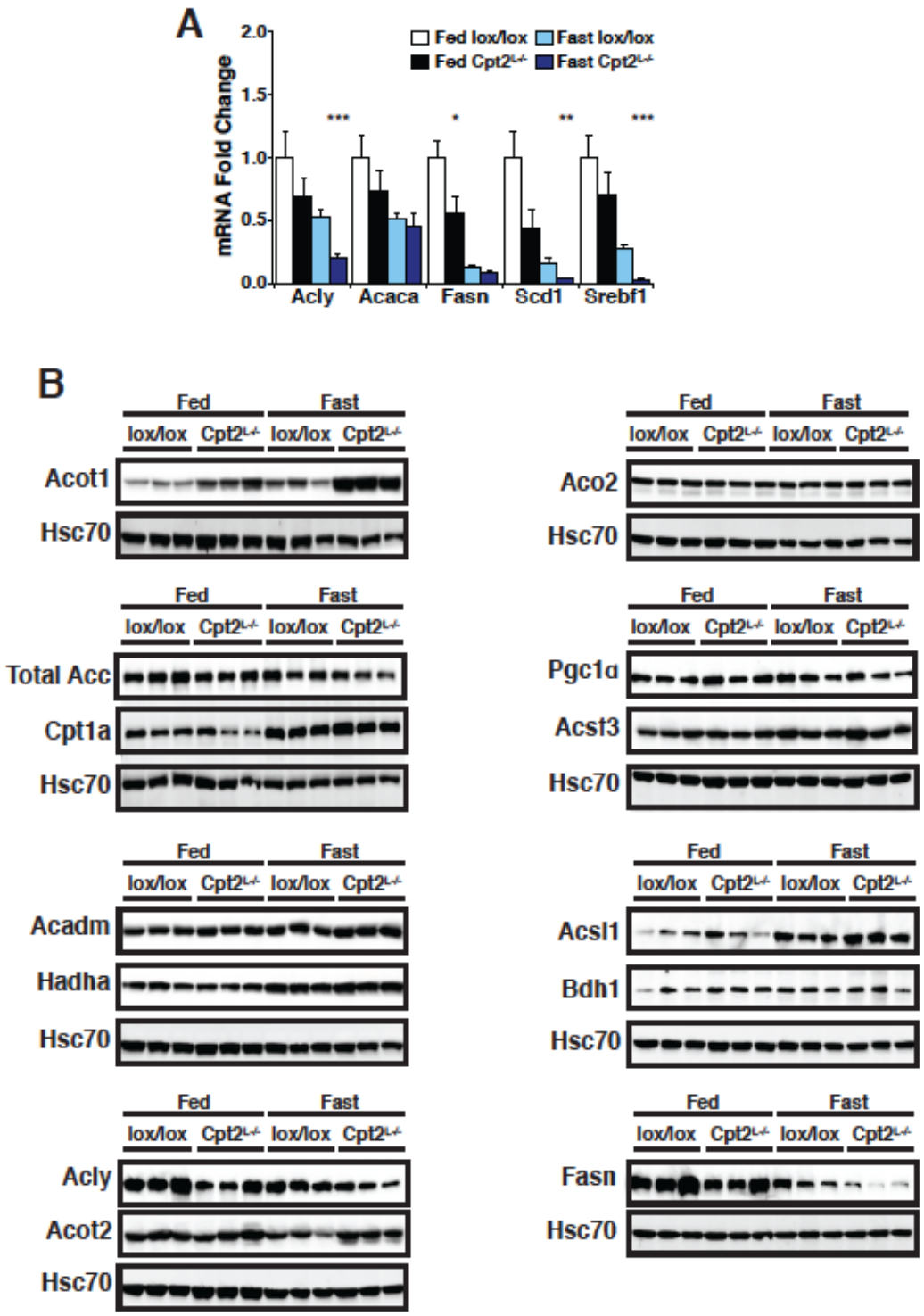

Figure 4-5. The loss of liver fatty acid oxidation alters fatty acid metabolism in the liver.

(A) Gene expression of *de novo* fatty acid biosynthesis genes of fed and 24h fasted $Cpt2^{lox/lox}$ and $Cpt2^{L-/-}$ mice (n=6).

(B) Western blots of proteins involved in fatty acid metabolism with Hsc70 as loading control (n=3).

Data are expressed as mean ± SEM. *p<0.05; **p<0.01; ***p<0.001.

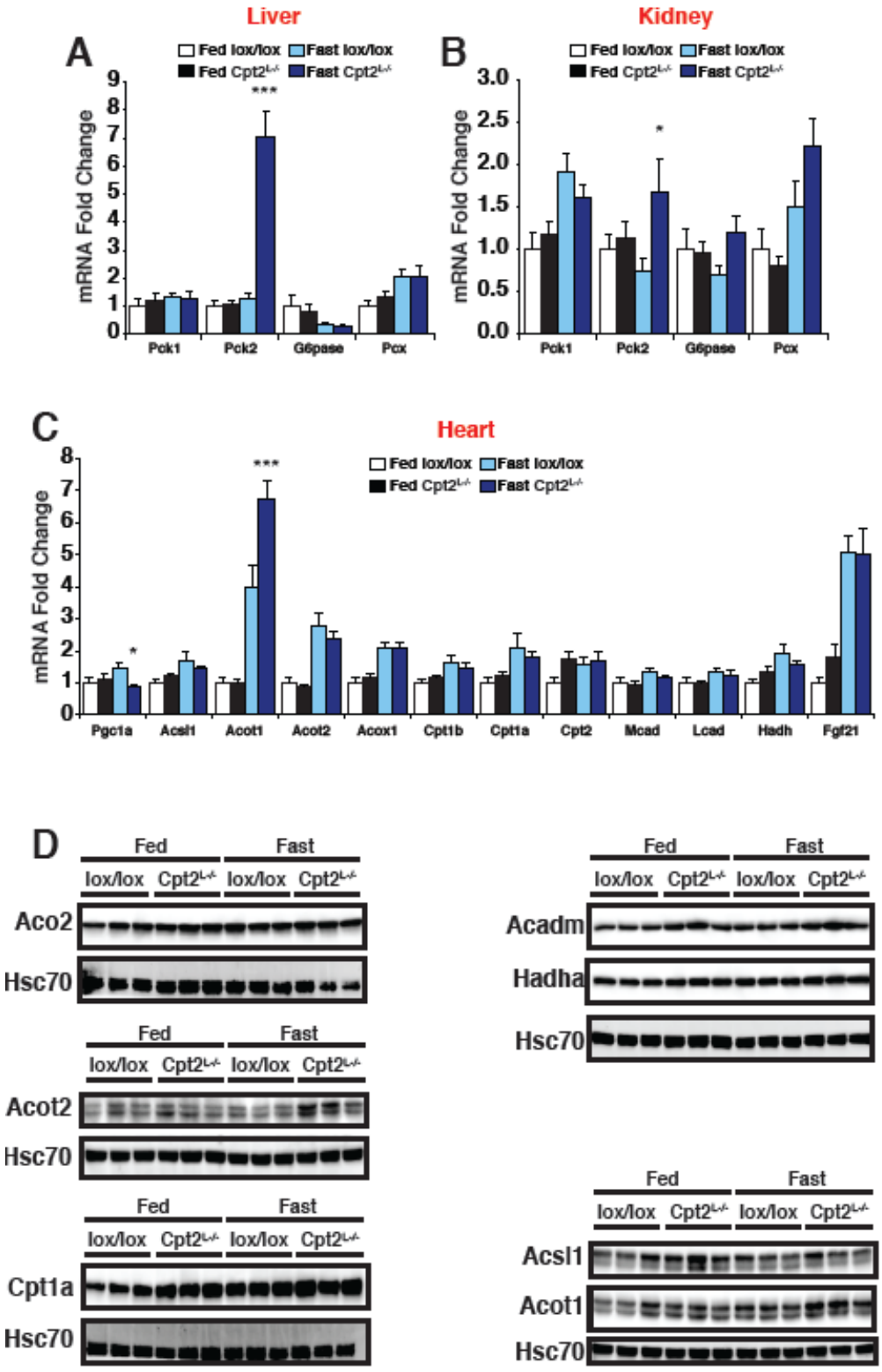
Liver
A
Fed lox/lox
Fast lox/lox
Fed Cpt2L-/-
Fast Cpt2L-/-
mRNA Fold Change
***
Pck1
Pck2
G6pase
Pcx
Kidney
B
*
Heart
C
Pgc1a
Acsl1
Acot1
Acot2
Acox1
Cpt1b
Cpt1a
Cpt2
Mcad
Lcad
Hadh
Fgf21
D
Fed
Fast
lox/lox
Cpt2L-/-
Aco2
Hsc70
Acot2
Cpt1a
Acadm
Hadha
Acsl1
Acot1

Figure 4-6. Gluconeogenic gene expression, cardiac and kidney fatty acid metabolism.

(A) Gene expression of gluconeogenic genes *Pck1, Pck2, G6pase* and *Pcx* in liver of fed and 24h fasted $Cpt2^{lox/lox}$ and $Cpt2^{L-/-}$ mice (n=6).

(B) Gene expression of gluconeogenic genes *Pck1, Pck2, G6pase* and *Pcx* in kidney of fed and 24h fasted $Cpt2^{lox/lox}$ and $Cpt2^{L-/-}$ mice (n=6).

(C) Gene expression of fatty acid oxidation genes in the heart of fed and 24h fasted $Cpt2^{lox/lox}$ and $Cpt2^{L-/-}$ mice (n=6).

(D) Western blots of fatty acid oxidation genes in the kidney with corresponding Hsc70 for each blot as a loading control.

Data are expressed as mean ± SEM. *p<0.05; **p<0.01; ***p<0.001.

Due to the robust transcriptional response in $Cpt2^{L-/-}$ mice, we decided to probe further into the transcriptional alterations in the livers of $Cpt2^{L-/-}$ mice. Therefore, we fasted $Cpt2^{lox/lox}$ and $Cpt2^{L-/-}$ mice for 24hrs for genome wide gene expression profiling on liver mRNA via DNA microarrays (**Table 4-1**). Microarray analysis revealed a dramatic transcriptional dysregulation in the livers of $Cpt2^{L-/-}$ mice upon fasting. In order to validate the microarray results in a larger cohort of mice, we analyzed a subset of genes identified in the microarray analysis by qRT-PCR in both fed and fasted $Cpt2^{lox/lox}$ and $Cpt2^{L-/-}$ mice (**Table 4-1**). Consistent with the robust transcriptional and protein induction of Acot1 and Acot2, other type I ACOTs, canonical Pparα target genes, were also identified in the microarray. Other canonical Pparα target genes were also dramatically up-regulated such as *pdk4* (~100 fold), *ehhadh* (~50 fold), cd*36*, (~10 fold), and *fabp3* (~160 fold) (**Table 4-1**). These data suggest that exogenous fatty acid derived Pparα ligands build up in the face of increased lipid delivery to the liver and are greatly potentiated in the absence of mitochondrial fatty acid oxidation.

We were surprised that although $Cpt2^{L-/-}$ mice had clear metabolic deficiencies, they were able to maintain systemic energy homeostasis even following a 24hr fast. Therefore, we were interested in determining how the $Cpt2^{L-/-}$ liver might be communicating these deficits with other tissues. Of interest was one of the most highly up-regulated genes in the livers of $Cpt2^{L-/-}$ mice (~50 fold), the secreted hepatokine *fgf21* (**Table 4-1, Figure 4-4C**). *Fgf21* is also a canonical Pparα target gene (*74, 75*). Consistent with the transcriptional increase in *fgf21*, serum Fgf21 was increased (~11.5 fold) in fasted $Cpt2^{L-/-}$ mice compared with $Cpt2^{lox/lox}$ littermate controls (**Figure 4-4D**). Additionally, *gdf15* and *igfbp1* mRNA were increased in fasted $Cpt2^{L-/-}$ liver and these

were also increased to a similar degree in $Cpt2^{L-/-}$ serum (**Figures 4-4C, D**). These secreted proteins have all been shown to increase systemic catabolism (*74-78*). These data suggest that the loss of hepatic fatty acid oxidation is mitigated in part by increasing systemic procatabolic hepatokines.

Fasting induces systemic catabolic gene expression in $Cpt2^{L-/-}$ mice.

Some metabolic processes that occur largely in the liver, such as gluconeogenesis, can be supplanted in part by the kidney. Therefore, we postulated that the kidney could be a major site of systemic compensation of energy homeostasis. First, we assessed the regulation of oxidative gene expression in the kidneys of fed and 24hr fasted $Cpt2^{lox/lox}$ and $Cpt2^{L-/-}$ mice. Fasting initiated a robust increase in the expression of genes involved in fatty acid oxidation in the kidneys of $Cpt2^{L-/-}$ mice similar to the elevation in liver (**Figure 4-7A**). A subset of these genes was also validated at the protein level (**Figure 4-7B**). Similar to the liver, gluconeogenic gene expression was not altered in $Cpt2^{L-/-}$ mice with the exception of *Pdk2* (**Figure 4-6B)**. Similar to the liver, gluconeogenic gene expression was not altered in $Cpt2^{L-/-}$ mice with the exception of *pck2* (**Figure 4-6B**). Upon dissection, the kidneys of 24hr fasted $Cpt2^{L-/-}$ mice were visibly lipid laden (**Figure 4-7C**). Although the wet weight of the kidneys of $Cpt2^{lox/lox}$ and $Cpt2^{L-/-}$ mice were similar, the kidneys of $Cpt2^{L-/-}$ mice exhibited a ~2fold increase in total triglycerides consistent with increased uptake of fatty acids (**Figures 4-7D,E**). These data support the kidney as a major site of compensation in fasted $Cpt2^{L-/-}$ mice.

Fgf21 has been shown to regulate ketogenic and oxidative genes in the liver in an autocrine manner. Fgf21 has also been postulated to affect adipocyte energy balance in an endocrine manner (*79*). Since fasting induces a robust increase in circulating Fgf21 in

$Cpt2^{L-/-}$ mice, we examined the some of the putative endocrine effects of Fgf21 treatment in a more physiological model. Interscapular BAT (iBAT) of $Cpt2^{L-/-}$ mice did not exhibit transcriptional increases in thermogenic genes (**Figure 4-7F**), but fasting elicited increases in *ucp1*, *cidea* and *fgf21* in inguinal WAT (iWAT) of $Cpt2^{L-/-}$ mice (**Figure 4-7G**) consistent with fasting induced Fgf21 target gene expression in this tissue (*80*). Adipose-derived Adiponectin has also been shown to be a pharmacologic target of Fgf21 (*81, 82*). However, we did not observe an increase in adiponectin mRNA in gonadal WAT (gWAT) nor did we observe changes in serum Adiponectin between fed or fasting $Cpt2^{lox/lox}$ and $Cpt2^{L-/-}$ mice (**Figure 4-7H**). Due to the robust contribution of skeletal muscle and heart to whole body fatty acid oxidation, we examined fatty acid oxidative gene expression in these tissues. Although the transcriptional response was not as robust as the kidney in these tissues, fasting induced a significant increase in *Acot1* and *Acot2* in $Cpt2^{L-/-}$ gastrocnemius muscle (**Figure 4-7I**) an induced a significant increase in *Acot1* in the $Cpt2^{L-/-}$ heart (**Figure4-6C**). Interestingly, along with liver and iWAT, skeletal muscle of $Cpt2^{L-/-}$ mice also exhibited a significant fasting-induced increase in *Fgf21* expression (**Figure 4-7J**). Together, these data suggest that loss of hepatic fatty acid oxidation may be mitigated in part by the induction of procatabolic hepatokines such as Fgf21 via both cell autonomous and non-cell autonomous mechanisms via both cell autonomous and non-cell autonomous mechanisms.

A ketogenic diet depletes adipose triglyceride stores and is lethal to $Cpt2^{L-/-}$ mice.

Given the putative requirements for hepatic fatty acid oxidation, we were surprised that $Cpt2^{L-/-}$ mice could survive a 24hr fast. To determine how $Cpt2^{L-/-}$ mice

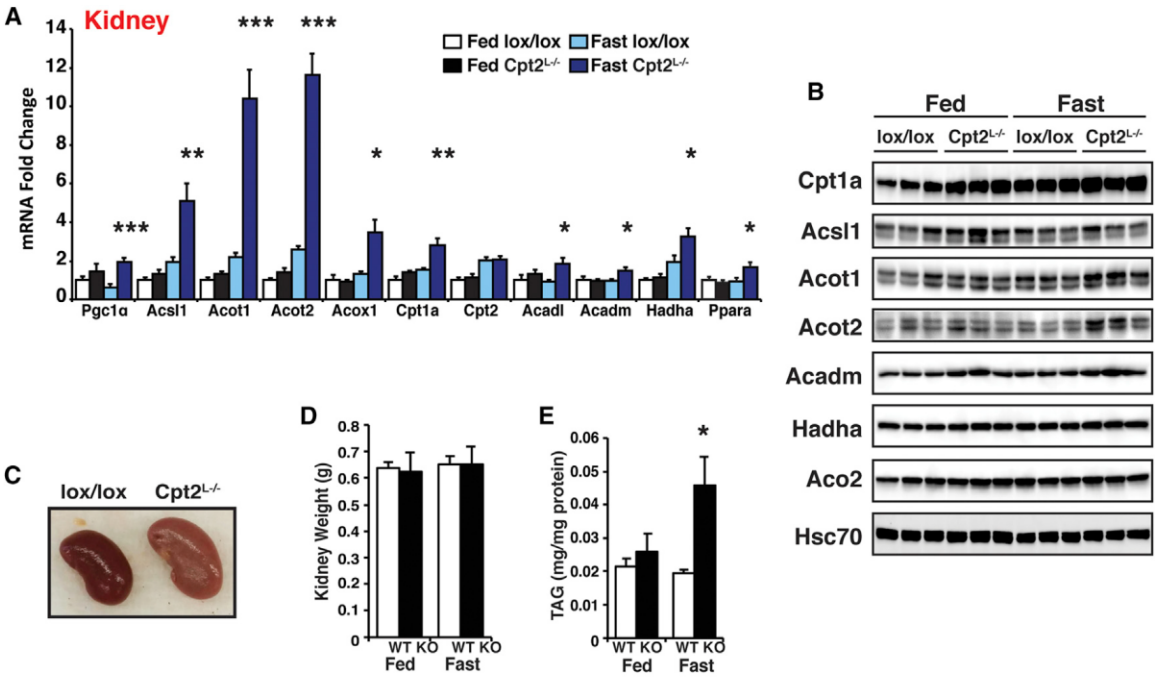
A
Kidney
mRNA Fold Change
Fed lox/lox
Fast lox/lox
Fed Cpt2L-/-
Fast Cpt2L-/-
Pgc1α
Acsl1
Acot1
Acot2
Acox1
Cpt1a
Cpt2
Acadl
Acadm
Hadha
Ppara
B
Fed
Fast
lox/lox
Cpt2L-/-
Cpt1a
Acsl1
Acot1
Acot2
Acadm
Hadha
Aco2
Hsc70
C
lox/lox
Cpt2L-/-
D
Kidney Weight (g)
WT KO
Fed
Fast
E
TAG (mg/mg protein)

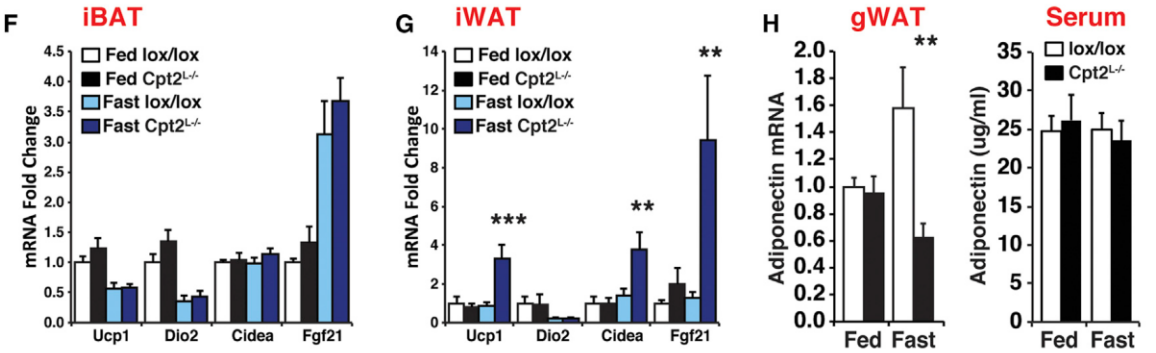
F
iBAT
mRNA Fold Change
Fed lox/lox
Fed Cpt2L-/-
Fast lox/lox
Fast Cpt2L-/-
Ucp1
Dio2
Cidea
Fgf21
G
iWAT
H
gWAT
Adiponectin mRNA
Fed
Fast
Serum
Adiponectin (ug/ml)
lox/lox
Cpt2L-/-

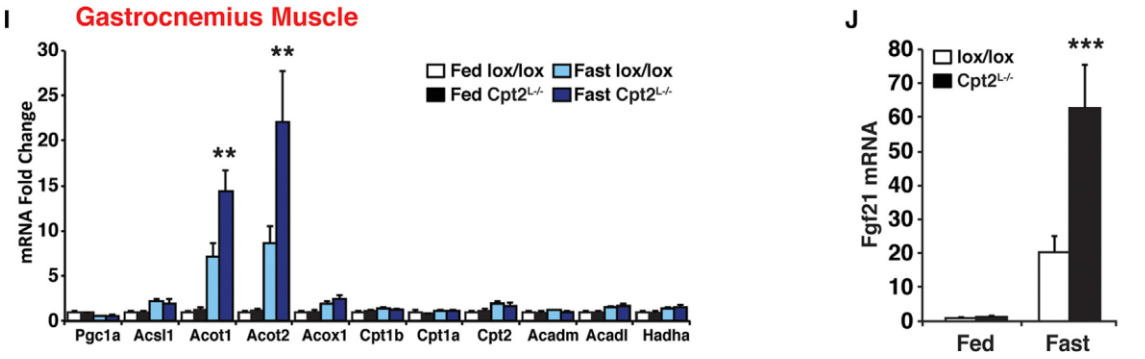
I
Gastrocnemius Muscle
mRNA Fold Change
Fed lox/lox
Fast lox/lox
Fed Cpt2L-/-
Fast Cpt2L-/-
Pgc1a
Acsl1
Acot1
Acot2
Acox1
Cpt1b
Cpt1a
Cpt2
Acadm
Acadl
Hadha
J
Fgf21 mRNA
lox/lox
Cpt2L-/-
Fed
Fast

Figure 4-7. Loss of hepatic fatty acid oxidation results in compensation from the kidney, muscle and adipose tissue.

(A) Gene expression of fatty acid oxidation genes in the kidney of fed and 24 hr fasted $Cpt2^{lox/lox}$ and $Cpt2^{L-/-}$ mice (n=6).
(B) Western blots of proteins in fatty acid metabolism. Composite of 5 blots. All blots were normalized to Hsc70 (**Figure 4-S3**).
(C) Gross kidney morphology in 24 hr fasted $Cpt2^{lox/lox}$ and $Cpt2^{L-/-}$ mice.
(D) Kidney wet weight of fed and 24 hr fasted $Cpt2^{lox/lox}$ and $Cpt2^{L-/-}$ mice (n=6-10).
(E) Kidney TAG content of fed and 24 hr fasted $Cpt2^{lox/lox}$ and $Cpt2^{L-/-}$ mice (n=5).
(F) iBAT gene expression of fed and 24 hr fasted $Cpt2^{lox/lox}$ and $Cpt2^{L-/-}$ mice (n=6).
(G) iWAT gene expression of fed and 24 hr fasted $Cpt2^{lox/lox}$ and $Cpt2^{L-/-}$ mice (n=6).
(H) gWAT adiponectin mRNA (n=6) and Adiponectin serum concentration (n=8) of fed and 24 hr fasted $Cpt2^{lox/lox}$ and $Cpt2^{L-/-}$ mice.
(I) Gene expression of fatty acid oxidation genes in the gastrocnemius muscle of fed and 24 hr fasted $Cpt2^{lox/lox}$ and $Cpt2^{L-/-}$ mice. (n=6).
(J) Gastrocnemius muscle mRNA of *Fgf21* in fed and 24 hr fasted $Cpt2^{lox/lox}$ and $Cpt2^{L-/-}$ mice (n=6).
(K) Gene expression of fatty acid oxidation genes in the gastrocnemius muscle of fed and 24 hr fasted $Cpt2^{lox/lox}$ and $Cpt2^{L-/-}$ mice (n=6).
(L) Gastrocnemius muscle mRNA of *Fgf21* in fed and 24 hr fasted $Cpt2^{lox/lox}$ and $Cpt2^{L-/-}$ mice (n=6).

Data are expressed as mean ± SEM. *p<0.05; **p<0.01; ***p<0.001.

would tolerate a long-term carbohydrate-limited diet, we placed 9-week old $Cpt2^{lox/lox}$ and $Cpt2^{L-/-}$ mice on a low carbohydrate ketogenic diet. After 6 days on the ketogenic diet, several $Cpt2^{L-/-}$ mice died and the remaining $Cpt2^{L-/-}$ mice exhibited a dramatic weight loss (**Figure 4-8A**). $Cpt2^{L-/-}$ mice exhibited hepatomegaly (**Figure 4-8B**) and significant liver damage as measured by serum ALT activity (**Figure 4-8C**). These physiologic indicators were accompanied by severe kyphosis and lethargy, suggesting a neurologic involvement. Additionally, $Cpt2^{L-/-}$ mice became hypoglycemic and hypoketotic with corresponding serum dyslipidemia (**Figure 4-8D**). Incredibly, upon dissection, $Cpt2^{L-/-}$ mice completely lacked observable white adipose tissue following 6 days on a ketogenic diet, consistent with the loss of body weight (**Figure 4-8E**). These data suggest that from a physiological standpoint, $Cpt2^{L-/-}$ mice could not differentiate starvation from a high calorie-low carbohydrate diet.

Fasting and a ketogenic diet share many metabolic features. Therefore, we assessed the gene expression signature of $Cpt2^{lox/lox}$ and $Cpt2^{L-/-}$ mice fed a ketogenic diet for 6 days. Consistent with the microarray data from 24hr fasting liver, the livers from $Cpt2^{L-/-}$ mice exhibited a dramatic increases in Pparα target gene expression compared to control mice (~170-fold increase in *Pdk4*, >50-fold increase in *Elovl7*) (**Table 4-1**). Also, oxidative gene expression in the livers of $Cpt2^{L-/-}$ mice was increased in ketogenic diet-fed mice (**Figure 4-8F**). Gluconeogenic gene expression, serum insulin and oxidative gene expression in the kidney, gastrocnemius muscle, and heart were also consistent with the fasting data (**Figure 4-9**). Finally, we measured the gene expression (**Table 4-1**) and serum concentrations of the secreted hepatokines Fgf21, Gdf15 and Igfbp1 (**Figure 4-8G**). Even through the ketogenic diet elicited a strong induction of those hepatokines in

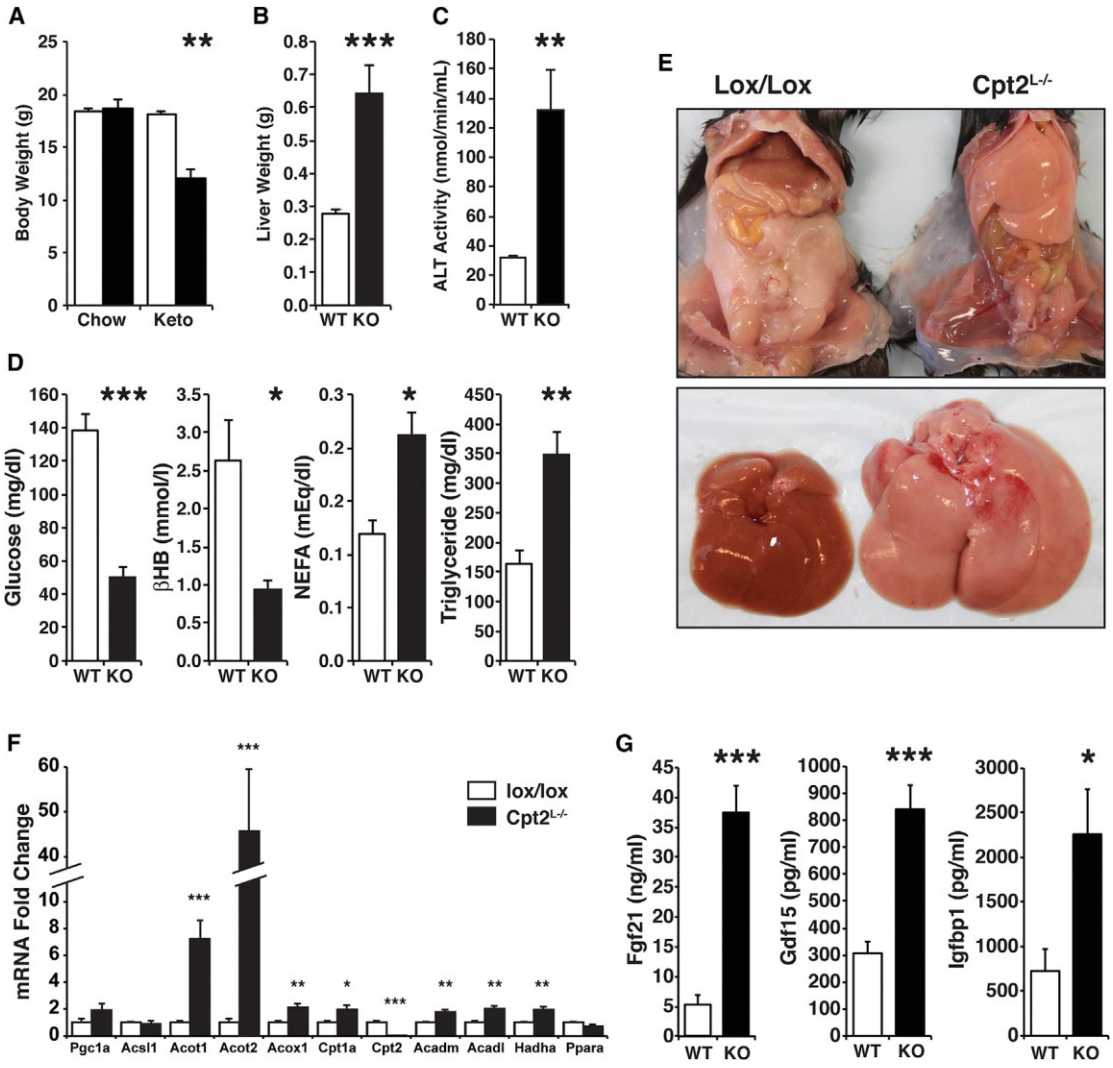

Figure 4-8. A ketogenic diet results in hypoglycemia, a depletion of adipose triglyceride and eventually lethality in Cpt2$^{L-/-}$ mice.

(A) Body weights of Cpt2$^{lox/lox}$ and Cpt2$^{L-/-}$ mice fed a normal chow or ketogenic diet for 6 days (normal chow, n=6-10; ketogenic diet, n=5-6).
(B) Wet weight of liver from Cpt2$^{lox/lox}$ and Cpt2$^{L-/-}$ mice fed a ketogenic diet for 6 days (n=5-6).
(C) Liver damage measured by serum ALT activity of Cpt2$^{lox/lox}$ and Cpt2$^{L-/-}$ mice fed a ketogenic diet (n=5).
(D) Serum metabolites in Cpt2$^{lox/lox}$ and Cpt2$^{L-/-}$ mice after a 6-day ketogenic diet (n=5-6).
(E) Gross morphology of Cpt2$^{lox/lox}$ and Cpt2$^{L-/-}$ mice fed a ketogenic diet.
(F) Gene expression of fatty acid oxidation genes in the liver of Cpt2$^{lox/lox}$ and Cpt2$^{L-/-}$ mice fed a ketogenic diet (n=6).
(G) Serum concentrations of Fgf21, Gdf15 and Igfbp1 of Cpt2$^{lox/lox}$ and Cpt2$^{L-/-}$ mice fed a ketogenic diet (n=6).
(H) Validation of results of microarray by qRTPCR in liver of Cpt2$^{lox/lox}$ and Cpt2$^{L-/-}$ mice fed a ketogenic diet (n=6).
(I) Gene expression of fatty acid oxidation genes in the liver of Cpt2$^{lox/lox}$ and Cpt2$^{L-/-}$ mice fed a ketogenic diet (n=6).
(J) Serum concentrations of Fgf21, Gdf15 and Igfbp1 of Cpt2$^{lox/lox}$ and Cpt2$^{L-/-}$ mice fed a ketogenic diet (n=6).

Data are expressed as mean ± SEM. *p<0.05; **p<0.01; ***p<0.001.

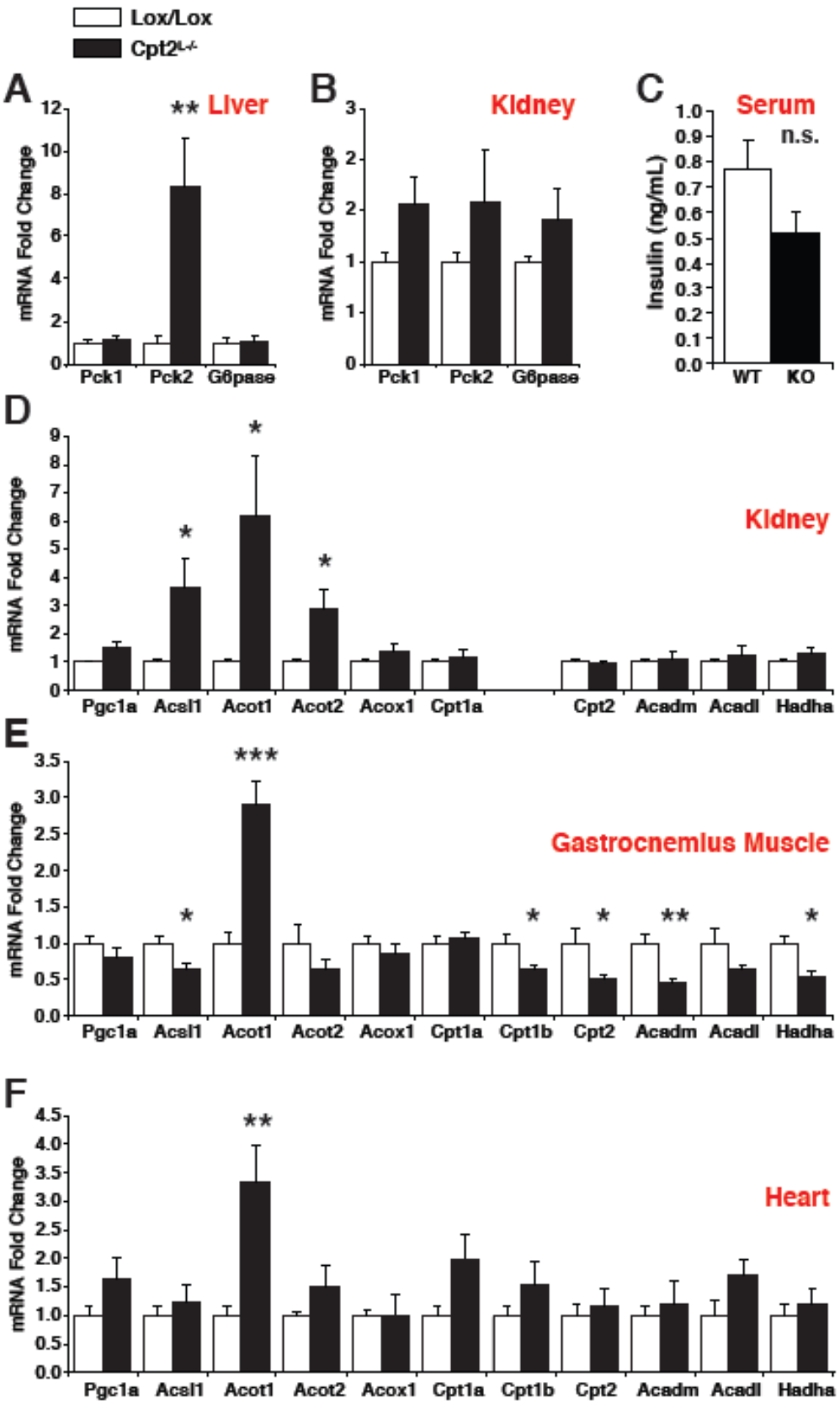
Lox/Lox
Cpt2L-/-
A
** Liver
mRNA Fold Change
Pck1
Pck2
G6pase
B
Kidney
mRNA Fold Change
Pck1
Pck2
G6pase
C
Serum
n.s.
Insulin (ng/mL)
WT
KO
D
Kidney
mRNA Fold Change
Pgc1a
Acsl1
Acot1
Acot2
Acox1
Cpt1a
Cpt2
Acadm
Acadl
Hadha
E
Gastrocnemius Muscle
mRNA Fold Change
Pgc1a
Acsl1
Acot1
Acot2
Acox1
Cpt1a
Cpt1b
Cpt2
Acadm
Acadl
Hadha
F
Heart
mRNA Fold Change
Pgc1a
Acsl1
Acot1
Acot2
Acox1
Cpt1a
Cpt1b
Cpt2
Acadm
Acadl
Hadha

Figure 4-9. A ketogenic diet results in compensation from kidney, gastrocnemius muscle and heart.

(A) Gene expression of gluconeogenic genes *Pck1, Pck2,* and *G6pase* in liver of $Cpt2^{lox/lox}$ and $Cpt2^{L-/-}$ mice fed a ketogenic diet (n=6).

(B) Gene expression of gluconeogenic genes *Pck1, Pck2,* and *G6pase* in kidney of $Cpt2^{lox/lox}$ and $Cpt2^{L-/-}$ mice fed a ketogenic diet (n=6).

(C) Serum concentrations of insulin in $Cpt2^{lox/lox}$ and $Cpt2^{L-/-}$ mice fed a ketogenic diet (n=5-7).

(D) Gene expression of fatty acid oxidation genes in kidney of $Cpt2^{lox/lox}$ and $Cpt2^{L-/-}$ mice fed a ketogenic diet (n=6).

(E) Gene expression of fatty acid oxidation genes in gastrocnemius muscle of $Cpt2^{lox/lox}$ and $Cpt2^{L-/-}$ mice fed a ketogenic diet (n=6).

(F) Gene expression of fatty acid oxidation genes in heart of $Cpt2^{lox/lox}$ and $Cpt2^{L-/-}$ mice fed a ketogenic diet (n=6).

Data are expressed as mean ± SEM. *p<0.05; **p<0.01; ***p<0.001.

control $Cpt2^{lox/lox}$ mice, $Cpt2^{L-/-}$ mice further exacerbated this increase in serum hepatokines. These data show that the ketogenic diet elicits a similar yet further exacerbated physiologic program in $Cpt2^{L-/-}$ mice compared to fasting.

To better determine the kinetics of the ketogenic-induced weight loss and hypoglycemia in mice deficient in hepatic fatty acid β-oxidation, we again placed $Cpt2^{lox/lox}$ and $Cpt2^{L-/-}$ mice on a ketogenic diet and measured their body weights and blood glucose daily over 4 days. $Cpt2^{lox/lox}$ and $Cpt2^{L-/-}$ mice had no significant differences in fed blood glucose (**Figure 4-10A**) or body weight (**Figure 4-10B**) over these 4 days although by day 4, $Cpt2^{L-/-}$ mice had accelerated body weight loss. This indicates that a lack of systemic gluconeogenesis was not the primary cause of lethality in $Cpt2^{L-/-}$ mice.

To determine the systemic metabolic effects of a loss of hepatic Cpt2, we measured blood and tissue acylcarnitines in $Cpt2^{lox/lox}$ and $Cpt2^{L-/-}$ mice before and over the 4-day ketogenic diet challenge. As the liver is a major site of carnitine biosynthesis, there were no changes in free carnitine in the liver; however, there was a significant suppression in free carnitine in the blood of $Cpt2^{L-/-}$ mice, indicating a systemic deficiency (**Figure 4-10C**). Total acylcarnitines and short chain acylcarnitines were significantly suppressed in both chow and ketogenic diet fed blood of $Cpt2^{L-/-}$ mice (**Figure 4-10D, Table 4-2**). However, the substrates specific for Cpt2, long chain acylcarnitines, showed a progressive increase in blood over time, indicating increased hepatic excursion of long chain acylcarnitines in $Cpt2^{L-/-}$ mice (**Figure 4-10E, Table 4-2**). Finally, we measured liver acylcarnitines in chow fed and 4-day ketogenic diet fed mice. Consistent with a block in fatty acid β-oxidation, $Cpt2^{L-/-}$ mice exhibited a suppression in

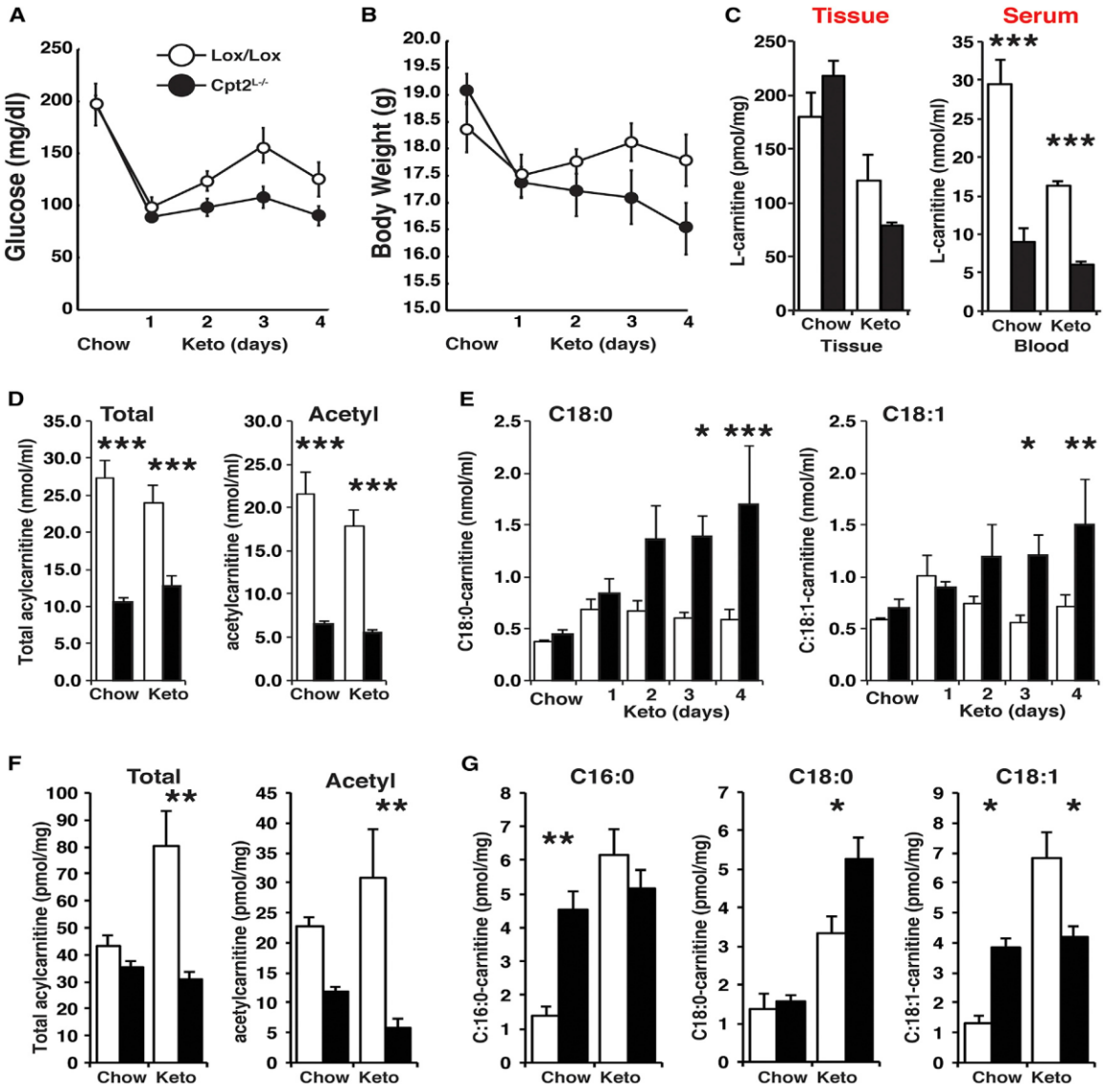

Figure 4-10. Time course of body weight, blood glucose and acylcarnitines in Cpt2$^{L-/-}$ mice fed a ketogenic diet.

(A) Blood glucose of Cpt2$^{lox/lox}$ and Cpt2$^{L-/-}$ mice during a 4-day ketogenic diet (n=5).
(B) Body weight of Cpt2$^{lox/lox}$ and Cpt2$^{L-/-}$ mice during a 4-day ketogenic diet (n=5).
(C) Liver and blood L-carnitine of Cpt2$^{lox/lox}$ and Cpt2$^{L-/-}$ mice following a 4-day ketogenic diet (n=5).
(D) Total blood acylcarnitines and acetylcarnitine of Cpt2$^{lox/lox}$ and Cpt2$^{L-/-}$ mice following a 4-day ketogenic diet (n=5).
(E) Daily blood long chain (C18:0, C18:1) acylcarnitines of Cpt2$^{lox/lox}$ and Cpt2$^{L-/-}$ mice during a 4-day ketogenic diet (n=5).
(F) Total liver acylcarnitines and acetylcarnitine of Cpt2$^{lox/lox}$ and Cpt2$^{L-/-}$ mice following a 4-day ketogenic diet (n=4-5).
(G) Total liver long chain (C16:0, C18:0, C18:1) acylcarnitines and acetylcarnitine of Cpt2$^{lox/lox}$ and Cpt2$^{L-/-}$ mice following a 4-day ketogenic diet (n=4-5).

Data are expressed as mean ± SEM. *p<0.05; **p<0.01; ***p<0.001.

liver acetylcarnitine that was exacerbated by the ketogenic diet (**Figure 4-10F**), and an increase in long chain acylcarnitines even in chow fed mice (**Figure 4-10G, Table 4-3**). These data show that a loss of hepatic fatty acid β-oxidation results in an accelerated depletion of adipose lipid stores and increased peripheral catabolism following fasting or a ketogenic diet that is ultimately unsustainable.

Discussion

The importance of fatty acid β-oxidation is made evident by multiple inborn errors in this pathway that cause serious human disease (*28, 83, 84*). For example, hypomorphic mutations in CPT2 result in metabolic disease of increasing severity. The most severe form presents as hypothermia, cardiomegaly, hepatomegaly and hypoglycemia in the first days of life from the important roles of fatty acid β-oxidation in adipocytes, heart and liver. Additionally, hypomorphic mutations in CPT1a result in hypoketotic-hypoglycemia (*54*) and a loss of CPT1a or CPT1b in mice is early embryonic lethal (*29, 30*). Given that the liver is critical for the adaptation to fasting and fatty acid β-oxidation is central to this response, we asked what the requirements of hepatic fatty acid β-oxidation are *in vivo*. Surprisingly, we found that mice with a hepatocyte-specific deletion of mitochondrial long chain fatty acid β-oxidation not only survived the perinatal period but also survived a 24hr fast with normal blood glucose but a lack of ketone bodies. Perhaps not surprisingly, survival during food deprivation has been so evolutionarily important that multiple compensatory systems are in place for such a critical adaptation.

While blood glucose is maintained within a tight range, ketones can change dramatically from micromolar to millimolar concentrations (*53*). Our data suggests that

the liver produces almost all of the circulating ketones. The total loss of ketone utilization via KO of *Oxct1* results in perinatal lethality in mice (*56*). Therefore we speculate that local ketone production (e.g. within the CNS) or a small amount of fatty acid independent ketogenesis may enable the survival of $Cpt2^{L-/-}$ mice during the perinatal period, a time of robust ketolysis (*85, 86*). Several effects of βHB indirectly associated with its metabolic role have been suggested (*87*). βHB is an endogenous ligand for at least two $G_{i/o}$-coupled GPCRs, HCAR2 and FFAR3, that suppress adipose lipolysis and sympathetic activity respectively (*88, 89*). Given the dramatic peripheral catabolism in ketogenic diet fed $Cpt2^{L-/-}$ mice that have suppressed circulating βHB, these nonmetabolic roles of ketones likely play a significant role in regulating systemic physiology during food deprivation. The inability to affect these two receptors would lead to enhanced fasting lipolysis consistent with $Cpt2^{L-/-}$ mice. Therefore, βHB is likely critical for restraining lipolysis, particularly under conditions where insulin is low.

Pparα has been postulated to be activated by fatty acid derived ligands. Some ligands are thought to be derived from *de novo* fatty acid synthesis (*90-92*), however that seems to be an unlikely driver of fasting gene expression in $Cpt2^{L-/-}$ mice. Alternatively, triglyceride hydrolysis has been shown to be critical for Pparα directed transcription. The loss of Atgl, the rate setting step in triglyceride hydrolysis, results in a loss of Pparα transcription presumably from the loss of an endogenous Pparα ligand produced upon hydrolysis (*93-96*). It will be interesting to determine if lipids derived from lipid droplet triglyceride hydrolysis are required for the increased Pparα mediated transcription in $Cpt2^{L-/-}$ mice or alternatively, if exogenous lipid uptake can directly activate Pparα target genes independent of lipid droplets.

One robust transcriptional target of Pparα is the hepatokine Fgf21 (*74, 75*). Although it is expressed in several tissues, most of the circulating Fgf21 is derived from hepatocytes (*97*). Fgf21 is induced by fasting and ketogenic feeding in rodents and acts largely to increase energy expenditure via an autocrine and endocrine manner (*79*). Fgf21 is emerging as a potential therapeutic for obesity and insulin resistance by increasing glucose uptake in adipocytes and increasing energy expenditure. The robust increase in circulating Fgf21 in $Cpt2^{L-/-}$ mice suggests that it provides some of the signal required to increase systemic catabolism to maintain energy homeostasis although Gdf15 and Igfbp1 likely also contribute. Consistent with $Cpt2^{L-/-}$ mice, humans with mitochondrial disease exhibit increased circulating FGF21 (*98*). The loss of the anti-catabolic βHB and the gain of procatabolic hepatokines such as Fgf21, Gdf15 and Igfbp1, likely all contribute to the exaggerated lipolysis seen in $Cpt2^{L-/-}$ mice upon fasting or ketogenic feeding, and mitigate hepatic energy expenditure defects in mice without the capacity for long chain mitochondrial fatty acid β-oxidation.

It is clear that the liver plays an important role in regulating systemic metabolism, and that hepatic fatty acid β-oxidation represents an important component, particularly when carbohydrate intake is limiting. However, our data shows that there is an incredible systemic adaptation mediated by the liver to regulate extra-hepatic metabolism to ensure survival. These data highlight the need to better understand the tissue-specific contributions of macronutrient metabolism to gain insight into the regulation of integrative metabolic physiology.

Table 4-1. Microarray on liver of 24-hr fasted $Cpt2^{lox/lox}$ and $Cpt2^{L-/-}$ mice.

Table 1. Fasting and Diet-Induced Gene Expression in $Cpt2^{L-/-}$ Liver

	Fasted	Fed		Fasted		Ketogenic Diet	
Gene	Array KO/WT	Lox/Lox	$Cpt2^{L-/-}$	Lox/Lox	$Cpt2^{L-/-}$	Lox/Lox	$Cpt2L^{-/-}$
Pdk4	30.5	1.0 ± 0.17	3.9 ± 0.39	1.2 ± 0.30	99.0 ± 16.22***	1.0 ± 0.34	178.9 ± 41.42**
Elovl7	13.3	1.0 ± 0.17	2.1 ± 0.33	0.9 ± 0.24	174.9 ± 31.58***	1.0 ± 0.46	58.7 ± 9.38***
Gpnmb	10.2	1.0 ± 0.26	2.2 ± 0.27	2.1 ± 0.51	301.7 ± 67.18***	1.0 ± 0.35	134.9 ± 12.60***
Cpt1b	8.9	1.0 ± 0.10	4.4 ± 1.25	6.1 ± 2.42	84.5 ± 14.39***	1.0 ± 0.23	9.9 ± 2.95*
Phospho1	7.6	1.0 ± 0.20	3.5 ± 0.22	1.8 ± 0.50	30.2 ± 7.71***	1.0 ± 0.26	15.3 ± 3.18***
Fgf21	6.0	1.0 ± 0.15	5.4 ± 1.00	4.9 ± 2.12	54.6 ± 7.02***	1.0 ± 0.26	13.9 ± 3.18**
Fabp3	5.8	1.0 ± 0.18	1.4 ± 0.24	2.4 ± 0.31	161.1 ± 21.31***	1.0 ± 0.19	32.0 ± 3.71***
Atf3	5.4	1.0 ± 0.16	2.1 ± 0.43	0.9 ± 0.10	28.4 ± 4.18***	1.0 ± 0.40	15.8 ± 2.58***
Cd68	5.0	1.0 ± 0.11	1.2 ± 0.27	0.8 ± 0.18	8.0 ± 1.09***	1.0 ± 0.19	2.1 ± 0.15**
Igfbp1	4.4	1.0 ± 0.16	1.4 ± 0.25	0.7 ± 0.18	4.8 ± 1.08***	1.0 ± 0.33	42.6 ± 13.62*
Acot2	4.4	1.0 ± 0.23	2.6 ± 0.52	5.8 ± 0.96	65.2 ± 11.33***	1.0 ± 0.30	45.7 ± 13.80***
Plin4	4.2	1.0 ± 0.17	1.0 ± 0.25	1.0 ± 0.23	7.6 ± 1.04***	1.0 ± 0.12	6.5 ± 1.07***
Jun	3.1	1.0 ± 0.17	1.8 ± 0.40	1.3 ± 0.42	5.8 ± 1.42***	1.0 ± 0.22	4.4 ± 0.46***
Cd36	3.0	1.0 ± 0.15	1.7 ± 0.25	1.5 ± 0.28	9.9 ± 2.51***	1.0 ± 0.26	7.5 ± 0.94***
Gdf15	3.0	1.0 ± 0.24	3.1 ± 0.49	1.0 ± 0.24	14.9 ± 2.81***	1.0 ± 0.33	10.1 ± 1.47***
Acot1	3.0	1.0 ± 0.10	2.1 ± 0.23	4.5 ± 1.05	18.7 ± 2.47***	1.0 ± 0.12	7.2 ± 1.41***
Agpat9	2.9	1.0 ± 0.15	4.0 ± 0.84	2.7 ± 0.49	10.1 ± 1.80***	1.0 ± 0.21	3.2 ± 0.52 **
Pex11a	2.9	1.0 ± 0.08	1.8 ± 0.30	1.4 ± 0.35	4.5 ± 0.73***	1.0 ± 0.07	2.2 ± 0.24***
Ehhadh	2.5	1.0 ± 0.21	1.4 ± 0.27	8.7 ± 1.54	49.4 ± 6.72***	1.0 ± 0.16	10.1 ± 1.95***
Acot6	2.5	1.0 ± 0.22	2.3 ± 0.44	2.2 ± 0.52	6.9 ± 1.59***	1.0 ± 0.20	1.8 ± 0.43
Myc	2.4	1.0 ± 0.17	1.2 ± 0.12	3.8 ± 0.95	10.8 ± 2.23***	1.0 ± 0.28	5.4 ± 1.24 **
Gpd2	2.2	1.0 ± 0.16	1.3 ± 0.29	0.7 ± 0.12	1.9 ± 0.38**	1.0 ± 0.20	2.7 ± 0.59 **
Mtor	2.2	1.0 ± 0.17	1.6 ± 0.28	1.3 ± 0.14	3.2 ± 0.51***	1.0 ± 0.07	2.0 ± 0.43 *
Plin5	2.2	1.0 ± 0.15	1.1 ± 0.28	1.6 ± 0.32	5.6 ± 0.55***	1.0 ± 0.19	4.4 ± 1.14 **
Plin3	2.2	1.0 ± 0.13	1.3 ± 0.19	1.2 ± 0.18	3.5 ± 0.46***	1.0 ± 0.15	2.8 ± 0.30***

Table 4-2. Daily blood acylcarnitine profile of $Cpt2^{lox/lox}$ and $Cpt2^{L-/-}$ mice fed a chow diet then a ketogenic diet for 4 days.

Acylcarnitines (nmol/ml)	Lox/Lox					Cpt2L-/-				
	Chow	1	2	3	4	Chow	1	2	3	4
Total	27.406 ± 2.206	26.094 ± 2.42	20.704 ± 1.351	21.222 ± 1.877§	23.928 ± 2.42§	7.15 ± 0.571####	8.366 ± 0.96####	9.27 ± 1.242####	9.53 ± 0.675####	10.616 ± 1.357####
C0	29.424 ± 3.309	17.332 ± 1.975§§§§	15.672 ± 2.025§§§§	16.672 ± 0.729§§§§	16.278 ± 1.634§§§§	4.478 ± 0.576####	3.56 ± 0.633####	4.005 ± 0.416####	3.748 ± 0.259####	3.803 ± 0.337####
C2	21.616 ± 2.423	19.296 ± 2.344	14.884 ± 0.989§§§	15.604 ± 1.234§§	17.858 ± 1.795	3.458 ± 0.3####	3.538 ± 0.579####	2.948 ± 0.151####	2.964 ± 0.391####	3.024 ± 0.344####
C3	0.644 ± 0.084	0.896 ± 0.141	0.684 ± 0.057	0.658 ± 0.078§	0.57 ± 0.099§	0.066 ± 0.005####	0.172 ± 0.021####	0.114 ± 0.007####	0.088 ± 0.006####	0.076 ± 0.015####
C3-DC	0.142 ± 0.031	0.118 ± 0.015	0.154 ± 0.013	0.11 ± 0.026	0.134 ± 0.015	0.06 ± 0.01##	0.052 ± 0.008#	0.082 ± 0.01#	0.05 ± 0.007	0.074 ± 0.01
C4	0.47 ± 0.106	0.332 ± 0.038	0.31 ± 0.039	0.328 ± 0.048	0.354 ± 0.038	0.166 ± 0.036###	0.206 ± 0.031	0.238 ± 0.025	0.254 ± 0.032	0.274 ± 0.057
C4-OH	0.23 ± 0.017	0.284 ± 0.014	0.328 ± 0.048	0.376 ± 0.079§§	0.44 ± 0.054§§	0.058 ± 0.015##	0.102 ± 0.018##	0.084 ± 0.017##	0.112 ± 0.017##	0.09 ± 0.006*,####
C4-DC	0.098 ± 0.011	0.098 ± 0.016	0.086 ± 0.005	0.112 ± 0.025	0.112 ± 0.032	0.048 ± 0.007	0.05 ± 0.013	0.05 ± 0.007	0.046 ± 0.005##	0.036 ± 0.004##
C5:1	0.014 ± 0.002	0.016 ± 0.002	0.02 ± 0.006	0.022 ± 0.006	0.018 ± 0.006	0.026 ± 0.008	0.012 ± 0.004	0.022 ± 0.006	0.012 ± 0.002	0.268 ± 0.241
C5	0.066 ± 0.006	0.062 ± 0.011	0.068 ± 0.024	0.096 ± 0.004	0.07 ± 0.005	0.024 ± 0.006#	0.026 ± 0.005	0.024 ± 0.004#	0.032 ± 0.006#	0.038 ± 0.007
C5-OH	0.088 ± 0.01	0.082 ± 0.008	0.062 ± 0.009	0.074 ± 0.01	0.098 ± 0.015	0.026 ± 0.005####	0.028 ± 0.006###	0.036 ± 0.005	0.034 ± 0.006##	0.028 ± 0.002####
C5-DC/C10-OH	0.026 ± 0.002	0.028 ± 0.006	0.032 ± 0.005	0.032 ± 0.006	0.034 ± 0.004	0.01 ± 0	0.022 ± 0.005	0.018 ± 0.004	0.028 ± 0.007	0.026 ± 0.008
C6	0.086 ± 0.012	0.098 ± 0.019	0.076 ± 0.005	0.084 ± 0.012	0.104 ± 0.018	0.052 ± 0.007	0.052 ± 0.008#	0.042 ± 0.002	0.062 ± 0.012	0.044 ± 0.007##
C8:1	0.042 ± 0.007	0.028 ± 0.004	0.032 ± 0.004	0.03 ± 0.004	0.036 ± 0.012	0.028 ± 0.002	0.024 ± 0.006	0.028 ± 0.006	0.026 ± 0.007	0.03 ± 0.005
C8	0.09 ± 0.023	0.084 ± 0.009	0.07 ± 0.008	0.092 ± 0.012	0.124 ± 0.035	0.038 ± 0.006	0.028 ± 0.004	0.022 ± 0.002	0.034 ± 0.007#	0.032 ± 0.004###
C10:1	0.122 ± 0.053	0.074 ± 0.011	0.058 ± 0.01	0.102 ± 0.03	0.114 ± 0.023	0.042 ± 0.004	0.052 ± 0.009	0.052 ± 0.013	0.044 ± 0.009	0.068 ± 0.012
C10	0.052 ± 0.009	0.054 ± 0.009§	0.06 ± 0.003	0.064 ± 0.008	0.09 ± 0.018*,§	0.026 ± 0.007	0.036 ± 0.008	0.028 ± 0.005	0.02 ± 0.003##	0.032 ± 0.005####
C12:1	0.032 ± 0.002	0.028 ± 0.004	0.03 ± 0.004	0.036 ± 0.006	0.034 ± 0.009	0.024 ± 0.006	0.028 ± 0.006	0.018 ± 0.004	0.024 ± 0.005	0.016 ± 0.004
C12	0.108 ± 0.02	0.098 ± 0.019	0.08 ± 0.006	0.122 ± 0.031	0.098 ± 0.014	0.056 ± 0.012	0.052 ± 0.008	0.048 ± 0.006	0.062 ± 0.006#	0.062 ± 0.007
C12:1-OH	0.04 ± 0.015	0.026 ± 0.002	0.024 ± 0.005	0.038 ± 0.021	0.022 ± 0.004	0.018 ± 0.004	0.018 ± 0.004	0.02 ± 0.004	0.022 ± 0.004	0.018 ± 0.004
C12-OH	0.03 ± 0.01	0.026 ± 0.002	0.034 ± 0.008	0.026 ± 0.006	0.03 ± 0.003	0.008 ± 0.002#	0.012 ± 0.002	0.016 ± 0.005	0.012 ± 0.002	0.014 ± 0.002
C14:2	0.05 ± 0.014	0.036 ± 0.009	0.028 ± 0.005	0.034 ± 0.007	0.036 ± 0.005	0.044 ± 0.007	0.024 ± 0.002	0.03 ± 0.007	0.036 ± 0.005	0.036 ± 0.004
C14:1	0.104 ± 0.025	0.108 ± 0.008	0.096 ± 0.012	0.122 ± 0.023	0.102 ± 0.014	0.084 ± 0.009	0.056 ± 0.009	0.062 ± 0.008	0.096 ± 0.017	0.062 ± 0.011
C14	0.172 ± 0.008*	0.304 ± 0.048	0.256 ± 0.025	0.264 ± 0.063	0.222 ± 0.033	0.14 ± 0.016	0.138 ± 0.014#	0.136 ± 0.012#	0.168 ± 0.024	0.158 ± 0.02
C14:1-OH	0.034 ± 0.005	0.05 ± 0.011	0.038 ± 0.008	0.052 ± 0.008	0.04 ± 0.007	0.024 ± 0.005	0.024 ± 0.005	0.024 ± 0.005	0.034 ± 0.005	0.024 ± 0.01
C14-OH	0.046 ± 0.015	0.048 ± 0.004	0.038 ± 0.002	0.06 ± 0.013	0.058 ± 0.006	0.018 ± 0.004#	0.016 ± 0.002#	0.014 ± 0.002	0.016 ± 0.002###	0.016 ± 0.004###
C16:1	0.122 ± 0.007	0.162 ± 0.032	0.11 ± 0.017	0.12 ± 0.027	0.126 ± 0.025	0.174 ± 0.017	0.14 ± 0.01	0.148 ± 0.026	0.198 ± 0.03	0.176 ± 0.025
C16	1.424 ± 0.041	1.392 ± 0.3	1.158 ± 0.139	0.996 ± 0.142	1.144 ± 0.136	0.942 ± 0.124	1.368 ± 0.129	1.726 ± 0.329	1.688 ± 0.211	2.012 ± 0.382*,#
C16:1-OH	0.062 ± 0.01	0.09 ± 0.014	0.076 ± 0.014	0.074 ± 0.019	0.092 ± 0.018	0.038 ± 0.009	0.064 ± 0.01§	0.108 ± 0.017*	0.114 ± 0.013*	0.148 ± 0.034***
C16-OH	0.054 ± 0.007*	0.07 ± 0.008	0.08 ± 0.008	0.074 ± 0.015	0.094 ± 0.024	0.018 ± 0.002	0.014 ± 0.004##	0.024 ± 0.007##	0.02 ± 0.003##	0.022 ± 0.004##
C18:2	0.254 ± 0.021	0.278 ± 0.05	0.216 ± 0.031	0.158 ± 0.023	0.226 ± 0.038	0.214 ± 0.027	0.214 ± 0.013	0.258 ± 0.046	0.274 ± 0.056	0.292 ± 0.038
C18:1	0.586 ± 0.012	1.01 ± 0.198	0.736 ± 0.081	0.552 ± 0.07	0.706 ± 0.113	0.714 ± 0.087	0.866 ± 0.065§	1.278 ± 0.316	1.336 ± 0.204#	1.66 ± 0.44*,§§,#
C18	0.378 ± 0.017	0.69 ± 0.1	0.674 ± 0.094	0.598 ± 0.052#	0.588 ± 0.098###	0.462 ± 0.04	0.876 ± 0.136§	1.5 ± 0.323**	1.554 ± 0.192**	1.918 ± 0.563****
C18:2-OH	0.032 ± 0.012	0.024 ± 0.004	0.016 ± 0.002	0.014 ± 0.005	0.024 ± 0.005	0.016 ± 0.004	0.014 ± 0.002	0.022 ± 0.006	0.014 ± 0.002	0.022 ± 0.002
C18:1-OH	0.044 ± 0.01	0.062 ± 0.008	0.054 ± 0.007	0.054 ± 0.014	0.072 ± 0.019	0.024 ± 0.002	0.022 ± 0.002	0.04 ± 0.01	0.046 ± 0.008	0.046 ± 0.018
C18-OH	0.034 ± 0.004	0.042 ± 0.008	0.042 ± 0.004	0.044 ± 0.005	0.06 ± 0.009*	0.01 ± 0##	0.01 ± 0###	0.014 ± 0.002##	0.01 ± 0.003####	0.016 ± 0.004####

Symbol	Significance
*	Chow vs. Keto; *$p<0.05$; **$p<0.01$; ***$p<0.001$; ****$p<0.0001$
#	Lox/Lox vs. Cpt2L-/-; #$p<0.05$; ##$p<0.01$; ###$p<0.001$; ####$p<0.0001$
§	Effect of time (day1-day5); §$p<0.05$; §§$p<0.01$; §§§$p<0.001$;§§§§$p<0.0001$

Table 4-3. Liver acylcarnitine profile of $Cpt2^{lox/lox}$ and $Cpt2^{L-/-}$ mice fed a chow diet or a ketogenic diet for 4 days.

Acylcarnitines (pmol/mg)	Lox/Lox		$Cpt2^{L-/-}$	
	Chow	Keto	Chow	Keto
Total	43.41 ± 3.58	80.34 ± 12.9*,##	35.23 ± 2.3	30.65 ± 3.23
C0	179.69 ± 21.85	120.04 ± 24.04	218.07 ± 13.26	79.63 ± 3.25***
C2	22.65 ± 1.67	30.83 ± 8.03	11.75 ± 0.9	5.88 ± 1.38 #
C3	4.87 ± 1.02	2.11 ± 0.4*	2.17 ± 0.38#	1.06 ± 0.12
C3-DC	1.27 ± 0.27	0.49 ± 0.09*	0.28 ± 0.03	0.08 ± 0.02##
C4	2.36 ± 0.38	2.58 ± 0.46	0.3 ± 0.05##	0.39 ± 0.03##
C4-OH	2.55 ± 0.61	1.9 ± 0.31	0.11 ± 0.01##	0.05 ± 0.01#
C4-DC	0.19 ± 0.05	0.84 ± 0.18**	0.11 ± 0.06	0.35 ± 0.08
C5:1	0.01 ± 0	0.01 ± 0	0.01 ± 0	0 ± 0#
C5	0.31 ± 0.06	0.32 ± 0.07	0.12 ± 0.01	0.03 ± 0.01##
C5-OH	0.15 ± 0.02	0.21 ± 0.04	0.09 ± 0.01	0.01 ± 0###
C5-DC/C10-OH	1.75 ± 0.55	4.79 ± 0.62*	4.91 ± 0.6##	3.64 ± 0.56
C6	0.17 ± 0.04	0.47 ± 0.08**	0.1 ± 0.01	0.05 ± 0.01###
C8:1	0.05 ± 0.01	0.09 ± 0.03	0.03 ± 0.01	0.05 ± 0
C8	0.2 ± 0.05	3.74 ± 0.9***	0.09 ± 0.01	0.1 ± 0.02###
C10:1	0.04 ± 0	0.11 ± 0.01****	0.03 ± 0	0.06 ± 0.01##
C10	0.04 ± 0.01	0.28 ± 0.06***	0.03 ± 0.01	0.06 ± 0.01##
C12:1	0.03 ± 0	0.23 ± 0.05***	0.03 ± 0.01	0.06 ± 0.01##
C12	0.19 ± 0.03	1.76 ± 0.26****	0.18 ± 0.03	0.32 ± 0.03####
C12:1-OH	0.09 ± 0.01	0.44 ± 0.06****	0.04 ± 0.01	0.04 ± 0####
C12-OH	0.58 ± 0.09	0.98 ± 0.11*	0.32 ± 0.06	0.28 ± 0.04###
C14:2	0.03 ± 0	0.33 ± 0.06****	0.06 ± 0.01	0.13 ± 0.02##
C14:1	0.1 ± 0.01	1.15 ± 0.24***	0.15 ± 0.02	0.22 ± 0.03##
C14	0.28 ± 0.06	3.36 ± 0.61****	0.57 ± 0.08	1.22 ± 0.1##
C14:1-OH	0.04 ± 0.01	0.44 ± 0.08****	0.05 ± 0.01	0.16 ± 0.02##
C14-OH	0.14 ± 0.04	1.13 ± 0.28**	0.04 ± 0.01	0.04 ± 0##
C16:1	0.26 ± 0.07	1.28 ± 0.21**	1.37 ± 0.18###	0.39 ± 0.09**,##
C16	1.37 ± 0.27	6.16 ± 0.76****	4.56 ± 0.51##	5.16 ± 0.56
C16:1-OH	0.09 ± 0.01	0.47 ± 0.07****	0.09 ± 0.01	0.36 ± 0.04**
C16-OH	0.09 ± 0.02	0.31 ± 0.08**	0.05 ± 0.01	0.05 ± 0.01##
C18:2	0.64 ± 0.08	2.8 ± 0.43***	2.07 ± 0.19##	0.82 ± 0.09*, ###
C18:1	1.32 ± 0.27	6.82 ± 0.84****	3.84 ± 0.3#	4.17 ± 0.4#
C18	1.37 ± 0.41	3.34 ± 0.43*	1.58 ± 0.13****	5.28 ± 0.54#
C18:2-OH	0.05 ± 0.01	0.12 ± 0.02**	0.02 ± 0	0.03 ± 0##
C18:1-OH	0.09 ± 0.02	0.3 ± 0.08*	0.04 ± 0.01	0.07 ± 0.01#
C18-OH	0.06 ± 0.01	0.15 ± 0.02***	0.02 ± 0	0.02 ± 0####

Symbol	Significance
*	Chow vs. Keto; *p<0.05; **p<0.01; ***p<0.005; ****p<0.001
#	Lox/Lox vs. Cpt2L-/-; #p<0.05; ##p<0.01; ###p<0.005; ####p<0.001

TISSUE SPECIFIC ROLES OF FATTY ACID OXIDATION

CHAPTER 5. Metabolomic profiling reveals a role for CPT1c in neuronal oxidative metabolism

Introduction

Although the mammalian brain is lipid rich and mutations in lipid metabolizing enzymes result in debilitating neurological disease, neurons are generally not thought to rely on mitochondrial fatty acid beta-oxidation for bioenergetic requirements. Neurons instead mainly utilize the oxidation of glucose for most of their bioenergetics needs, although, during prolonged fasting, ketone bodies (i.e. acetoacetate and beta hydroxybutyrate) can also be used (60). Most neurons have a low amount of the rate-setting enzymes in mitochondrial long chain fatty acid catabolism, namely, the malonyl-CoA sensitive Carnitine Palmitoyltransferase 1 (CPT1a and CPT1b) enzymes which limit most neurons potential for mitochondrial fatty acid beta-oxidation (146).

Carnitine acyltransferases are enzymes that catalyze the exchange of acyl groups between carnitine and Coenzyme A (CoA) to facilitate the transport acyl chains between the cytoplasm to the mitochondrial matrix (147). CPT1 isoenzymes (EC 2.3.1.21) preferentially are positioned on the outer mitochondrial membrane and transfer long chain acyl groups from CoA to carnitine. CPT1a and CPT1b are malonyl-CoA sensitive and therefore inhibited when malonyl-CoA levels are high (e.g. during high glucose flux). The malonyl-CoA insensitive CPT2, on the other hand, is located in the mitochondrial matrix and reversibly transfers the acyl chain back to CoA to facilitate beta-oxidation. Although neurons have a relative dearth of CPT1a and CPT1b [2], they express a CPT1 homologue, CPT1c (148).

CPT1c has a high primary amino acid sequence similarity and identity to the canonical CPT enzymes. Therefore, it was surprising that definitive acyltransferase activity or enhanced oxidation of fatty acids could not be shown for CPT1c (148-150).

CPT1c KO mice exhibit both behavioral and metabolic deficits (150-153). Over-expression of CPT1c in the brain of developing transgenic mice results in microencephaly (70). Therefore, it is clear that CPT1c plays an important role in brain function. Although there were several metabolites identified that have been altered after over-expression (70, 154) or knockout of CPT1c (151), the reaction that CPT1c catalyzes has remained elusive.

Here we used an unbiased metabolomic approach to broadly understand the consequence of CPT1c deletion to gain insight into the biochemical and physiological roles of CPT1c function. Similar to previous work in heterologous systems, we did not see changes consistent with a role for CPT1c in long chain fatty acid beta oxidation. However, there were changes in several fatty acid derived metabolites including endocannabinoids, which may explain the suppressed food intake in these models. Also, some of the most abundant changes were in redox biochemistry consistent with several models of CPT1c function recently proposed.

Experimental Procedures

Animals

Mice with a targeted knockout of exons 1 and 2 of the cpt1c gene were propagated and genotyped as previously described (149, 150). Mice were fed a standard lab chow (Harlan 2018) after weaning. All procedures were performed in accordance with the National Institutes of Health Guide for the Care and Use of Laboratory Animals and under the approval of the Johns Hopkins Medical School Animal Care and Use Committee.

Western blot analysis

A polyclonal rabbit antibody against CPT1c was used as a primary antibody for CPT1c detection in WT and CPT1c KO mice (149, 150). Anti-rabbit horseradish peroxidase (HRP) was used as a secondary antibody, and the blots for CPT1c were developed using ECL reagent. Mouse monoclonal anti-HSC70 (Santa Cruz biotech) and mouse monoclonal anti beta-actin (Sigma) was used as primary antibodies for loading control. Cy3 conjugated fluorescent secondary antibody was used for both HSC70 and beta-actin antibodies.

Metabolomic measurements and profiling

Unbiased metabolomics analysis of whole brain samples from WT and CPT1c KO mice (n=8/group) that were fasted overnight was performed using liquid chromatography/ tandem mass spectrometry (HPLC/MS/MS^2) and gas chromatography/mass spectrometry (GC/MS) platforms. The platform was able to screen and identify several metabolites in multiple classes, such as amino acids, lipids, and nucleotides. A complete list of the metabolites identified in this study is given in Tables 6-1, 6-2, 6-3 and 6-4. General platform methods about metabolomics measurements and profiling are described in the metabolomics study done by Eckel-Mahan et al. (155)

Statistical analysis

Pair-wise comparisons between CPT1c WT and KO were performed using Welch' s two-sample t-tests. From the p -values, any value below the significance level of 0.05 was interpreted as statistically significant.

Results

Carnitine Palmitoyltransferase-1c KO mice

Although CPT1c is widely expressed in transformed cells and tumors (156), we

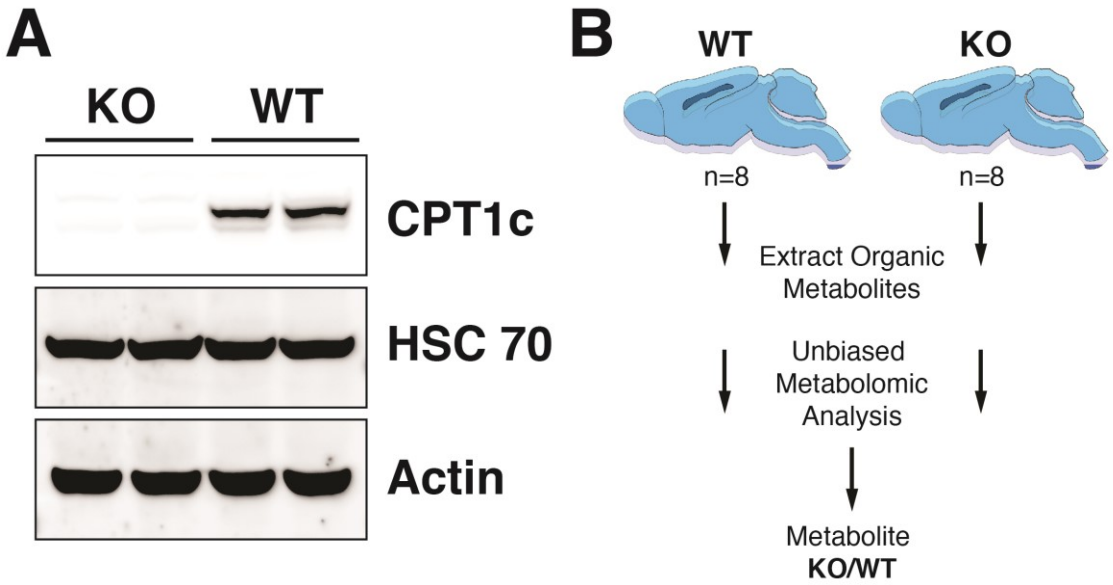

Figure 5-1. CPT1c KO mice and metabolomics profiling.

(A) CPT1c protein from homogenized brains of WT and CPT1c KO mice were analyzed by western blot using the anti-CPT1c antibody. Hsc70 and Actin were used for loading controls.

(B) A schematic pathway of metabolomics profiling for KO and WT brains. A commercial supplier of metabolic analysis homogenized 8 brain samples from independent mice to extract organic metabolites for performing unbiased metabolomics analysis using a mixture of GC-MS and LC-MS/MS.

have only been able to reliably detect CPT1c in neurons *in vivo*. To understand the endogenous function of CPT1c, we performed metabolomics profiling on brains of CPT1c KO mice and their littermate controls. Therefore, we collected and snap froze the brains of CPT1c KO and WT littermate sex matched adult mice after an overnight fast. Western blot analysis of WT and CPT1c KO mice showed that KO mice were indeed completely deficient of CPT1c (**Figure 5-1A**). These samples were then homogenized and the small organic metabolites were extracted and analyzed by a mixture of GC-MS and LC-MS/MS by a commercial supplier of metabolomic analyses (**Figure 5-1B**). Below, we detail the changes in steady-state biochemical between WT and KO brains that were identified through an unbiased metabolomic screen.

Fatty acid oxidative metabolites show no difference in overall trend in CPT1c KO mice

Given the high primary amino acid homology of CPT1c to other CPTs, it would follow that CPT1c may be involved in fatty acid beta oxidation or at least in long chain acyl-CoA metabolism. If CPT1c was involved in fatty acid oxidation, we would expect that the deletion of CPT1c would decrease the level of acyl-carnitines and potentially increase the levels of other long chain acyl-CoA dependent biosyntheses. A broad range of lipid species were identified in the metabolomic screen (**Table 5-1**). No changes were seen in oleoyl-carnitine, beta-hydroxybutyrate, or acetyl-carnitine, as we would have expected (**Figure 5-2A**). However, the metabolomics analysis did show that free carnitine, 3-dehydrocarnitine, glutaroylcarnitine, and betaine were significantly changed (**Figure 5-2A**).

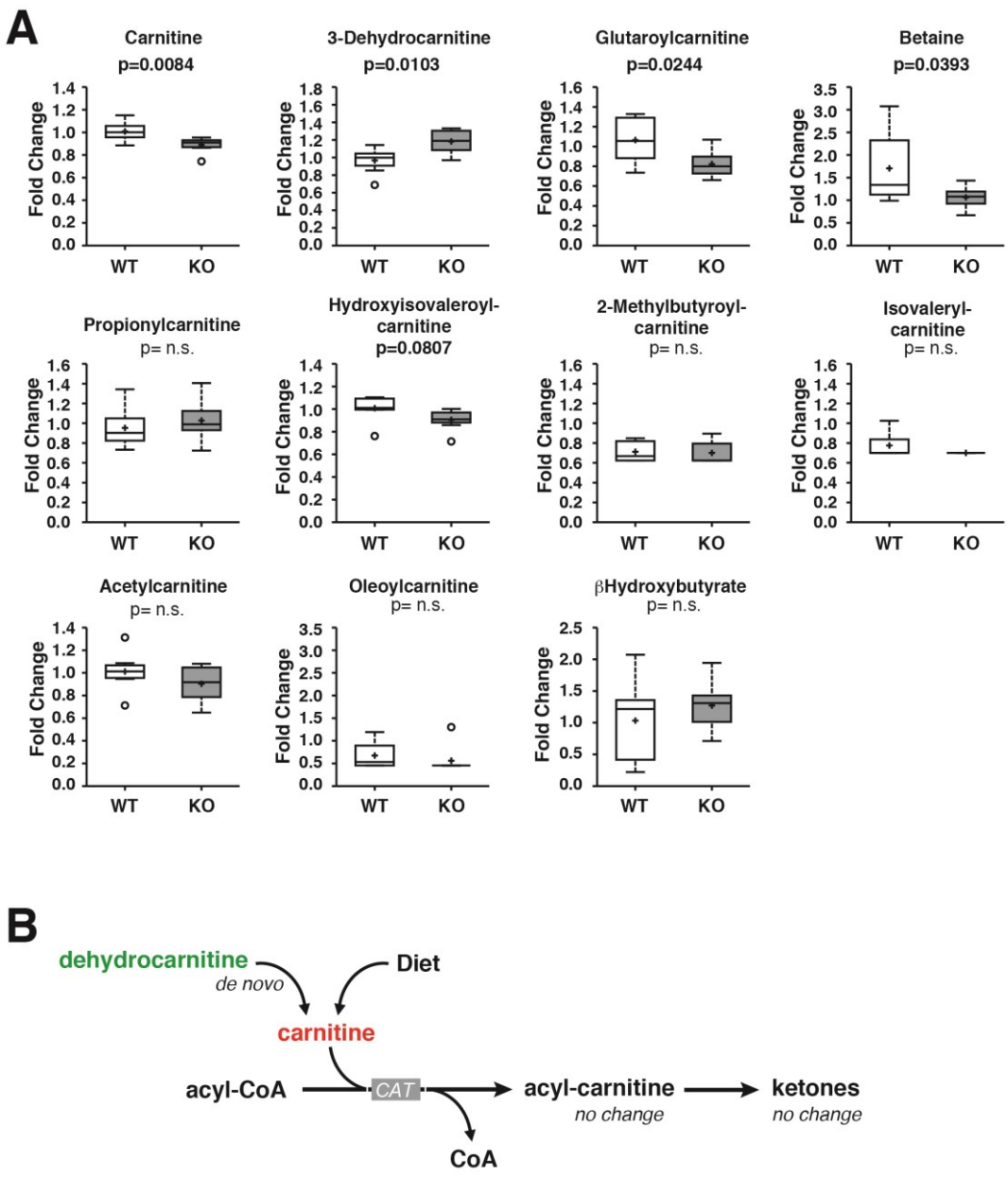

Figure 5-2. Loss of CPT1c results in decreased free carnitine and no change in fatty acid oxidative metabolites in the brain.

(A) Biochemicals involved in carnitine, amino acid and fatty acid metabolism from WT and CPT1c KO brains were compared through metabolomics analyses, revealing a statistically significant change in levels of free carnitine (p=0.084), 3-dehydrocarnitine (p=0.0103), glutaroylcarnitine (p=0.0244) and betaine (p=0.0383).

(B) Schematic of biochemical pathways altered in CPT1c KO mice. Based on this schematic pathway, glutaroyl carnitine and betaine may affect the level of free carnitine, since these biochemical play a role in carnitine biosynthesis.

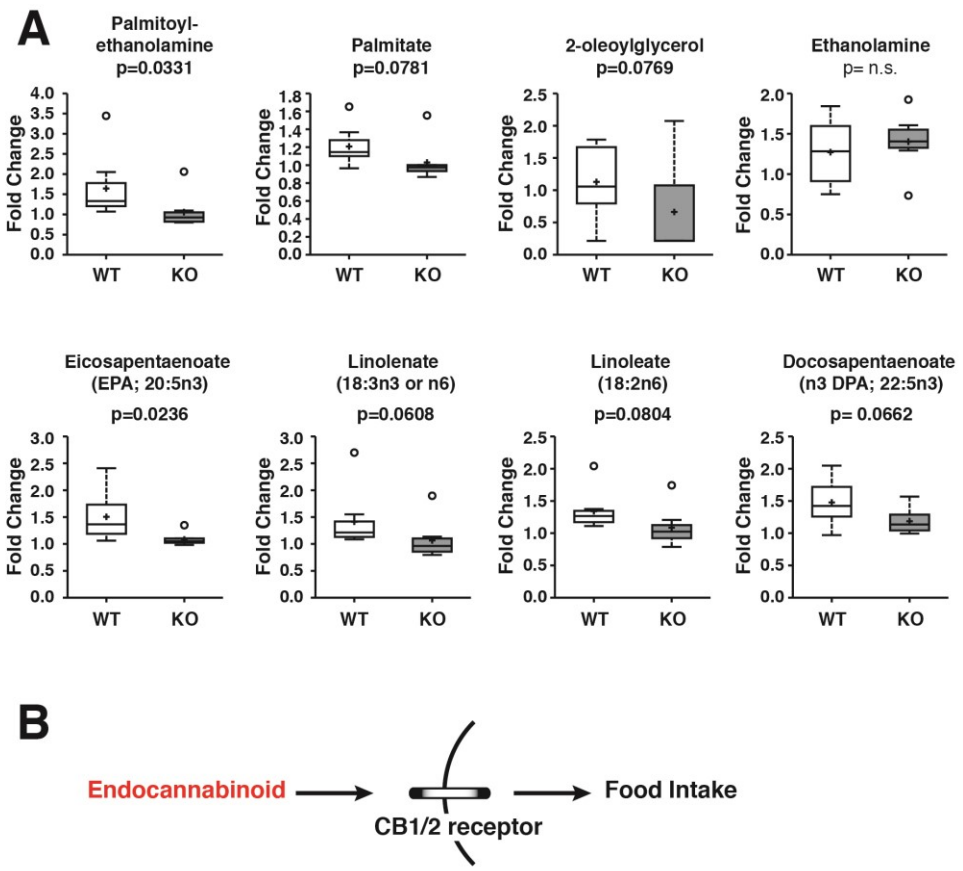

Figure 5-3. Loss of CPT1c results in decreased endocannabinoids in the brain.

(A) Biochemicals involved in fatty acid biochemistry from WT and CPT1c KO mouse brains were compared to determine if metabolomics analyses showed any statistically significant changes. There was an overall decreasing trend in endocannabinoids in CPT1c KO mice. Specifically, eicosapentaenoate (p=0.0236) and palmitoylethanolamine (p=0.0331) significantly decreased in CPT1c KO mice.

(B) A schematic of how a decrease in endocannabinoids can induce a decrease in food intake by interacting with CB1 and CB2 cannabinoid receptors.

Among the metabolites that showed a statistically significant difference, only 3-dehydrocarnitine increased in CPT1c KO mice while glutaroyl carnitine, betaine and free carnitine decreased. Glutaroyl carnitine and betaine are biochemicals that are involved in carnitine biosynthesis (**Figure 5-2B; Table 5-2**). Glutaroyl carnitine is involved in lysine metabolism, which is one of the amino acids that is used to synthesize carnitine. In the carnitine biosynthesis pathway, betaine takes the form of butyrobetaine to synthesize L-carnitine (157). As a result, it is possible that the decrease in glutaroyl carnitine and betaine could have caused free carnitine levels to decrease in CPT1c KO mice. Previous studies also tested hypothalamic and cortical explants from WT and CPT1c KO mice for their ability to oxidize fatty acids, but there was no evidence that unique properties in neurons existed to allow activation of fatty acid oxidation by CPT1c (149). CPT1c over-expressed in heterologous cells in vitro also did not show a change in fatty acid oxidation (149). Therefore, our results remain consistent with previous findings that CPT1c, although it is highly homologous with its isoforms CPT1a and CPT1b, does not participate substantially in neuronal mitochondrial fatty acid oxidation.

Loss of CPT1c results in decreased levels of endogenous endocannabinoids

Several studies have investigated the neurological role of endocannabinoids on food intake (158). A study investigated the role of endocannabinoids in regulating food intake in the tongue, gut and different brain regions, suggesting that the cannabinoid system plays a role in modulating the activity of neural pathways that regulate food intake and energy expenditure (158). The brain cannabinoid system, as shown in **Figure 5-3B**, regulates food intake through the interaction of endogenous ligands and

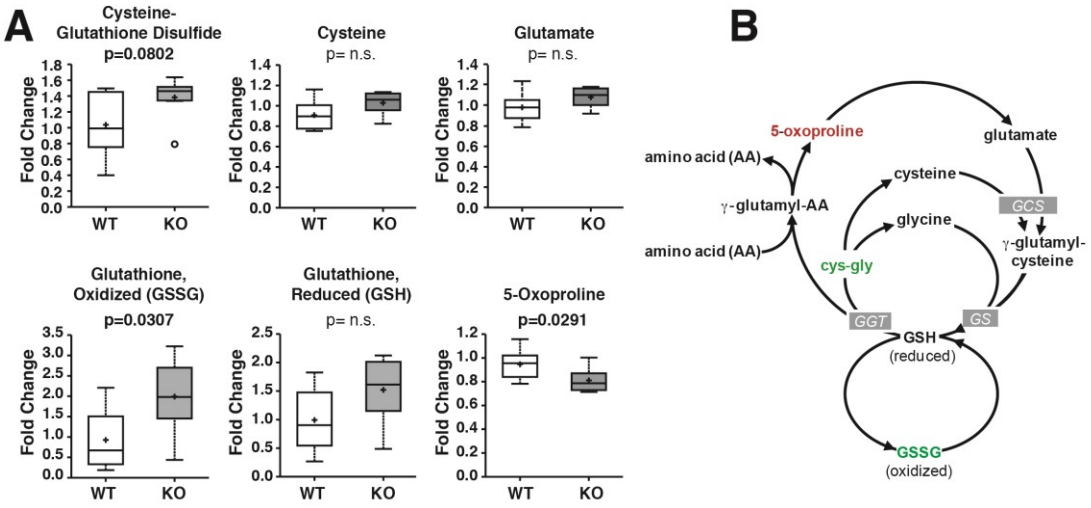

Figure 5-4. Loss of CPT1c results in elevated oxidative demands in the brain.

(A) In a comparison of biochemical involved in redox homeostasis in WT and CPT1c KO mouse brains, GSSG and 5-oxoproline were statistically significant. GSSG levels increased in CPT1c KO mice with a p-value of 0.0307, while 5-oxoproline decreased in KO mice (p=0.0291). The biochemical shown displayed an overall increasing trend in CPT1c KO mice.

(B) A schematic of the gamma-glutamyl redox cycle. Based on the pathway, an increase in the biochemical from Fig 4A may cause the cells to become more sensitive to oxidative stress.

cannabinoid receptors. From our metabolomics analyses, there was a significant decrease in palmitoylethanolamine and a trend for a decrease in 2-oleolylglycerol in CPT1c KO mouse brains compared to WT mouse brains (**Figure 5-3**). There was no significant difference between WT and CPT1c KO mice for free nonesterified fatty acids (**Table 5-1**). Among the metabolites shown in **Figure 5-3A**, eicosapentaenoate and palmitoylethanolamine showed a significant decrease in CPT1c KO mice with a p-value of 0.0236 and 0.0331, respectively. There was also a slight increase in ethanolamine between WT and CPT1c KO mice, and decrease in 2-oleoylglycerol (p=0.0769), an endogenous cannabinoid (CB) CB-1 agonist (**Figure 5-3A**).

Loss of CPT1c results in increased levels of glutathione

The oxidized form of GSH (GSSG) and 5-oxoproline, biochemicals involved in the gamma-glutamyl redox cycle, resulted in a statistically significant difference in CPT1c KO mice (**Table 5-2**). GSSG and cysteineglutathione disulfide levels increased while 5-oxoproline levels decreased in CPT1c KO mice (**Figure 5-4A**). Based on the schematic redox pathway shown in **Figure 5-4B**, our results suggest that CPT1c may play a role in oxidative metabolism. This is consistent with findings in cancer metabolism. Zaugg et al. depleted the levels of CPT1c in MCF-7 cells to determine whether these cells were sensitive to oxidative stress. Hypoxia was used as a stress inducer, and they found that CPT1c depletion caused an increased sensitivity to oxidative stress, implying that CPT1c may play a crucial role in protecting the cells from stress from the environment (156). Furthermore, the loss of CPT1c resulted in an increase in ceramides (151, 152), a key mediator of oxidative stress (159, 160). However, the mechanism and role of CPT1c in oxidative metabolism remains unknown.

Discussion

Role of CPT1c in behavior and physiology

Carnitine acyltransferases are enzymes that catalyze the exchange of acyl groups between carnitine and CoA to facilitate the transport of acyl groups from the cytoplasm to the mitochondrial matrix. Carnitine acetyltransferase (CRAT) and carnitine octonyltransferase (CROT) facilitate transport short- and medium-chain acyl-CoA, while CPT1 facilitate transports long chain acyl-CoA to the mitochondria. CPT1 enzymes are encoded by three genes in mammals that are localized in different tissues and have different properties. CPT1a, which is enriched in the liver, has been heavily studied due to its crucial role in β -oxidation and human fatty oxidation disorders (OMIM #255120) and is lethal when knocked out in mice (28). CPT1b is localized mainly in the muscle and is a regulator for the use of fatty acids in muscle and is also lethal when knocked out in mice (27). These two enzymes, which are present on the outer mitochondrial membrane, play a critical role in regulating and facilitating fatty acid beta-oxidation.

The brain specific CPT1c is highly homologous to its closely related genes, CPT1a and CPT1b (148). However, despite its high homology, CPT1c does not catalyze acyl transfer from long chain acyl-CoA to carnitine (148-150). Other distinguishing properties of CPT1c include a longer C-terminus and localization in the endoplasmic reticulum (ER) instead of the mitochondria (154). Although it does not facilitate acyl transfer in the cell, CPT1c most likely remains sensitive to the endogenous allosteric CPT1 inhibitor, malonyl-CoA, binding with a similar affinity as CPT1a (148, 150). Moreover, while other isoenzymes are expressed in a broad range of organisms, CPT1c seems to have risen late in evolution, raising the question whether CPT1c has a specific

role in mammalian brain function.

Several studies used CPT1c knockout (KO) and CPT1c transgenic mice to investigate the role of CPT1c in the CNS. Knockout studies showed that loss of CPT1c did not affect the viability or fertility of the mice, but resulted in a suppression in food intake and decrease in body weight when they were fed a normal or low-fat diet (150, 153). Paradoxically, when high fat diet was given to CPT1c KO mice, they exhibited diet-induced obesity, which ultimately resulted in a diabetic phenotype (149, 150). Even though fatty acid oxidative metabolites showed no significant change based on the metabolomic analysis, due to a decrease in peripheral energy expenditure CPT1c KO mice were more susceptible to obesity and diabetes when fed a high fat diet. This suggests that CPT1c has a hypothalamic function in protecting the body from adverse weight gain when the mice were fed a high fat diet. Transgenic CPT1c mice (CPT1c-TgN), on the other hand, which allowed conditional expression of CPT1c in a tissue-specific manner via cre-lox recombination, showed enhanced expression of CPT1c and they were protected from diet-induced obesity even on a high-fat diet (70).

CPT1c KO mice also showed impaired spatial learning (151). Cpt1c deficiency was shown to alter dendritic spine morphology by increasing immature filopodia and reducing mature mushroom and stubby spines. Compared to WT mice, CPT1c KO mice showed a higher escape latency, implying that they had a delay in the acquisition phase (151). Based on this study, CPT1c deficiency interfered with consolidating new information but did not affect retaining information or motor behavior. As a result, there may be other physiological roles of CPT1c in addition to regulating food intake and energy expenditure consistent with its broad expression throughout the nervous system

(151).

Endocannabinoid regulation of food intake

Endocannabinoids are endogenous ligands that bind to cannabinoid receptors to regulate many aspects of physiology and behavior. Specifically, the brain endocannabinoid system regulates food intake via the hypothalamus, where it activates necessary mediators to induce appetite after a short-term food deprivation. CB1 receptor KO mice showed reduced food intake, similar to CPT1c KO mice (161, 162). Based on our results, CPT1c could be interacting with the cannabinoid system, causing an overall decreasing trend in endocannabinoids in CPT1c KO mice. In this context, the loss of CPT1c could have influenced the endocannabinoid system and its function to regulate food intake and body weight, which may explain the suppressed food intake in CPT1c KO mice (149, 153). Therefore, a decrease in endocannabinoids based on metabolomic profiling may suggest a putative role of the endocannabinoid system in suppressing food intake in CPT1c KO mice. However, it is unclear if CPT1c affects endocannabinoid metabolism directly or more likely indirectly by altering neuronal specific fatty acid metabolism.

Glutathione and redox metabolism

Neurons are particularly sensitive to oxidative stress and damage caused by reactive oxygen species (ROS). On the cellular level, there are many endogenous metabolic stress inducers, such as ROS produced from the mitochondria and cytosolic enzymes, such as cyclooxygenase and lipoxygenase. There are also various exogenous conditions that can also promote the level of ROS species to increase, such as H_2O_2 and hypoxia, that induces irreversible cellular damage or cell death. As shown by the pathway

in **Figure 5-4B**, reduced glutathione (GSH) and oxidized glutathione (GSSG) are tightly regulated in order to maintain cellular redox homeostasis and to protect the cells from oxidative damage (160). Carrasco et al. showed that CPT1c expression correlated with ceramide production and loss of CPT1c resulted in reduced ceramide levels. (151). A recent study on the role of CPT1c in cancer cells in response to metabolic stress showed that CPT1c could participate in protecting cells from stress. In addition, they postulated that metabolic stress could alter regulation of the CPT1c gene, reducing ATP production and increasing sensitivity towards metabolic stress (156). Here, we showed that CPT1c deficiency results in an increased oxidative environment. This may indicate that although CPT1c does not contribute in large part to beta-oxidation, it may be involved in other neuron specific oxidative metabolism. Alternatively, CPT1c may need to be activated in a yet to identified stress-induced manner. Barger et al. (163) showed that CPT1c was required for leukemia growth under low glucose conditions. Therefore, CPT1c may have a context dependent role in fatty acid catabolism. Although here we show that CPT1c could play a role in oxidative stress, the precise role of CPT1c in relation to oxidative stress remains unknown.

PATHWAY	SUB PATHWAY	BIOCHEMICAL NAME	KEGG	CPT1c KO CPT1c WT	Welch's Two-Sample t-Test	CAS	PUBCHEM
Lipid	Essential fatty acid	linoleate (18:2n6)	C01595	0,93	0,4643	60-33-3;	5280450
		linolenate [alpha or gamma; (18:3n3 or 6)]	C06427	1,04	0,4808		
		dihomo-linolenate (20:3n3 or n6)	C03242	0,81	0,0608		5312529
		eicosapentaenoate (EPA; 20:5n3)	C06428	0,72	0,0236	10-2005-9;10417-94-4;	446284
		docosapentaenoate (n3 DPA; 22:5n3)	C16513	0,80	0,0662	2234-74-4 ;	
		docosapentaenoate (n6 DPA; 22:5n6)	C06429	0,77	0,3030	25182-74-5;	6441454
		docosahexaenoate (DHA; 22:6n3)	C06429	0,89	0,2879	6217-54-5;	445580
	Medium chain fatty acid	caproate (6:0)	C01585	0,98	0,5408	142-62-1;	8892
		caprylate (8:0)	C06423	0,99	0,9309	124-07-2;	379
		pelargonate (9:0)	C01601	0,89	0,1531	112-05-0;	5461016
		laurate (12:0)	C02679	1,01	0,9051	143-07-7;	3893
	Long chain fatty acid	myristate (14:0)	C06424	0,99	0,8942	544-63-8;	11005
		myristoleate (14:1n5)	C08322	1,26	0,1786	544-64-9 ;	5281119
		palmitate (16:0)	C00249	0,85	0,0781	57-10-3;	985
		palmitoleate (16:1n7)	C08362	0,93	0,3794	373-49-9;	445638
		margarate (17:0)		0,86	0,2288	506-12-7;	10465
		10-heptadecenoate (17:1n7)		0,81	0,1051	29743-97-3;	5312435
		stearate (18:0)	C01530	0,94	0,4536	57-11-4;	5281
		oleate (18:1n9)	C00712	0,88	0,2434	112-80-1;	445639
		10-nonadecenoate (19:1n9)		0,72	0,0470	73033-09-7;	5312513
		eicosenoate (20:1n9 or 11)		0,78	0,1453		
		dihomo-linoleate (20:2n6)	C16525	0,75	0,0804	2091-39-6;	6439848
		arachidonate (20:4n6)	C00219	0,94	0,4832	506-32-1;	444899
		docosadienoate (22:2n6)	C16533	0,84	0,3185	7370-49-2 ;	5282807
		adrenate (22:4n6)	C16527	0,81	0,1467	2091-25-0;	5282844
	Fatty acid, ester	n-Butyl Oleate		0,96	0,7046	142-77-8;	5354342
	Fatty acid, dicarboxylate	2-hydroxyglutarate	C02630	1,00	0,8616	40951-21-1;	43
	Fatty acid, amide	oleamide		1,22	0,7962	301-02-0;	5283387
		stearamide	C13846	1,19	0,6546	124-26-5;	31292
	Eicosanoid	prostaglandin D2	C00696	1,20	0,1092	41598-07-6;	448457
		prostaglandin E2	C00584	0,93	0,3928	363-24-6;	5280360
		5-HETE		0,99	0,8472	73307-52-5;	9862886
		15-HETE	C04742	0,83	0,9669	54845-95-3;	5280724
	Endocannabinoid	palmitoyl ethanolamide		0,64	0,0331		4671
	Fatty acid & BCAA metabolism	propionylcarnitine	C03017	1,08	0,4494	17298-37-2 ;	107738
	Carnitine metabolism	carnitine	C00487	0,88	0,0084	461-05-2;	288
		3-dehydrocarnitine*	C02636	1,22	0,0103	10457-99-5;	6991982
		acetylcarnitine	C02571	0,89	0,2172	5080-50-2;	7045767
		oleoylcarnitine		0,83	0,3694		
	Fatty alcohol, long chain	1-octadecanol	D01924	1,01	0,8513	112-92-5;	8221
	Glycerolipid metabolism	choline phosphate	C00588	0,97	0,4914	72556-74-2;	1014
		ethanolamine	C00189	1,10	0,4703	141-43-5;	
		phosphoethanolamine	C00346	1,06	0,5812	1071-23-4;	52323241015
		glycerol	C00116	0,97	0,6203	56-81-5;	753
		glycerol 3-phosphate (G3P)	C00093	0,98	0,6926	29849-82-9;	754
		glycerophosphorylcholine (GPC)	C00670	0,96	0,9071	28319-77-9;	657272
		cytidine 5'-diphosphocholine	C00307	1,25	0,0583	33818-15-4;	13805
	Inositol metabolism	myo-inositol	C00137	0,94	0,0882	87-89-8;	
		chiro-inositol		0,77	0,1568	643-12-9;	
		inositol 1-phosphate (I1P)		1,01	0,8432	106032-59-1;	
		scyllo-inositol	C06153	0,90	0,1635	488-59-5;	
	Ketone bodies	3-hydroxybutyrate (BHBA)	C01089	1,23	0,2197	625-72-9;	441
	Lysolipid	1-palmitoylglycerophosphoethanolamine		1,12	0,8591		9547069
		2-palmitoylglycerophosphoethanolamine*		0,83	0,1926		
		1-stearoylglycerophosphoethanolamine		1,20	0,7882	69747-55-3;	9547068
		1-oleoylglycerophosphoethanolamine		1,14	0,8654		9547071
		2-oleoylglycerophosphoethanolamine*		1,07	0,9602		
		1-arachidonoylglycerophosphoethanolamine*		1,06	0,8488		
		2-arachidonoylglycerophosphoethanolamine*		0,45	0,2213		
		2-docosahexaenoylglycerophosphoethanolamine*		0,48	0,3141		
		1-palmitoylglycerophosphocholine		0,47	0,1450	17364-16-8;	86554
		2-palmitoylglycerophosphocholine*		0,59	0,2106		
		1-stearoylglycerophosphocholine		0,51	0,1452	19420-57-6;	497299
		2-stearoylglycerophosphocholine*		1,00			10208382
		1-oleoylglycerophosphocholine		0,56	0,1923	19420-56-5;	16081932
		2-oleoylglycerophosphocholine*		0,65	0,3441		
		1-arachidonoylglycerophosphocholine*	C05208	1,00			
		2-arachidonoylglycerophosphocholine*		0,89	0,4485		
		1-docosahexaenoylglycerophosphocholine*		1,00			
		2-docosahexaenoylglycerophosphocholine*		0,86	0,4614		
		1-palmitoylglycerophosphoinositol*		0,85	0,2160		
		1-stearoylglycerophosphoinositol		0,77	0,1315		
		1-arachidonoylglycerophosphoinositol*		0,87	0,3521		
		1-oleoylglycerophosphoserine		0,92	0,6515		9547099
		2-oleoylglycerophosphoserine*		0,80	0,1921		
		1-palmitoylplasmenylethanolamine*		1,23	0,5225		
	Monoacylglycerol	1-palmitoylglycerol (1-monopalmitin)		0,83	0,1685	542-44-9;	14900
		1-stearoylglycerol (1-monostearin)	D01947	0,92	0,3625	123-94-4;	24699
		2-stearoylglycerol (2-monostearin)		0,75	0,1774	621-61-4;	79075
		1-oleoylglycerol (1-monoolein)		0,80	0,1139	111-03-5;	5283468
		2-oleoylglycerol (2-monoolein)		0,59	0,0769	3443-84-3;	5319879
	Sphingolipid	sphingosine	C00319	0,71	0,3009	123-78-4;	5353955
		palmitoyl sphingomyelin		0,84	0,1297		9939941
		stearoyl sphingomyelin	C00550	1,07	0,2147	85187-10-6;85187-10-6 ;	6453725
	Mevalonate metabolism	3-hydroxy-3-methylglutarate	C03761	1,07	0,4426	503-49-1;	5459993
	Sterol/Steroid	cholesterol	C00187	1,00	0,9987	57-88-5;	6432564
		7-alpha-hydroxycholesterol	C03594	1,24	0,2998	566-27-8;	107722
		7-beta-hydroxycholesterol	C03594	1,11	0,2969	566-27-8;	473141
		24(S)-hydroxycholesterol	C13550	0,94	0,5728	2140-46-7;	
		corticosterone	C02140	0,59	0,2402	50-22-6;	5753

Table 5-1. Biochemicals involved in lipid metabolic pathways

PATHWAY	SUB PATHWAY	BIOCHEMICAL NAME	KEGG	CPT1c KO CPT1c WT	Welch's Two-Sample t-Test	CAS	PUBCHEM
Amino acid	Glycine, serine and threonine metabolism	glycine	C00037	0,91	0,1984	56-40-6;	5257127750
		serine	C00065	0,98	0,6400	56-45-1;	59516857581
		N-acetylserine		1,16	0,2513	97-14-3;	65249
		homoserine	C02989	1,04	0,5460	672-15-1;	126476971022
		3-phosphoserine	C01005	1,06	0,4516	407-41-0;	
		threonine	C00188	0,98	0,8340	72-19-5;	69710196288
		allo-threonine	C05519	0,98	0,7264	28954-12-3;	992896995276
		betaine	C00719	0,62	0,0393	107-43-7;	247
	Alanine and aspartate metabolism	alanine	C00041	0,99	0,8540	56-41-7;	59507311724
		beta-alanine	C00099	0,95	0,7707	56-41-7;107-95-9;	2394755801
		N-acetylalanine	C02847	0,96	0,7172	97-69-8;	88064
		aspartate	C00049	1,02	0,5759	56-84-8;	5960
		N-acetylaspartate (NAA)	C01042	0,98	0,7849	997-55-7;997-55-7 ;	65065
	Glutamate metabolism	glutamate	C00025	1,10	0,1218	56-86-0;	611
		glutamine	C00064	0,96	0,3866	56-85-9;	69920865961
		gamma-aminobutyrate (GABA)	C00334	1,07	0,4581	56-12-2;	6992099119
		N-acetylglutamate	C00624	1,21	0,1108	5817-08-3;	1549099
		N-acetyl-aspartyl-glutamate (NAAG)	C12270	1,04	0,6033	3106-85-2;	5255
		N-acetylglutamine	C02716	0,79	0,1871	2490-97-3;	182230
	Histidine metabolism	histidine	C00135	1,11	0,1815	5934-29-2;	7733651426
	Lysine metabolism	lysine	C00047	0,81	0,0655	56-87-1;	5962
		2-aminoadipate	C00956	0,99	0,9856	542-32-5;1118-90-7;	469
		pipecolate	C00408	0,91	0,4383	4043-87-2;	849
		glutaroyl carnitine		0,77	0,0244	102636-82-8;	
	Phenylalanine & tyrosine metabolism	phenylalanine	C00079	0,93	0,0731	63-91-2;	69256656140
		tyrosine	C00082	1,10	0,1569	60-18-4;	60576942100
		3-(4-hydroxyphenyl)lactate	C03672	1,28	0,1580	6482-98-0;	9378
	Tryptophan metabolism	tryptophan	C00078	1,10	0,1009	73-22-3;	69235166305
		C-glycosyltryptophan*		1,00	0,9578		
		5-hydroxyindoleacetate	C05635	0,99	0,9982	54-16-0;	1826
	Valine, leucine and isoleucine metabolism	isoleucine	C00407	0,99	0,7705	73-32-5;	791
		leucine	C00123	0,92	0,1061	61-90-5;	70457986106
		valine	C00183	1,00	0,9896	72-18-4;	69710186287
		alpha-hydroxyisovalerate		0,92	0,9081	600-37-3;	99823
		2-methylbutyroylcarnitine		0,98	0,7985	31023-25-3;	6426901
		isovalerylcarnitine		0,90	0,1479		6426851
		hydroxyisovaleroyl carnitine		0,90	0,0807	99159-87-2;	
	Cysteine, methionine, SAM, taurine metabolism	cysteine	C00097	1,13	0,0835	52-90-4;56-89-3;	58626419722
		cystine	C00491	0,86	0,5529	56-89-3;	595
		taurine	C00245	1,03	0,7783	107-35-7;	11234068592
		S-adenosylhomocysteine (SAH)	C00021	0,96	0,4778	979-92-0;	
		methionine	C00073	0,95	0,1654	63-68-3;	69920876137
		N-acetylmethionine	C02712	0,88	0,1362	65-82-7;	448580
		2-hydroxybutyrate (AHB)	C05984	1,23	0,5077	3347-90-8;	440864
	Urea cycle; arginine-, proline-, metabolism	arginine	C00062	0,95	0,0964	1119-34-2;	5246487232
		ornithine	C00077	0,90	0,2453	3184-13-2;	6262
		urea	C00086	0,71	0,2913	57-13-6;	117616150869
		proline	C00148	0,97	0,6099	147-85-3;	1457426971047
		N-acetylornithine	C00437	1,26	0,3497	6205-08-9;	6992102439232
		trans-4-hydroxyproline	C01157	1,03	0,6431	51-35-4;	58106971053
		argininosuccinate	C03406	0,86	0,3803	156637-58-0;	828
	Creatine metabolism	creatine	C00300	1,03	0,2564	57-00-1;	586
		creatinine	C00791	1,20	0,1694	60-27-5;	588
	Butanoate metabolism	2-aminobutyrate	C02261	1,03	0,8503	1492-24-6;	4396916971251
	Polyamine metabolism	5-methylthioadenosine (MTA)	C00170	1,08	0,2023	2457-80-9;	439176
		putrescine	C00134	0,83	0,4688	110-60-1;	
		spermidine	C00315	1,04	0,6645	124-20-9;	1102
		spermine	C00750	0,99	0,4470	71-44-3;	1103
	Guanidino and acetamido metabolism	4-guanidinobutanoate	C01035	0,98	0,7911	463-003;463-00-3;	500
	Glutathione metabolism	glutathione, reduced (GSH)	C00051	1,53	0,1024	70-18-8;	124886
		5-oxoproline	C01879	0,86	0,0291	98-79-3;	7405
		glutathione, oxidized (GSSG)	C00127	2,15	0,0307	103239-24-3;	6535911215652
		cysteine-glutathione disulfide		1,33	0,0802	13081-14-6;	4247235
Peptide	Dipeptide derivative	carnosine	C00386	0,98	0,8057	305-84-0;	4392246992100
		homocarnosine	C00884	1,00	0,9807	3650-73-5;	10243361
	gamma-glutamyl	gamma-glutamylleucine		0,91	0,1529	2566-39-4;	151023
		gamma-glutamylglutamate		1,24	0,1880	1116-22-9;	92865
		gamma-glutamylglutamine		0,93	0,4450	10148-81-9;	150914
		gamma-glutamylphenylalanine		0,93	0,5544	7432-24-8;	111299

Table 5-2. Biochemicals in the amino acid and peptide pathways

PATHWAY	SUB PATHWAY	BIOCHEMICAL NAME	KEGG	CPT1c KO / CPT1c WT	Welch's Two-Sample t-Test	CAS	PUBCHEM
Carbohydrate	Aminosugars metabolism	N-acetylglucosamine	C00140	1.03	0.7477	7512-17-6;	24139
		erythronate*		0.98	0.7434	13752-84-6;	2781043
		N-acetylneuraminate	C00270	1.03	0.4494	131-48-6;	
	Fructose, mannose, galactose, starch, and sucrose metabolism	fructose	C00095	0.98	0.8393	57-48-7;	5984
		mannose	C00159	0.94	0.6417	3458-28-4;	161658
		mannose-6-phosphate	C00275	0.97	0.7187	70442-25-0;104872-94-8;	
		sorbitol	C00794	0.92	0.5926	6706-59-8;	107428
	Glycolysis, gluconeogenesis, pyruvate metabolism	1,5-anhydroglucitol (1,5-AG)	C07326	0.95	0.7426	154-58-5;	
		glycerate	C00258	0.96	0.4928	600-19-1;	752
		glucose-6-phosphate (G6P)	C00668	0.96	0.5074	103192-55-8;	
		glucose	C00293	0.86	0.1984	50-99-7;	79025
		fructose-6-phosphate	C05345	0.83	0.1261	103213-47-4;	
		Isobar: fructose 1,6-diphosphate, glucose 1,6-diphosphate		0.98	0.8050		
		3-phosphoglycerate	C00597	0.80	0.1220	80731-10-8;	
		dihydroxyacetone phosphate (DHAP)	C00111	1.02	0.6910	102783-56-2;	4643300
		1,3-dihydroxyacetone	C00184	1.12	0.4601	62147-49-3;	670
		pyruvate	C00022	0.83	0.0193	127-17-3;	107735
		lactate	C00186	1.06	0.3677	79-33-4;	612
	Nucleotide sugars, pentose metabolism	arabitol	C00474	1.30	0.0435	488-82-4;	94154
		ribitol	C00474	0.86	0.1732	488-81-3;	
		sedoheptulose-7-phosphate	C05382	0.91	0.4130	2646-35-7;	616
		ribose 5-phosphate	C00117	1.39	0.0353	18265-46-8;108321-05-7;	447634
		Isobar: ribulose 5-phosphate, xylulose 5-phosphate		1.06	0.5400		
		arabinose	C00181	1.08	0.5432	28697-53-2;	66308
Energy	Krebs cycle	citrate	C00158	1.02	0.5785	77-92-9;	311
		alpha-ketoglutarate	C00026	0.79	0.2702	305-72-6;328-50-7;22202-68-2;	51
		succinate	C00042	0.88	0.5010	110-15-6;	1110
		fumarate	C00122	0.94	0.5055	100-17-8;	
		malate	C00149	1.11	0.2256	6915-15-7;	525
	Oxidative phosphorylation	phosphate	C00009	0.98	0.3284	7664-38-2 ;	1061
		pyrophosphate (PPi)	C00013	0.84	0.4801	1466-09-3;	644102

Table 5-3. Biochemicals from the carbohydrate and energy pathways

PATHWAY	SUB PATHWAY	BIOCHEMICAL NAME	KEGG	CPT1c KO CPT1c WT	Welch's Two-Sample t-Test	CAS	PUBCHEM
Nucleotide	Purine metabolism, (hypo)xanthine/inosine containing	xanthine	C00385	1.02	0.7727	69-89-6;	1188
		hypoxanthine	C00262	0.98	0.4343	68-94-0;	790
		inosine		1.00	0.8754	58-63-9;	
	Purine metabolism, adenine containing	adenine	C00147	1.11	0.0801	73-24-5;	190
		adenosine	C00212	0.86	0.1407	58-61-7;	60961
		N1-methyladenosine	C02494	0.94	0.3601	15763-06-1;	5460178
		adenosine 2'-monophosphate (2'-AMP)	C00946	1.00		130-49-4;	
		adenosine 5'-monophosphate (AMP)	C00020	0.89	0.2000	149022-20-8;	15938965
	Purine metabolism, guanine containing	guanosine	C00387	1.01	0.9130	118-00-3;	6802
	Purine metabolism, urate metabolism	urate	C00366	1.06	0.4983	69-93-2;120K5305;	
		allantoin	C02350	0.76	0.1685	97-59-6;	204
	Pyrimidine metabolism, cytidine containing	cytidine	C00475	0.94	0.1562	65-46-3;	6175
		cytidine 5'-monophosphate (5'-CMP)	C00055	1.01	0.8988	63-37-6;	7058165
	Pyrimidine metabolism, orotate	orotate	C00295	0.86	0.2325	50887-69-9;	967
	Pyrimidine metabolism, uracil containing	uracil	C00106	0.97	0.5212	66-22-8;	1174
		uridine	C00299	0.91	0.0141	58-96-8;	6029
		pseudouridine	C02067	0.99	0.7648	1445-07-4;	
	Purine and pyrimidine metabolism	methylphosphate		0.85	0.1460	7023-27-0;	13130
Cofactors and vitamins	Ascorbate and aldarate metabolism	ascorbate (Vitamin C)	C00072	0.87	0.1924	134-03-2;	
		dehydroascorbate	C05422	1.70	0.2338	490-83-5;	835
		threonate	C01620	0.96	0.5529	70753-61-6;	151152
	Hemoglobin and porphyrin	heme*	C00032	0.69	0.3695	14875-96-8;	
	Nicotinate and nicotinamide metabolism	nicotinamide	C00153	1.00	0.9275	98-92-0;	936
		nicotinamide adenine dinucleotide (NAD+)	C00003	0.87	0.0469	53-84-9;	1089765158925280000
	Pantothenate and CoA metabolism	pantothenate	C00864	0.94	0.7951	137-08-6;	6613
		phosphopantetheine	C01134	0.85	0.0841	NA;	115254
	Pyridoxal metabolism	pyridoxal	C00250	1.05	0.5803	65-22-5;	1050
	Riboflavin metabolism	flavin adenine dinucleotide (FAD)	C00016	0.93	0.1085	146-14-5;84366-81-4;	643975
		riboflavin (Vitamin B2)	C00255	0.93	0.2187	83-88-5;	493570
		flavin mononucleotide (FMN)	C00061	0.96	0.7167	130-40-5;	710
	Tocopherol metabolism	alpha-tocopherol	C02477	1.04	0.6234	59-02-9;10191-41-0;	14985
Xenobiotics	Chemical	glycolate (hydroxyacetate)	C00160	1.06	0.7194	79-14-1;	3698251757
		glycerol 2-phosphate	C02979	1.02	0.9683	819-83-0;	2526
		2-phenoxyethanol	D11488	0.94	0.9231	122-99-6;	
		2-pyrrolidinone		0.84	0.6590	616-45-5 ;	12025
	Food component/Plant	ergothioneine	C05570	0.88	0.0968	58511-63-0;	3032311
	Sugar, sugar substitute, starch	erythritol	C00503	0.89	0.0966	149-32-6;	

Table 5-4. Biochemicals in nucleotide, cofactors and vitamins, and xenobiotic pathways

TISSUE SPECIFIC ROLES OF FATTY ACID OXIDATION

CHAPTER 6. Conclusions and Future Directions

Conclusions

Through this thesis, a conditional knockout of Cpt2 has allowed us to understand the role of fatty acid oxidation *in vivo*. It has long been suggested that mitochondrial dysfunction and suppressed BAT or WAT fatty acid oxidation contributes to changes in body weight and glucose tolerance. Some strategies to reverse obesity include increasing adipose energy expenditure to improve systemic obesity-related complications. However, through the adipocyte-specific deletion of Cpt2 mouse model, I found that although adipocyte fatty acid oxidation was an important metabolic process for environmental and nutritional homeostasis, it did not alter body weight or improve glucose tolerance.

In BAT, fatty acid oxidation was crucial for acute adaptation to cold by providing energy required for heat generation and transcriptional regulation of BAT thermogenesis. Although $Cpt2^{A-/-}$ mice were unable to maintain their body temperature in the cold, they were able to maintain energy homeostasis via alternative mechanisms during moderate environmental challenges. Due to the large potential to alter energy expenditure, it is tempting to suggest that defects in brown or beige adipocytes can lead to an obesogenic phenotype at thermoneutrality. However, my studies have shown that incompetent BAT does not potentiate obesity, even at thermoneutrality. Surprisingly, fatty acid oxidation was required to maintain the identity and morphology of BAT. This suggests that adipocyte fatty acid oxidation plays a major role in mediating and regulating molecular, cellular and physiological adaptations to maintain body temperature and energy homeostasis.

The molecular mechanisms by which high fat diets contribute to metabolic pathologies are not well understood, but several themes have emerged. Implicated in the

etiology and progression of obesity-related pathologies is oxidative stress, ER stress and inflammation originating locally at adipose depots but acting systemically to promote insulin resistance. Hence, it has been suggested that preventing local adipose tissue inflammation may have beneficial systemic effects against insulin resistance. In contrast, the loss of fatty acid oxidation in BAT and WAT suppressed oxidative stress and inflammation upon a high-fat diet feeding, but it did not improve systemic insulin resistance. Furthermore, the loss of fatty acid oxidation in adipose tissue did not alter body weight in varying environmental conditions when mice were either fed a high fat or low fat diet.

In the liver, fatty acid oxidation is crucial to maintain energy homeostasis upon prolonged fasting via gluconeogenesis or ketogenesis. In fact, gluconeogenesis is predominantly carried out in the liver with minor contributions from the kidney and gut. In the hepatocyte-specific deletion of Cpt2 mouse model, it is clear that the liver plays an important role in regulating systemic metabolism, especially when carbohydrate intake is limiting. However, my studies indicate that in the absence of fatty acid oxidation in the liver, the kidney is capable of maintaining glucose homeostasis. Additionally, the liver was able to mediate systemic adaptations, such as increase catabolism through circulating hepatokine Fgf21, to maintain energy homeostasis and ensure survival during prolonged fasting. However, when carbohydrate intake was limited through a ketogenic diet, $Cpt2^{L-/-}$ mice were not able to survive upon a heavy lipid burden. Overall, the control of energy expenditure represents a critical evolutionarily conserved survival mechanism that is likely regulated by multiple overlapping and compensatory systems, which may present a continuing challenge for treatments aimed at reversing human obesity.

Future Directions

What would be the physiological, molecular and biochemical response when $Cpt2^{L-/-}$ mice are put on a 60% high fat diet?

Studying the role of fatty acid oxidation in the liver has opened a whole new field of research in understanding how the liver regulates alternative mechanisms to maintain energy homeostasis and ensure survival in the absence of fatty acid oxidation. In my initial studies, I have shown that other tissues were able to contribute to maintain glucose and energy homeostasis during prolonged fasting (24hr fast) via increasing systemic catabolism via Pparα-regulated hepatokines Fgf21, Gdf15 and Igfbp1 under a standard chow diet. Therefore, it would be interesting to see if the same physiological and molecular effects take place upon a high fat diet feeding.

Preliminary data have shown that male and female $Cpt2^{L-/-}$ mice are resistant to body weight gain upon a 60% high-fat diet feeding and had significantly less fat mass than $Cpt2^{lox/lox}$ control mice. It would be important to determine which metabolic factor is preventing $Cpt2^{L-/-}$ mice from gaining weight. Is it Fgf21 or Atgl that is increasing lipolysis in adipose depots to maintain energy homeostasis? Also, by performing qRT-PCR, we can also investigate the transcriptional response of these mice on a high fat diet. What changes would we see in Pparα regulated genes? Would they have more severe hepatomegaly than 24hr fasted mice? Would these mice still be able to maintain energy homeostasis? It would also be helpful to generate Cpt2 and Fgf21 or Cpt2 and Atgl liver-specific double knockout mouse models and repeat the same experiments to see if we can rescue any of the phenotypes previously seen. Furthermore, using these double knockout

mouse models, we can investigate if systemic catabolism is still increased during fed, 24hr fasted and high fat diet conditions.

What is the effect of Cpt2 on insulin sensitivity and insulin signaling?

Consistent with my initial studies presented in chapter 4, $Cpt2^{L-/-}$ mice on a 60% high fat diet for 16 weeks had suppressed circulating β-hydroxybutyrate and insulin, but, surprisingly, had normal levels of glucose. Additionally, $Cpt2^{L-/-}$ mice had improved glucose tolerance and insulin sensitivity compared to control mice when these two tolerance tests were administered before the body weights of control and $Cpt2^{L-/-}$ mice were different. Insulin signaling in the liver is mediated via the hepatic insulin receptor and downstream kinases (164). Furthermore, Akt is known to affect the mTorc1 pathway and insulin-induced *de novo* lipogenesis (164). Therefore, performing an acute insulin stimulation to look at the insulin receptor and downstream targets in the insulin signaling pathway would be important to understand the role of hepatic fatty acid oxidation and its regulation in insulin release and glucose homeostasis. Additionally, since we saw a huge suppression in insulin, using radiolabeled substrates to perform an *in vivo* lipogenesis experiment would be helpful to understand how changes in insulin can affect DNL in the liver.

REFERENCE

1. Y. H. Tseng, A. M. Cypess, C. R. Kahn, Cellular bioenergetics as a target for obesity therapy. *Nat Rev Drug Discov* **9**, 465 (Jun, 2010).
2. C. Guerra, R. A. Koza, H. Yamashita, K. Walsh, L. P. Kozak, Emergence of brown adipocytes in white fat in mice is under genetic control. Effects on body weight and adiposity. *The Journal of clinical investigation* **102**, 412 (Jul 15, 1998).
3. K. I. Stanford *et al.*, Brown adipose tissue regulates glucose homeostasis and insulin sensitivity. *The Journal of clinical investigation* **123**, 215 (Jan 2, 2013).
4. P. Bostrom *et al.*, A PGC1-alpha-dependent myokine that drives brown-fat-like development of white fat and thermogenesis. *Nature* **481**, 463 (Jan 26, 2012).
5. J. Wu *et al.*, Beige adipocytes are a distinct type of thermogenic fat cell in mouse and human. *Cell* **150**, 366 (Jul 20, 2012).
6. F. M. Fisher *et al.*, FGF21 regulates PGC-1alpha and browning of white adipose tissues in adaptive thermogenesis. *Genes & development* **26**, 271 (Feb 1, 2012).
7. C. Vernochet, M. E. McDonald, S. R. Farmer, Brown adipose tissue: a promising target to combat obesity. *Drug News Perspect* **23**, 409 (Sep, 2010).
8. A. Whittle, J. Relat-Pardo, A. Vidal-Puig, Pharmacological strategies for targeting BAT thermogenesis. *Trends in pharmacological sciences* **34**, 347 (Jun, 2013).
9. A. Whittle, A. Vidal-Puig, When BAT is lacking, WAT steps up. *Cell Res* **23**, 868 (Jul, 2013).
10. A. L. Carey, B. A. Kingwell, Brown adipose tissue in humans: Therapeutic potential to combat obesity. *Pharmacol Ther*, (May 26, 2013).
11. M. J. Vosselman *et al.*, Brown adipose tissue activity after a high-calorie meal in humans. *The American journal of clinical nutrition* **98**, 57 (Jul, 2013).
12. M. J. Vosselman, W. D. van Marken Lichtenbelt, P. Schrauwen, Energy dissipation in brown adipose tissue: From mice to men. *Molecular and cellular endocrinology*, (Apr 28, 2013).
13. J. Grundlingh, P. I. Dargan, M. El-Zanfaly, D. M. Wood, 2,4-dinitrophenol (DNP): a weight loss agent with significant acute toxicity and risk of death. *J Med Toxicol* **7**, 205 (Sep, 2011).
14. M. Yen, M. B. Ewald, Toxicity of weight loss agents. *J Med Toxicol* **8**, 145 (Jun, 2012).
15. W. D. van Marken Lichtenbelt *et al.*, Cold-activated brown adipose tissue in healthy men. *The New England journal of medicine* **360**, 1500 (Apr 9, 2009).
16. A. M. Cypess *et al.*, Identification and importance of brown adipose tissue in adult humans. *The New England journal of medicine* **360**, 1509 (Apr 9, 2009).
17. M. Saito *et al.*, High incidence of metabolically active brown adipose tissue in healthy adult humans: effects of cold exposure and adiposity. *Diabetes* **58**, 1526 (Jul, 2009).
18. K. A. Virtanen *et al.*, Functional brown adipose tissue in healthy adults. *The New England journal of medicine* **360**, 1518 (Apr 9, 2009).

19. J. Krishnan *et al.*, Dietary obesity-associated Hif1alpha activation in adipocytes restricts fatty acid oxidation and energy expenditure via suppression of the Sirt2-NAD+ system. *Genes & development* **26**, 259 (Feb 1, 2012).
20. L. Ye *et al.*, TRPV4 is a regulator of adipose oxidative metabolism, inflammation, and energy homeostasis. *Cell* **151**, 96 (Sep 28, 2012).
21. T. Sawada *et al.*, Perilipin overexpression in white adipose tissue induces a brown fat-like phenotype. *PLoS One* **5**, e14006 (2010).
22. C. Vernochet *et al.*, Adipose-specific deletion of TFAM increases mitochondrial oxidation and protects mice against obesity and insulin resistance. *Cell metabolism* **16**, 765 (Dec 5, 2012).
23. R. Singh *et al.*, Autophagy regulates adipose mass and differentiation in mice. *The Journal of clinical investigation* **119**, 3329 (Nov, 2009).
24. M. Harms, P. Seale, Brown and beige fat: development, function and therapeutic potential. *Nature medicine* **19**, 1252 (Oct, 2013).
25. L. P. Kozak, Brown fat and the myth of diet-induced thermogenesis. *Cell metabolism* **11**, 263 (Apr 7, 2010).
26. N. Longo, C. Amat di San Filippo, M. Pasquali, Disorders of carnitine transport and the carnitine cycle. *Am J Med Genet C Semin Med Genet* **142C**, 77 (May 15, 2006).
27. S. Ji *et al.*, Homozygous carnitine palmitoyltransferase 1b (muscle isoform) deficiency is lethal in the mouse. *Molecular genetics and metabolism* **93**, 314 (Mar, 2008).
28. L. R. Nyman *et al.*, Homozygous carnitine palmitoyltransferase 1a (liver isoform) deficiency is lethal in the mouse. *Mol Genet Metab* **86**, 179 (Sep-Oct, 2005).
29. M. E. Patti *et al.*, Coordinated reduction of genes of oxidative metabolism in humans with insulin resistance and diabetes: Potential role of PGC1 and NRF1. *Proceedings of the National Academy of Sciences of the United States of America* **100**, 8466 (Jul 8, 2003).
30. M. E. Patti, S. Corvera, The role of mitochondria in the pathogenesis of type 2 diabetes. *Endocr Rev* **31**, 364 (Jun, 2010).
31. I. Dahlman *et al.*, Downregulation of electron transport chain genes in visceral adipose tissue in type 2 diabetes independent of obesity and possibly involving tumor necrosis factor-alpha. *Diabetes* **55**, 1792 (Jun, 2006).
32. M. Kaaman *et al.*, Strong association between mitochondrial DNA copy number and lipogenesis in human white adipose tissue. *Diabetologia* **50**, 2526 (Dec, 2007).
33. B. B. Lowell *et al.*, Development of obesity in transgenic mice after genetic ablation of brown adipose tissue. *Nature* **366**, 740 (Dec 23-30, 1993).
34. S. Enerback *et al.*, Mice lacking mitochondrial uncoupling protein are cold-sensitive but not obese. *Nature* **387**, 90 (May 1, 1997).
35. C. Guerra *et al.*, Abnormal nonshivering thermogenesis in mice with inherited defects of fatty acid oxidation. *The Journal of clinical investigation* **102**, 1724 (Nov 1, 1998).

36. J. M. Ellis *et al.*, Adipose acyl-CoA synthetase-1 directs fatty acids toward beta-oxidation and is required for cold thermogenesis. *Cell metabolism* **12**, 53 (Jul 7, 2010).
37. R. J. Tolwani *et al.*, Medium-chain acyl-CoA dehydrogenase deficiency in gene-targeted mice. *PLoS genetics* **1**, e23 (Aug, 2005).
38. A. M. Schuler *et al.*, Synergistic heterozygosity in mice with inherited enzyme deficiencies of mitochondrial fatty acid beta-oxidation. *Molecular genetics and metabolism* **85**, 7 (May, 2005).
39. E. D. Abel *et al.*, Adipose-selective targeting of the GLUT4 gene impairs insulin action in muscle and liver. *Nature* **409**, 729 (Feb 8, 2001).
40. P. R. Shepherd *et al.*, Adipose cell hyperplasia and enhanced glucose disposal in transgenic mice overexpressing GLUT4 selectively in adipose tissue. *J. Biol. Chem.* **268**, 22243 (1993).
41. W. He *et al.*, Adipose-specific peroxisome proliferator-activated receptor gamma knockout causes insulin resistance in fat and liver but not in muscle. *Proceedings of the National Academy of Sciences of the United States of America* **100**, 15712 (Dec 23, 2003).
42. H. Bottcher, P. Furst, Decreased white fat cell thermogenesis in obese individuals. *Int J Obes Relat Metab Disord* **21**, 439 (Jun, 1997).
43. P. Hallgren, E. Raddatz, C. H. Bergh, P. Kucera, L. Sjostrom, Oxygen consumption in collagenase-liberated rat adipocytes in relation to cell size and age. *Metabolism: clinical and experimental* **33**, 897 (Oct, 1984).
44. P. Hallgren, L. Sjostrom, H. Hedlund, L. Lundell, L. Olbe, Influence of age, fat cell weight, and obesity on O2 consumption of human adipose tissue. *The American journal of physiology* **256**, E467 (Apr, 1989).
45. K. H. Pietilainen *et al.*, Global transcript profiles of fat in monozygotic twins discordant for BMI: pathways behind acquired obesity. *PLoS Med* **5**, e51 (Mar 11, 2008).
46. T. Wang, Y. Zang, W. Ling, B. E. Corkey, W. Guo, Metabolic partitioning of endogenous fatty acid in adipocytes. *Obes Res* **11**, 880 (Jul, 2003).
47. J. Villarroya, M. Giralt, F. Villarroya, Mitochondrial DNA: an up-and-coming actor in white adipose tissue pathophysiology. *Obesity (Silver Spring)* **17**, 1814 (Oct, 2009).
48. C. M. Kusminski, P. E. Scherer, Mitochondrial dysfunction in white adipose tissue. *Trends Endocrinol Metab* **23**, 435 (Sep, 2012).
49. F. W. Kiefer *et al.*, Retinaldehyde dehydrogenase 1 regulates a thermogenic program in white adipose tissue. *Nature medicine* **18**, 918 (Jun, 2012).
50. C. Vernochet, C. R. Kahn, Mitochondria, obesity and aging. *Aging (Albany NY)* 4, 859 (Dec, 2012).
51. K. L. Hoehn *et al.*, Acute or chronic upregulation of mitochondrial fatty acid oxidation has no net effect on whole-body energy expenditure or adiposity. *Cell metabolism* 11, 70 (Jan, 2010).
52. D. P. Olson, T. Pulinilkunnil, G. W. Cline, G. I. Shulman, B. B. Lowell, Gene knockout of Acc2 has little effect on body weight, fat mass, or food intake. *Proceedings of the National Academy of Sciences of the United States of America* 107, 7598 (Apr 20, 2010).

53. Reddy JK and Rao MS. Liver metabolism and liver inflammation. II. Fatty liver disease and fatty acid oxidation. *American Journal of Physiology-Gastrointestinal and Liver Physiology* 290(5): G852-858, 2006.
54. Browning JD and Horton JD. Molecular mediators of hepatic steatosis and liver injury. *J Clin Invest* 114: 147–152, 2004.
55. Evans RM, Barish GD, and Wang YX. PPARs and the complex journey to obesity. *Nat Med* 10: 1–7, 2004.
56. Matsusue K, Haluzik M, Lambert G, Yim SH, Gavrilova O, Ward JM, Brewer B Jr, Reitman ML, and Gonzalez FJ. Liver-specific disruption of PPARγ in leptin-deficient mice improves fatty liver but aggravates diabetic phenotypes. *J Clin Invest* 111: 737–747, 2003.
57. Yu S, Matsusue K, Kashireddy P, Cao WQ, Yeldandi V, Yeldandi AV, Rao MS, Gonzalez FJ, and Reddy JK. Adipocyte-specific gene expression and adipogenic steatosis in the mouse liver due to peroxisome proliferator-activated receptor γ1 (PPARγ1) overexpression. *J Biol Chem* 278: 498–505, 2003.
58. Hashimoto T, Cook WS, Qi C, Yeldandi AV, Reddy JK, and Rao MS. Defect in peroxisome proliferator-activated receptor α-inducible fatty acid oxidation determines the severity of hepatic steatosis. *J Biol Chem* 275: 28918–28928, 2000.
59. Rao MS and Reddy JK. PPARα in the pathogenesis of fatty liver disease. *Hepatology* 40: 783–786, 2004.
60. Cahill GF, Jr. Fuel metabolism in starvation. *Annu Rev Nutr.* 2006;26(1-22.
61. L IJ, Mandel H, Oostheim W, Ruiter JP, Gutman A, and Wanders RJ. Molecular basis of hepatic carnitine palmitoyltransferase I deficiency. *J Clin Invest.* 1998;102(3):527-31.
62. Glass, C.K., and Olefsky, J.M. (2012). Inflammation and lipid signaling in the etiology of insulin resistance. Cell Metab. 15, 635–645.
63. Hotamisligil, G.S. (2010). Endoplasmic reticulum stress and the inflammatory basis of metabolic disease. Cell 140, 900–917.
64. Keaney, J.F., Jr., Larson, M.G., Vasan, R.S., Wilson, P.W., Lipinska, I., Corey, D., Massaro, J.M., Sutherland, P., Vita, J.A., and Benjamin, E.J.; Framingham Study (2003). Obesity and systemic oxidative stress: clinical correlates of oxidative stress in the Framingham Study. Arterioscler. Thromb. Vasc. Biol. 23, 434–439.
65. Ahmadian, M., Abbott, M.J., Tang, T., Hudak, C.S., Kim, Y., Bruss, M., Hellerstein, M.K., Lee, H.Y., Samuel, V.T., Shulman, G.I., et al. (2011). Desnutrin/ATGL is regulated by AMPK and is required for a brown adipose phenotype. Cell Metab. 13, 73 9–748.
66. Lodhi, I.J., Yin, L., Jensen-Urstad, A.P., Funai, K., Coleman, T., Baird, J.H., El Ramahi, M.K., Razani, B., Song, H., Fu-Hsu, F., et al. (2012). Inhibiting adipose tissue lipogenesis reprograms thermogenesis and PPARg activation to decrease diet-induced obesity. Cell Metab. 16, 189–201.
67. Wolfgang, M.J., and Lane, M.D. (2006). Control of energy homeostasis: role of enzymes and intermediates of fatty acid metabolism in the central nervous system. Annu. Rev. Nutr. 26, 23–44.
68. Houstis, N., Rosen, E.D., and Lander, E.S. (2006). Reactive oxygen species

have a causal role in multiple forms of insulin resistance. Nature 440, 944–948.
69. Eguchi, J., Wang, X., Yu, S., Kershaw, E.E., Chiu, P.C., Dushay, J., Estall, J.L., Klein, U., Maratos-Flier, E., and Rosen, E.D. (2011). Transcriptional control of adipose lipid handling by IRF4. Cell Metab. 13, 249–259.
70. Reamy, A.A., and Wolfgang, M.J. (2011). Carnitine palmitoyltransferase-1c gain-of-function in the brain results in postnatal microencephaly. J. Neurochem. 118, 388–398.
71. Rodriguez, S., and Wolfgang, M.J. (2012). Targeted chemical-genetic regulation of protein stability in vivo. Chem. Biol. 19, 391–398.
72. Ellis, J.M., Mentock, S.M., Depetrillo, M.A., Koves, T.R., Sen, S., Watkins, S.M., Muoio, D.M., Cline, G.W., Taegtmeyer, H., Shulman, G.I., et al. (2011). Mouse cardiac acyl coenzyme a synthetase 1 deficiency impairs Fatty Acid oxidation and induces cardiac hypertrophy. Mol. Cell. Biol. 31, 1252–1262.
73. Haynie, K.R., Vandanmagsar, B., Wicks, S.E., Zhang, J., and Mynatt, R.L. (2014). Inhibition of carnitine palymitoyltransferase1b induces cardiac hypertrophy and mortality in mice. Diabetes Obes. Metab. 16, 757–760.
74. Hsiao, Y.S., Jogl, G., Esser, V., and Tong, L. (2006). Crystal structure of rat carnitine palmitoyltransferase II (CPT-II). Biochem. Biophys. Res. Commun. 346, 974–980.
75. Golozoubova, V., Hohtola, E., Matthias, A., Jacobsson, A., Cannon, B., and Nedergaard, J. (2001). Only UCP1 can mediate adaptive nonshivering thermogenesis in the cold. FASEB J. 15, 2048–2050.
76. Ukropec, J., Anunciado, R.P., Ravussin, Y., Hulver, M.W., and Kozak, L.P. (2006). UCP1-independent thermogenesis in white adipose tissue of cold acclimated Ucp1$^{-/-}$ mice. J. Biol. Chem. 281, 31894–31908.
77. Abu-Elheiga, L., Matzuk, M.M., Abo-Hashema, K.A., and Wakil, S.J. (2001). Continuous fatty acid oxidation and reduced fat storage in mice lacking acetyl-CoA carboxylase 2. Science 291, 2613–2616.
78. Nelson, R.A., Wahner, H.W., Jones, J.D., Ellefson, R.D., and Zollman, P.E. (1973). Metabolism of bears before, during, and after winter sleep. Am. J. Physiol. 224, 491–496.
79. Liu, X., Rossmeisl, M., McClaine, J., Riachi, M., Harper, M.E., and Kozak, L.P. (2003). Paradoxical resistance to diet-induced obesity in UCP1-deficient mice. J. Clin. Invest. 111, 399–407.
80. Furukawa, S., Fujita, T., Shimabukuro, M., Iwaki, M., Yamada, Y., Nakajima, Y., Nakayama, O., Makishima, M., Matsuda, M., and Shimomura, I. (2004). Increased oxidative stress in obesity and its impact on metabolic syndrome. J. Clin. Invest. 114, 1752–1761.
81. Feldmann, H.M., Golozoubova, V., Cannon, B., and Nedergaard, J. (2009). UCP1 ablation induces obesity and abolishes diet-induced thermogenesis in mice exempt from thermal stress by living at thermoneutrality. Cell Metab. 9, 203–209.
82. Kontani, Y., Wang, Y., Kimura, K., Inokuma, K.I., Saito, M., Suzuki-Miura, T., Wang, Z., Sato, Y., Mori, N., and Yamashita, H. (2005). UCP1 deficiency increases susceptibility to diet-induced obesity with age. Aging Cell 4, 147–155.
83. Bal, N.C., Maurya, S.K., Sopariwala, D.H., Sahoo, S.K., Gupta, S.C., Shaikh,

S.A., Pant, M., Rowland, L.A., Bombardier, E., Goonasekera, S.A., et al. (2012). Sarcolipin is a newly identified regulator of muscle-based thermogenesis in mammals. Nat. Med. 18, 1575–1579.

84. Leonardsson, G., Steel, J.H., Christian, M., Pocock, V., Milligan, S., Bell, J., So, P.W., Medina-Gomez, G., Vidal-Puig, A., White, R., and Parker, M.G. (2004). Nuclear receptor corepressor RIP140 regulates fat accumulation. Proc. Natl. Acad. Sci. USA 101, 8437–8442.
85. Wang, H., Zhang, Y., Yehuda-Shnaidman, E., Medvedev, A.V., Kumar, N., Daniel, K.W., Robidoux, J., Czech, M.P., Mangelsdorf, D.J., and Collins, S. (2008). Liver X receptor alpha is a transcriptional repressor of the uncoupling protein 1 gene and the brown fat phenotype. Mol. Cell. Biol. 28, 2187–2200.
86. Ozaki, K., Sano, T., Tsuji, N., Matsuura, T., and Narama, I. (2011). Carnitine is necessary to maintain the phenotype and function of brown adipose tissue. Lab. Invest. 91, 704–710.
87. Muoio, D.M., Noland, R.C., Kovalik, J.P., Seiler, S.E., Davies, M.N., DeBalsi, K.L., Ilkayeva, O.R., Stevens, R.D., Kheterpal, I., Zhang, J., et al. (2012). Muscle-specific deletion of carnitine acetyltransferase compromises glucose tolerance and metabolic flexibility. Cell Metab. 15, 764–777.
88. Liu, M., Bai, J., He, S., Villarreal, R., Hu, D., Zhang, C., Yang, X., Liang, H., Slaga, T.J., Yu, Y., et al. (2014). Grb10 promotes lipolysis and thermogenesis by phosphorylation-dependent feedback inhibition of mTORC1. Cell Metab. 19, 967–980.
89. Müller, T.D., Lee, S.J., Jastroch, M., Kabra, D., Stemmer, K., Aichler, M., Abplanalp, B., Ananthakrishnan, G., Bhardwaj, N., Collins, S., et al. (2013). p62 links **b**-adrenergic input to mitochondrial function and thermogenesis. J. Clin. Invest. 123, 469–478.
90. Neess, D., Bek, S., Bloksgaard, M., Marcher, A.B., Færgeman, N.J., and Mandrup, S. (2013). Delayed hepatic adaptation to weaning in ACBP-/- mice is caused by disruption of the epidermal barrier. Cell Rep. 5, 1403–1412.
91. , R.J., Hamm, D.A., Tian, L., Sharer, J.D., Vockley, J., Rinaldo, P., Matern, D., Schoeb, T.R., and Wood, P.A. (2005). Medium-chain acyl-CoA dehydrogenase deficiency in gene targeted mice. PLoS genetics 1, e23.
92. Fedorenko, A., Lishko, P.V., and Kirichok, Y. (2012). Mechanism of fatty-acid-dependent UCP1 uncoupling in brown fat mitochondria. Cell 151, 400-413.
93. Lee, J., Ellis, J.M., and Wolfgang, M.J. (2015). Adipose fatty acid oxidation is required for thermogenesis and potentiates oxidative stress-induced inflammation. Cell Rep 10, 266-279.
94. Chace, D.H., Hillman, S.L., Van Hove, J.L., and Naylor, E.W. (1997). Rapid diagnosis of MCAD deficiency: quantitative analysis of octanoylcarnitine and other acylcarnitines in newborn blood spots by tandem mass spectrometry. Clin. Chem. 43, 2106–2113.
95. Sandlers, Y., Moser, A.B., Hubbard, W.C., Kratz, L.E., Jones, R.O., and Raymond, G.V. (2012). Combined extraction of acyl carnitines and 26:0 lysophosphatidylcholine from dried blood spots: prospective newborn screening for X-linked adrenoleukodystrophy. Mol. Genet. Metab. 105, 416–420.
96. Cohen, P., Levy, J.D., Zhang, Y., Frontini, A., Kolodin, D.P., Svensson, K.J.,

Lo, J.C., Zeng, X., Ye, L., Khandekar, M.J., et al. (2014). Ablation of PRDM16 and beige adipose causes metabolic dysfunction and a subcutaneous to visceral fat switch. Cell 156, 304-316.
97. Harms, M.J., Ishibashi, J., Wang, W., Lim, H.W., Goyama, S., Sato, T., Kurokawa, M., Won, K.J., and Seale, P. (2014). Prdm16 is required for the maintenance of brown adipocyte identity and function in adult mice. Cell Metab 19, 593-604.
98. Haemmerle, G., Moustafa, T., Woelkart, G., Buttner, S., Schmidt, A., van de Weijer, T., Hesselink, M., Jaeger, D., Kienesberger, P.C., Zierler, K., et al. (2011). ATGL-mediated fat catabolism regulates cardiac mitochondrial function via PPAR-alpha and PGC-1. Nat Med 17, 1076-1085.
99. Mottillo, E.P., Bloch, A.E., Leff, T., and Granneman, J.G. (2012). Lipolytic products activate peroxisome proliferator-activated receptor (PPAR) alpha and delta in brown adipocytes to match fatty acid oxidation with supply. The Journal of biological chemistry 287, 25038-25048.
100. Schoiswohl, G., Stefanovic-Racic, M., Menke, M.N., Wills, R.C., Surlow, B.A., Basantani, M.K., Sitnick, M.T., Cai, L., Yazbeck, C.F., Stolz, D.B., et al. (2015). Impact of reduced ATGL-mediated adipocyte lipolysis on obesity-associated insulin resistance and inflammation in male mice. Endocrinology, en20151322.
101. Bartelt, A., Bruns, O.T., Reimer, R., Hohenberg, H., Ittrich, H., Peldschus, K., Kaul, M.G., Tromsdorf, U.I., Weller, H., Waurisch, C., et al. (2011). Brown adipose tissue activity controls triglyceride clearance. Nat. Med. 17, 200–205.
102. Kazak, L., Chouchani, E.T., Jedrychowski, M.P., Erickson, B.K., Shinoda, K., Cohen, P., Vetrivelan, R., Lu, G.Z., Laznik-Bogoslavski, D., Hasenfuss, S.C., et al. (2015). A creatine-driven substrate cycle enhances energy expenditure and thermogenesis in beige fat. Cell 163, 643–655.
103. West, A.P., Khoury-Hanold, W., Staron, M., Tal, M.C., Pineda, C.M., Lang, S.M., Bestwick, M., Duguay, B.A., Raimundo, N., MacDuff, D.A., et al. (2015). Mitochondrial DNA stress primes the antiviral innate immune response. Nature 520, 553-557.
104. Fisher, F.M., Kleiner, S., Douris, N., Fox, E.C., Mepani, R.J., Verdeguer, F., Wu, J., Kharitonenkov, A., Flier, J.S., Maratos-Flier, E., et al. (2012). FGF21 regulates PGC-1alpha and browning of white adipose tissues in adaptive thermogenesis. Genes & development 26, 271-281.
105. Samms, R.J., Smith, D.P., Cheng, C.C., Antonellis, P.P., Perfield, J.W., 2nd, Kharitonenkov, A., Gimeno, R.E., and Adams, A.C. (2015). Discrete Aspects of FGF21 In Vivo Pharmacology Do Not Require UCP1. Cell Rep 11, 991-999.
106. Veniant, M.M., Sivits, G., Helmering, J., Komorowski, R., Lee, J., Fan, W., Moyer, C., and Lloyd, D.J. (2015). Pharmacologic Effects of FGF21 Are Independent of the "Browning" of White Adipose Tissue. Cell Metab 21, 731-738.
107. Eng, J.W., Reed, C.B., Kokolus, K.M., Pitoniak, R., Utley, A., Bucsek, M.J., Ma, W.W., Repasky, E.A., and Hylander, B.L. (2015). Housing temperature-induced stress drives therapeutic resistance in murine tumour models through beta2-adrenergic receptor activation. Nature communications 6, 6426.

108. Kokolus, K.M., Capitano, M.L., Lee, C.T., Eng, J.W., Waight, J.D., Hylander, B.L., Sexton, S., Hong, C.C., Gordon, C.J., Abrams, S.I., et al. (2013). Baseline tumor growth and immune control in laboratory mice are significantly influenced by subthermoneutral housing temperature. Proceedings of the National Academy of Sciences of the United States of America 110, 20176-20181.
109. Owen OE, Morgan AP, Kemp HG, Sullivan JM, Herrera MG, and Cahill GF, Jr. Brain metabolism during fasting. *J Clin Invest.* 1967;46(10):1589-95.
110. Cotter DG, d'Avignon DA, Wentz AE, Weber ML, and Crawford PA. Obligate role for ketone body oxidation in neonatal metabolic homeostasis. *The Journal of biological chemistry.* 2011;286(9):6902-10.
111. Mutel E, Gautier-Stein A, Abdul-Wahed A, Amigo-Correig M, Zitoun C, Stefanutti A, Houberdon I, Tourette JA, Mithieux G, and Rajas F. Control of blood glucose in the absence of hepatic glucose production during prolonged fasting in mice: induction of renal and intestinal gluconeogenesis by glucagon. *Diabetes.* 2011;60(12):3121-31.
112. McGarry JD, and Brown NF. The mitochondrial carnitine palmitoyltransferase system. From concept to molecular analysis. *Eur J Biochem.* 1997;244(1):1-14.
113. Isackson PJ, Bennett MJ, Lichter-Konecki U, Willis M, Nyhan WL, Sutton VR, Tein I, and Vladutiu GD. CPT2 gene mutations resulting in lethal neonatal or severe infantile carnitine palmitoyltransferase II deficiency. *Mol Genet Metab.* 2008;94(4):422-7.
114. Kurtz DM, Rinaldo P, Rhead WJ, Tian L, Millington DS, Vockley J, Hamm DA, Brix AE, Lindsey JR, Pinkert CA, et al. Targeted disruption of mouse long-chain acyl-CoA dehydrogenase gene reveals crucial roles for fatty acid oxidation. *Proceedings of the National Academy of Sciences of the United States of America.* 1998;95(26):15592-7.
115. Spiekerkoetter U, and Wood PA. Mitochondrial fatty acid oxidation disorders: pathophysiological studies in mouse models. *Journal of inherited metabolic disease.* 2010;33(5):539-46.
116. Zhang D, Christianson J, Liu ZX, Tian L, Choi CS, Neschen S, Dong J, Wood PA, and Shulman GI. Resistance to high-fat diet-induced obesity and insulin resistance in mice with very long-chain acyl-CoA dehydrogenase deficiency. *Cell Metab.* 2010;11(5):402-11.
117. Zhang D, Liu ZX, Choi CS, Tian L, Kibbey R, Dong J, Cline GW, Wood PA, and Shulman GI. Mitochondrial dysfunction due to long-chain Acyl-CoA dehydrogenase deficiency causes hepatic steatosis and hepatic insulin resistance. *Proceedings of the National Academy of Sciences of the United States of America.* 2007;104(43):17075-80.
118. Postic C, Shiota M, Niswender KD, Jetton TL, Chen Y, Moates JM, Shelton KD, Lindner J, Cherrington AD, and Magnuson MA. Dual roles for glucokinase in glucose homeostasis as determined by liver and pancreatic beta cell-specific gene knock-outs using Cre recombinase. *The Journal of biological chemistry.* 1999;274(1):305-15.
119. Ellis JM, Bowman CE, and Wolfgang MJ. Metabolic and Tissue-Specific Regulation of Acyl-CoA Metabolism. *PLoS One.* 2015;10(3):e0116587.

120. Ellis JM, Wong GW, and Wolfgang MJ. Acyl coenzyme A thioesterase 7 regulates neuronal fatty acid metabolism to prevent neurotoxicity. *Molecular and cellular biology.* 2013;33(9):1869-82.
121. Lee J, Choi J, Aja S, Scafidi S, and Wolfgang MJ. Loss of Adipose Fatty Acid Oxidation Does Not Potentiate Obesity at Thermoneutrality. *Cell Rep.* 2016;14(6):1308-16.
122. Nomura M, Liu J, Rovira, II, Gonzalez-Hurtado E, Lee J, Wolfgang MJ, and Finkel T. Fatty acid oxidation in macrophage polarization. *Nat Immunol.* 2016;17(3):216-7.
123. Boles RG, Buck EA, Blitzer MG, Platt MS, Cowan TM, Martin SK, Yoon H, Madsen JA, Reyes-Mugica M, and Rinaldo P. Retrospective biochemical screening of fatty acid oxidation disorders in postmortem livers of 418 cases of sudden death in the first year of life. *The Journal of pediatrics.* 1998;132(6):924-33.
124. Rinaldo P, Matern D, and Bennett MJ. Fatty acid oxidation disorders. *Annual review of physiology.* 2002;64(477-502.
125. Badman MK, Pissios P, Kennedy AR, Koukos G, Flier JS, and Maratos-Flier E. Hepatic fibroblast growth factor 21 is regulated by PPARalpha and is a key mediator of hepatic lipid metabolism in ketotic states. *Cell Metab.* 2007;5(6):426-37.
126. Inagaki T, Dutchak P, Zhao G, Ding X, Gautron L, Parameswara V, Li Y, Goetz R, Mohammadi M, Esser V, et al. Endocrine regulation of the fasting response by PPARalpha-mediated induction of fibroblast growth factor 21. *Cell Metab.* 2007;5(6):415-25.
127. Wheatcroft SB, and Kearney MT. IGF-dependent and IGF-independent actions of IGF-binding protein-1 and -2: implications for metabolic homeostasis. *Trends Endocrinol Metab.* 2009;20(4):153-62.
128. Hsiao EC, Koniaris LG, Zimmers-Koniaris T, Sebald SM, Huynh TV, and Lee SJ. Characterization of growth-differentiation factor 15, a transforming growth factor beta superfamily member induced following liver injury. *Molecular and cellular biology.* 2000;20(10):3742-51.
129. Johnen H, Lin S, Kuffner T, Brown DA, Tsai VW, Bauskin AR, Wu L, Pankhurst G, Jiang L, Junankar S, et al. Tumor-induced anorexia and weight loss are mediated by the TGF-beta superfamily cytokine MIC-1. *Nat Med.* 2007;13(11):1333-40.
130. Fisher FM, and Maratos-Flier E. Understanding the Physiology of FGF21. *Annual review of physiology.* 2015.
131. Fisher FM, Kleiner S, Douris N, Fox EC, Mepani RJ, Verdeguer F, Wu J, Kharitonenkov A, Flier JS, Maratos-Flier E, et al. FGF21 regulates PGC-1alpha and browning of white adipose tissues in adaptive thermogenesis. *Genes Dev.* 2012;26(3):271-81.
132. Holland WL, Adams AC, Brozinick JT, Bui HH, Miyauchi Y, Kusminski CM, Bauer SM, Wade M, Singhal E, Cheng CC, et al. An FGF21-adiponectin-ceramide axis controls energy expenditure and insulin action in mice. *Cell Metab.* 2013;17(5):790-7.

133. Lin Z, Tian H, Lam KS, Lin S, Hoo RC, Konishi M, Itoh N, Wang Y, Bornstein SR, Xu A, et al. Adiponectin mediates the metabolic effects of FGF21 on glucose homeostasis and insulin sensitivity in mice. *Cell Metab.* 2013;17(5):779-89.
134. Wanders RJ, Vreken P, den Boer ME, Wijburg FA, van Gennip AH, and L IJ. Disorders of mitochondrial fatty acyl-CoA beta-oxidation. *Journal of inherited metabolic disease.* 1999;22(4):442-87.
135. Brivet M, Boutron A, Slama A, Costa C, Thuillier L, Demaugre F, Rabier D, Saudubray JM, and Bonnefont JP. Defects in activation and transport of fatty acids. *Journal of inherited metabolic disease.* 1999;22(4):428-41.
136. Auestad N, Korsak RA, Morrow JW, and Edmond J. Fatty acid oxidation and ketogenesis by astrocytes in primary culture. *J Neurochem.* 1991;56(4):1376-86.
137. Guzman M, and Blazquez C. Ketone body synthesis in the brain: possible neuroprotective effects. *Prostaglandins, leukotrienes, and essential fatty acids.* 2004;70(3):287-92.
138. Newman JC, and Verdin E. Ketone bodies as signaling metabolites. *Trends Endocrinol Metab.* 2014;25(1):42-52.
139. Kimura I, Inoue D, Maeda T, Hara T, Ichimura A, Miyauchi S, Kobayashi M, Hirasawa A, and Tsujimoto G. Short-chain fatty acids and ketones directly regulate sympathetic nervous system via G protein-coupled receptor 41 (GPR41). *Proceedings of the National Academy of Sciences of the United States of America.* 2011;108(19):8030-5.
140. Taggart AK, Kero J, Gan X, Cai TQ, Cheng K, Ippolito M, Ren N, Kaplan R, Wu K, Wu TJ, et al. (D)-beta-Hydroxybutyrate inhibits adipocyte lipolysis via the nicotinic acid receptor PUMA-G. *The Journal of biological chemistry.* 2005;280(29):26649-52.
141. Chakravarthy MV, Lodhi IJ, Yin L, Malapaka RR, Xu HE, Turk J, and Semenkovich CF. Identification of a physiologically relevant endogenous ligand for PPARalpha in liver. *Cell.* 2009;138(3):476-88.
142. Chakravarthy MV, Pan Z, Zhu Y, Tordjman K, Schneider JG, Coleman T, Turk J, and Semenkovich CF. "New" hepatic fat activates PPARalpha to maintain glucose, lipid, and cholesterol homeostasis. *Cell Metab.* 2005;1(5):309-22.
143. Chakravarthy MV, Zhu Y, Lopez M, Yin L, Wozniak DF, Coleman T, Hu Z, Wolfgang M, Vidal-Puig A, Lane MD, et al. Brain fatty acid synthase activates PPARalpha to maintain energy homeostasis. *J Clin Invest.* 2007;117(9):2539-52.
144. Markan KR, Naber MC, Ameka MK, Anderegg MD, Mangelsdorf DJ, Kliewer SA, Mohammadi M, and Potthoff MJ. Circulating FGF21 is liver derived and enhances glucose uptake during refeeding and overfeeding. *Diabetes.* 2014;63(12):4057-63.
145. Davis RL, Liang C, Edema-Hildebrand F, Riley C, Needham M, and Sue CM. Fibroblast growth factor 21 is a sensitive biomarker of mitochondrial disease. *Neurology.* 2013;81(21):1819-26.
146. Cahoy JD, Emery B, Kaushal A, Foo LC, Zamanian JL, Christopherson KS, Xing Y, Lubischer JL, Krieg PA, Krupenko SA, et al: A transcriptome database

for astrocytes, neurons, and oligodendrocytes: a new resource for understanding brain development and function. J Neurosci 2008, 28(1):264–278.
147. Wolfgang MJ, Lane MD: The role of hypothalamic malonyl-CoA in energy homeostasis. J Biol Chem 2006, 281(49):37265–37269.
148. Price N, van der Leij F, Jackson V, Corstorphine C, Thomson R, Sorensen A, Zammit V: A novel brain-expressed protein related to carnitine palmitoyltransferase I. Genomics 2002, 80(4):433–442.
149. Wolfgang MJ, Cha SH, Millington DS, Cline G, Shulman GI, Suwa A, Asaumi M, Kurama T, Shimokawa T, Lane MD: Brain-specific carnitine palmitoyl-transferase-1c: role in CNS fatty acid metabolism, food intake, and body weight. J Neurochem 2008, 105(4):1550–1559.
150. Wolfgang MJ, Kurama T, Dai Y, Suwa A, Asaumi M, Matsumoto S, Cha SH, Shimokawa T, Lane MD: The brain-specific carnitine palmitoyltransferase-1c regulates energy homeostasis. Proc Natl Acad Sci USA 2006, 103(19):7282–7287.
151. Carrasco P, Sahun I, McDonald J, Ramirez S, Jacas J, Gratacos E, Sierra AY, Serra D, Herrero L, Acker-Palmer A, et al: Ceramide levels regulated by carnitine palmitoyltransferase 1C control dendritic spine maturation and cognition. J Biol Chem 2012, 287(25):21224–21232.
152. Gao S, Zhu G, Gao X, Wu D, Carrasco P, Casals N, Hegardt FG, Moran TH, Lopaschuk GD: Important roles of brain-specific carnitine palmitoyltransferase and ceramide metabolism in leptin hypothalamic control of feeding. Proc Natl Acad Sci USA 2011, 108(23):9691–9696.
153. Gao XF, Chen W, Kong XP, Xu AM, Wang ZG, Sweeney G, Wu D: Enhanced susceptibility of Cpt1c knockout mice to glucose intolerance induced by a high-fat diet involves elevated hepatic gluconeogenesis and decreased skeletal muscle glucose uptake. Diabetologia 2009, 52(5):912–920.
154. Sierra AY, Gratacos E, Carrasco P, Clotet J, Urena J, Serra D, Asins G, Hegardt FG, Casals N: CPT1c is localized in endoplasmic reticulum of neurons and has carnitine palmitoyltransferase activity. J Biol Chem 2008, 283(11):6878–6885.
155. Eckel-Mahan KL, Patel VR, Mohney RP, Vignola KS, Baldi P, Sassone-Corsi P: Coordination of the transcriptome and metabolome by the circadian clock. Proc Natl Acad Sci USA 2012, 109(14):5541–5546.
156. Zaugg K, Yao Y, Reilly PT, Kannan K, Kiarash R, Mason J, Huang P, Sawyer SK, Fuerth B, Faubert B, et al: Carnitine palmitoyltransferase 1C promotes cell survival and tumor growth under conditions of metabolic stress. Genes Dev 2011, 25(10):1041–1051.
157. Sharma S, Black SM: Carnitine homeostasis, mitochondrial function, and cardiovascular disease. Drug Discov Today Dis Mech 2009, 6(1–4): e31–e39.
158. Dipatrizio NV, Piomelli D: The thrifty lipids: endocannabinoids and the neural control of energy conservation. Trends Neurosci 2012, 35(7):403–411.
159. Sanvicens N, Cotter TG: Ceramide is the key mediator of oxidative stress-induced apoptosis in retinal photoreceptor cells. J Neurochem 2006, 98(5): 1432–1444.

160. Andrieu-Abadie N, Gouaze V, Salvayre R, Levade T: Ceramide in apoptosis signaling: relationship with oxidative stress. Free Radic Biol Med 2001, 31(6): 717–728.
161. Cardinal P, Bellocchio L, Clark S, Cannich A, Klugmann M, Lutz B, Marsicano G, Cota D: Hypothalamic CB1 cannabinoid receptors regulate energy balance in mice. Endocrinology 2012, 153(9): 4136–4143.
162. Cota D, Marsicano G, Tschop M, Grubler Y, Flachskamm C, Schubert M, Auer D, Yassouridis A, Thone-Reineke C, Ortmann S, et al: The endogenous cannabinoid system affects energy balance via central orexigenic drive and peripheral lipogenesis. J Clin Invest 2003, 112(3): 423–431.
163. Barger JF, Gallo CA, Tandon P, Liu H, Sullivan A, Grimes HL, Plas DR: S6K1 determines the metabolic requirements for BCR-ABL survival. Oncogene 2012, doi: 10.1038/onc.2012.70 [Epub ahead of print].
164. Titchenell PM, Quinn WJ, Lu M, Chu Q, Lu W, Li C, Chen H, Monks BR, Chen J, Rabinowitz JD and Birnbaum MJ: Direct Hepatocyte Insulin Signaling is Required for Lipogenesis but is Dispensable for the Suppression of Glucose Production. Cell Metab 2016, 23: 1154-1166.

CURRICULUM VITAE

Jieun Lee

Education and Training

Degrees/Year	Institution	Discipline
Ph.D/2011-2016	Johns Hopkins School of Medicine	Biological Chemistry
Bachelor of Science/2011 (*Summa Cum Laude*)	American University	Biochemistry

Employment and other positions

Position/Year	Institution	Discipline
Research Assistant 2008-2011	AU Biomaterials Design Lab	Biomaterials Design
Undergraduate Volunteer 2010-2011	Johns Hopkins School of Medicine-Wilmer Eye Institute	Endocrinology/Pathology
Guest Researcher 2010-2011	National Institute of Standards and Technology (NIST)	BFRL/Polymer Division 866

Awards and Honors

2016	David I. Macht Research Award Young Investigator's Day, Johns Hopkins University School of Medicine
2015	Poster award at Johns Hopkins School of Medicine First Annual Biological Chemistry Retreat Title: Requirement of adipose tissue fatty acid oxidation
2007-2011	Frederick Douglas Distinguished Scholars Scholarship
2011	University Student Award for Outstanding Scholarship at the Undergraduate Level
2011	Outstanding Research Honors Award
2009-2011	Shaskan Family Endowed Scholarship for Outstanding Undergraduate Students
2009-2011	Korean American Scholarship Foundation Merit Award
2009-2011	Ernest M. Aiken Educational Fund
2010	Korean Embassy Award for Undergraduate Students
2008-2010	Barbara Bohn Wright Award
2009	Poster Award at the 19th Annual Robin Mathias Conference in Washington D.C.
2009	Sejong Merit Award for Outstanding Undergraduate Students
2007-2009	Ruth McFeeter Scholarship for Academic Merit

Talks/Conferences

2016	Young Investigator's Day-Johns Hopkins University School of Medicine (Poster) Title: Requirement of adipose tissue fatty acid oxidation
2016	Navigating Lipid Research in Baltimore-Carnegie Institution for Science (Talk) Title: Hepatic fatty acid oxidation restrains systemic catabolism during starvation
2016	Navigating Lipid Research in Baltimore-Carnegie Institution for Science (Poster) Title: Requirement of hepatic fatty acid oxidation
2015	Gordon Research Conferences: Lipids, Molecular & Cellular Biology of (Poster) Title: Requirement of adipose tissue fatty acid oxidation
2015	Johns Hopkins School of Medicine First Annual Biological Chemistry Retreat (Poster) Title: Requirement of adipose tissue fatty acid oxidation
2014	Johns Hopkins School of Medicine BCMB Retreat (Talk) Title: Role of adipocyte fatty acid oxidation in obesity and diabetes
2009	238th National ACS Conference in Washington D.C. (Talk) Title: Hydrophobically modified cellulose using 1,2-Epoxy-3-phenoxypropane and glycidyl phenyl-POSS
2009	19th Annual Robyn Raffert Mathias Research Conference (Poster) Title: The thermal stability of hybrid plastic using POSS-modified L040-6
2009	Cellulose Nanocomposites Symposium at the 10th International Conference on Wood and Biofiber Plastic Composites, Forest Products Society (Poster) Title: POSS modified cellulose nanofibrils

Peer-Reviewed Publications:

1. Lam WY, Becker AM, Kennerly KM, Wong R, Curtis JD, Llufrio EM, McCommis KS, Fahrmann J, Pizzato HA, Nunley RM, Lee J, Wolfgang MJ, Patti GJ, Finck BN, Pearce EL, Bhattacharya D. Mitochondrial pyruvate import promotes long-term survival of antibody-secreting plasma cells. *Immunity* 45(1), 60-73 (2016).

2. Lee J, Choi J, Scafidi S, Wolfgang MJ. Hepatic fatty acid oxidation restrains systemic catabolism during starvation. *Cell Reports* 16(1), 201-12 (2016).

3. Nomura M, Liu J, Rovira II, Gonzalez-Hurtado E, Lee J, Wolfgang MJ, Finkel T. Re-assessing the role of fatty acid oxidation in macrophage polarization. *Nat. Immunol* 17, 216-217 (2016).

4. Lee J, Choi J, Aja S, Wolfgang MJ. Loss of adipose fatty acid oxidation does not potentiate obesity at thermoneutrality. *Cell Reports* 14, 1-9 (2016).

5. Lee J, Choi J, Wolfgang MJ, Neurometabolomic roles of ApoE and Ldl-R in mouse brain. *J Bioenerg Biomembr* 48(1), 13-21 (February, 2016).

6. Lee J, Ellis JM, Wolfgang MJ, Adipose fatty acid oxidation is required for thermogenesis and potentiates oxidative stress-induced inflammation. *Cell Reports* 10, 1-14 (January, 2015).

7. Fox DM, Lee J, Citro CJ, Novy M. Flame Retarded Poly(lactic acid) Using POSS-Modified Cellulose Thermal and Combustion Properties of Intumescing Composites. *Polym. Degrad. Stab*. 98, 590-596 (2013).

8. Lee J & Wolfgang MJ. Metabolomic profiling reveals a role for CPT1c in neuronal oxidative metabolism. *BMC Biochem* 13:23 (2012).

9. Fox DM, Lee J, Zammarano M, Kim YS, Katsoulis D, Eldred DV, Haverhals L, Trulove PC, De Long HC, Gilman JW. Char-Forming Behavior of Nanofibrillated Cellulose Treated with GlycidylPhenyl POSS. *Carbohydrate Polymers* 88:847-858 (2012).

10. Fox DM, Lee J, Jones JM, Zammarano M, Gilman JW. "Microencapsulated POSS in Cellulose Using 1-Ethyl-3-Methylimidazolium Acetate," in Proc. Int. Symp. Molten Salts and Ionic Liquids, *ECS Transactions* 33(7): 99-108 (2010).

11. Fox DM, Lee J, Ford E, Balsley E, Zammarano M, Batko S, Gilman JW. "POSS modified cellulose for improving flammability characteristics of polystyrene." *Proc. 10th Int. Conf. Wood Biofiber Plastic Composites, Forest Products Society* 337-342 (2010).'

Leadership Experience

- Joseph Choi – Undergraduate Research Student, University of Maryland-Baltimore County*;* 2014-present
- Elsie Gonzalez-Hurtado – Department of Biological Chemistry, Postbaccalaureate Education Program (PREP), Johns Hopkins School of Medicine; 2015-Present
- Emily Fray – Biochemistry, Cellular and Molecular Biology (BCMB) PhD student, Johns Hopkins School of Medicine; 2015.